POLITECNICO DI MILANO

DIPARTIMENTO DI ELETTRONICA, INFORMAZIONE E BIOINGEGNERIA

DOCTORAL PROGRAMME IN INFORMATION TECHNOLOGY

The Capacity of Amplitude-Constrained Vector Gaussian Channels

Doctoral Dissertation of:

Antonino Favano

Supervisor:

Prof. Luca Barletta

Co-Supervisor:

Dr. Marco Ferrari

Tutor:

Prof. Paolo Martelli

The Chair of the Doctoral Program:

Prof. Luigi Piroddi

2022 – XXXV Cycle

Acknowledgements

I would like to thank the following people.

My supervisor Prof. Luca Barletta for his valuable guidance and his continuous support throughout the duration of my research.

My co-supervisor Dr. Marco Ferrari for his insightful advice and constant assistance and Prof. Maurizio Magarini for his fruitful comments and for encouraging me to pursue a PhD.

My family for their unwavering support.

Abstract

ENERGY efficiency is one of the most important features of modern wireless communication systems. The components having a stronger impact on the power consumption of wireless systems are radio frequency chains. To improve their energy efficiency and reduce the associated costs, it is useful to limit the peak power of the transmitted signals. Therefore, power constraints are used to accurately model the limitations imposed on such communication systems and provide a reliable information theoretic baseline to efficiently maximize the achievable mutual information.

In this work, it is investigated the capacity of both nonfading and fading vector Gaussian channels subject to input power constraints. The considered transmitter configurations are those employing either one or several concurrent power constraints. Results on the capacity-achieving distribution are presented for nonfading channels. Moreover, accurate estimates of the optimal input distribution and of the resulting channel capacity are derived.

Two families of upper bounds are proposed for fading channels. The first family relies on a sphere packing argument and can be applied to any convex input constraint. The second family of upper bounds is specifically devised for multiple parallel power constraints.

List of Publications

- A. Favano, M. Ferrari, M. Magarini and L. Barletta, "A Sphere Packing Bound for Vector Gaussian Fading Channels under Peak Amplitude Constraints," in IEEE Transactions on Information Theory, 2022
- A. Favano, L. Barletta and A. Dytso, "On the Capacity Achieving Input of Amplitude Constrained Vector Gaussian Wiretap Channel," 2022 IEEE International Symposium on Information Theory (ISIT), 2022, pp. 850-855
- A. Favano, M. Ferrari, M. Magarini and L. Barletta, "The Capacity of the Amplitude-Constrained Vector Gaussian Channel," 2021 IEEE International Symposium on Information Theory (ISIT), 2021, pp. 426-431
- A. Favano, M. Ferrari, M. Magarini and L. Barletta, "A Sphere Packing Bound for AWGN MIMO Fading Channels under Peak Amplitude Constraints," 2020 IEEE Information Theory Workshop (ITW), 2021, pp. 1-5
- A. Favano, M. Ferrari, M. Magarini and L. Barletta, "Capacity Bounds for Amplitude-Constrained AWGN MIMO Channels with Fading," 2020 IEEE International Symposium on Information Theory (ISIT), 2020, pp. 2032-2037

Contents

List of Figures

List of Acronyms

AWGN Additive White Gaussian Noise

ICT Information and Communication Technologies

MIMO Multiple-Input Multiple-Output

PDF Probability Density Function

PMF Probability Mass Function

SNR Signal-to-Noise Ratio

TA Total Amplitude

PA Per-Antenna

AS Antenna Subsets

EPI Entropy Power Inequality

P-EPI Piecewise Entropy Power Inequality

SP Sphere Packing

G-SP Generalized Sphere Packing

P-SP Piecewise Sphere Packing

KKT Karush–Kuhn–Tucker

QPC Quasi Parallel Channels

Notation

$\mathbf{x}$	Bold letters are vectors
X	Uppercase Letters are random variables
X_i	ith element of the random vector $\mathbf{X}$
$\mathcal{X}$	Calligraphic letters are subsets of vector spaces
$\mathrm{Vol}_n(\mathcal{X})$	n-dimensional volume of the set $\mathcal{X}$
$\|\mathbf{x}\|$	Euclidean norm of the vector $\mathbf{x}$
H	Uppercase sans serif letters are matrices
$\mathsf{H}_{i,j}$	Element (i, j) of the matrix H
H^T	Transpose of the matrix H
$\det(\mathsf{H})$	Determinant of the matrix H
$\mathcal{N}(\boldsymbol{\mu}, \Sigma)$	Multivariate Gaussian distribution of mean vector $\boldsymbol{\mu}$ and covariance matrix Σ
$\mathcal{CN}(\boldsymbol{\mu}, \Sigma)$	Multivariate complex Gaussian distribution of mean vector $\boldsymbol{\mu}$ and covariance matrix Σ
$\chi^2_n(\xi)$	Noncentral chi-squared distribution with n degrees of freedom and noncentrality parameter ξ
$\mathbf{0}_n$	n-dimensional vector of zeros
I_n	$n \times n$ identity matrix
$\mathcal{B}^n$	n-dimensional unitary ball centered at the origin
$\mathcal{B}^n_{\mathsf{R}}$	n-dimensional ball of radius R and centered at the origin
$\mathcal{S}^n_{\mathsf{R}}$	n-dimensional hypersphere of radius R and centered at the origin
$I_n(z)$	Modified Bessel function of the first kind of order n and argument z

$\mathsf{E}[\mathbf{X}]$	Expected value of $\mathbf{X}$
$\mathsf{H}(\mathbf{X})$	Entropy of $\mathbf{X}$
$\mathsf{h}(\mathbf{X})$	Differential entropy of $\mathbf{X}$
$\mathsf{I}(\mathbf{X}\,;\mathbf{Y})$	Mutual information of $\mathbf{X}$ and $\mathbf{Y}$
$\mathrm{supp}(f)$	Support of the function f
$f_{\mathbf{X}}$	Probability density function of $\mathbf{X}$
$P_{\mathbf{X}}$	Probability mass function of $\mathbf{X}$
$F_{\mathbf{X}}$	Cumulative distribution function of $\mathbf{X}$
C	Channel capacity

Chapter 1

Introduction

Channel capacity is one of the fundamental concepts in information theory and provides the maximum information rate that a channel can sustain while guaranteeing an arbitrarily small error probability. The capacity of an Additive White Gaussian Noise (AWGN) channel subject to average power constraints was first introduced in Shannon's most celebrated work [1]. As communication technologies progressed, the interest in faster and more efficient transceivers grew substantially. In the pursuit of higher information rates, multi-antenna communication systems were envisioned as a technology capable to offer significant capacity gains [2–4], prompting an intense research effort. The derivation of Shannon's channel capacity was extended to the case of multi-antenna systems in [5] by Telatar. Because of the rapid growth of the cellular industry and of wireless communication systems as a whole, also multi-user Multiple-Input Multiple-Output (MIMO) systems were extensively studied [6–11]. Another extremely relevant research topic that ignited even more the interest in wireless communications is that of massive MIMO systems. These systems enable a

dramatic increase in terms of throughput, obtained by employing a large number (in the order of hundreds) of antennas [12–17]. Massive MIMO systems, together with device-to-device communications, Internet of things, and ultra-dense networks have received increasing attention because of the unstoppable growth of mobile devices and applications [18].

As the number of antennas and devices scale, the consequences in terms of power consumption and environmental impact caused by wireless systems become unsustainable [19]. Moreover, the amount of transmitted data and new applications dealing with sensitive information, exacerbates the privacy concerns in communication systems [20].

As of today, the demand for higher information rates has not slowed down. It is currently estimated that the Information and Communication Technologies (ICT) industry is responsible for about 2–3% of all the carbon footprint generated by human activities [21–23]. As a consequence, in the last years the theme of Green Communications has gained more and more traction in the world of ICT.

A particularly representative case, in wireless communication systems, is that of the cellular industry. In wireless cellular networks, base stations are the elements having the strongest impact in terms of power usage [24]. Moreover, within the base station, the power amplifiers typically account for roughly $50 - 80\%$ of the total power consumption [25]. Due to their nonlinear characteristic, power amplifiers become inefficient when they are fed with an input power out of their linear range. Since power amplifiers are ubiquitous in communication transceivers and since their employment will dramatically increase with massive MIMO technologies, a countermeasure to im-

prove the overall efficiency of communication systems is worthwhile. A solution is to reduce the power consumption by strictly constraining the peak power, or equivalently the peak amplitude, of the transmitted signals. To maximize the mutual information under such constraints, it is fundamental to accurately characterize the problem from an information theoretic viewpoint. While average power constraints have been thoroughly investigated in the literature, peak power constraints have received far less attention.

One of the first and most notable result is the evaluation of the channel capacity under both peak and average power constraints derived in [26]. The author proves that the capacity-achieving distribution is discrete and comprises a finite number of mass points. In [27], similar insights on the structure of the optimal input distribution are derived for the quadrature case. Moreover, the authors of [28] further generalize the results of [27] and prove that the capacity-achieving input distribution for vector Gaussian channels has, again, uniform phase and a finite and discrete number of amplitude mass points. Then, the support of the capacity-achieving distribution comprises of n-dimensional concentric hyperspheres. In [29], the authors provide an upper bound on the number of hyperspheres. Other important contributions and results on the structure of the optimal input Probability Density Function (PDF) are presented in [30–32].

In [33], the author presents a simple and tight upper bound on the capacity of scalar Gaussian channels subject to amplitude constraints. In [34], the authors extend and refine the bound in [33] to MIMO channels. Specifically, the authors of [34] consider a nonfading MIMO channel and an amplitude constraint on the norm of the input vector.

For the scalar case, a further improvement on the *refined* upper bound of [34] is presented in [35].

For scalar systems the structure of amplitude constraints is well defined, i.e., it is an interval. On the other hand, in multi-dimensional systems the constraint region can be any n-dimensional subset of $\mathbb{R}^n$.

For instance, in [34] the amplitude constraint is set on the norm of the input vector. Therefore, the resulting constraint region is an n-dimensional closed ball centered at the origin. Furthermore, the bounds derived in [34] hold just for nonfading channels.

In the case of fading channels, far less has been done. The structure of the optimal input distribution is known just for real and complex-valued scalar models. In [36, 37], the authors show that, for scalar Gaussian channels with independent and unknown fading, the capacity-achieving distribution is still discrete and comprising a finite number of mass points, for both peak and average power constraints. However, the mathematical tools used by [36, 37] for the scalar case cannot be used to the MIMO case. The main available results for fading MIMO channels are the derivation of capacity bounds. Furthermore, these works consider a different fading model, characterized by a random, but known and fixed, fading channel matrix. In [38], the authors evaluate bounds on the capacity of fading 2×2 MIMO systems for rectangular input constraint regions. Moreover, the authors of [39] derived much more general upper and lower bounds, valid for any n-dimensional constraint region and any arbitrary full rank fading channel matrices. Despite being applicable to a wide variety of cases, the capacity gap between upper and lower bounds presented in [39] is far from zero in most scenarios and there

is still room for improvement.

Amplitude-constrained models are relevant for several kinds of wireless communication paradigms. The most renowned ones are microwave wireless and free-space optical communications. The results derived in each scenario can often be adapted to the other case with some modifications. The main difference is that, since free-space optical communications deal with intensity signals, the constraint region has to lie in the positive real n-dimensional vector space $\mathbb{R}_+^n$. For more details on the capacity of optical intensity channels under peak and average power constraints, see [40–46]. In this work, the focus will be on microwave wireless communications.

1.1 Contributions

The main results presented in this work are bounds on the capacity of MIMO vector Gaussian channels affected by fading and insights on the capacity-achieving input distribution of nonfading channels. Throughout this work, the fading model is characterized via a matrix which is random, but fixed and known at both the transmitter and the receiver. The results are applied to amplitude constraints induced by commonly used transmitter configurations.

Nonfading Vector Gaussian Channels:

In [47], we derived new insights on the structure of the capacity-achieving input distribution. Furthermore, we presented a numerical procedure to estimate the optimal input distribution and the channel capacity. Similar results are extended to the case of nonfading wiretap channels in [48].

Fading Vector Gaussian Channels:

In [49], for two kinds of amplitude constraints, we derived upper and lower bounds on the channel capacity tighter than the best available at the time [39]. We considered constraints on the norm of the input vector and constraints on the amplitude of each input entry. In [50], we presented an upper bounds based on a sphere packing argument that improves, again, on the results of [39]. The derived sphere packing upper bounds is valid for any constraint region and any channel matrix. The results derived in [50] are further examined and exemplified in [51]. Furthermore, in [52] we presented an alternative upper bound that specifically targets transmitter configurations employing multiple parallel power constraints.

1.2 Structure of the Thesis

Chapter 2.1 formally defines key concepts used throughout this work, such as the channel models, the channel capacity definition, the considered amplitude constraints, and so on. Part I introduces the results achieved for nonfading channels. Chapter 3 includes several results on the capacity-achieving distribution for the considered amplitude constraints. Furthermore, the results on the classic vector Gaussian channel are adapted to the wiretap case. Part II includes the results derived for fading channels. In Chapter 4, it is derived an upper bound based on a sphere packing argument suitable for any convex constraint region and any full rank channel matrix, as well as, an upper bound suitable for specific kind of input constraints. Chapter 5 provides numerical results for both the upper bounds presented in Chapter 4 and compares their performance. Finally, Chapter 6 concludes this work.

Chapter 2

Amplitude-Constrained Channel Capacity

In this chapter, the main features of the considered channel models are presented. Several concepts and definitions about amplitude-constrained vector Gaussian channels, useful throughout this work, are introduced. Furthermore, the amplitude constraints of main interest are formally defined, as well as a discussion about the practical transmitter configurations inducing such constraints.

2.1 Channel Model

The focus of this work is on microwave wireless communication systems. In such systems, the transmitted and received signals, by each antenna, are assumed to have complex baseband representation. Therefore, the main considered channel model is a complex-valued MIMO AWGN channel. Let us denote by N_{Tx} the number of transmitting antennas and by N_{Rx} the number of receiving antennas. This

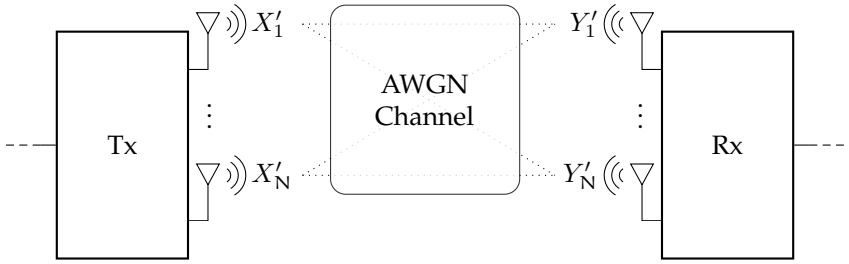

Figure 2.1: *Diagram of a vector AWGN channel model.*

work focuses on the special case where $\mathsf{N}_{\mathrm{Tx}} = \mathsf{N}_{\mathrm{Rx}} = \mathsf{N}$. Nonetheless, notice that the channel models presented in this chapter can be still applied to certain systems with $\mathsf{N}_{\mathrm{Tx}} \neq \mathsf{N}_{\mathrm{Rx}}$. Specifically, the authors of [41] show that for any channel model such that $\mathsf{N}_{\mathrm{Tx}} < \mathsf{N}_{\mathrm{Rx}}$ and $\mathrm{rank}(\mathsf{H}) = \mathsf{N}_{\mathrm{Tx}}$ there exists an equivalent $\mathsf{N}_{\mathrm{Tx}} \times \mathsf{N}_{\mathrm{Tx}}$ channel, i.e., the case considered in this work.

Let us begin by describing the resulting channel model in presence of fading.

Definition 2.1.1 (Fading Channel Model)

The $\mathsf{N} \times \mathsf{N}$ fading complex-valued channel model is given by

$$\mathbf{Y}' = \mathsf{H}'\mathbf{X}' + \mathbf{Z}', \tag{2.1}$$

where $\mathbf{Y}'$ is the output vector, $\mathbf{X}'$ is the input vector, H' is the channel matrix, and $\mathbf{Z}'$ is the AWGN. The output vector $\mathbf{Y}' \in \mathbb{C}^{\mathsf{N}}$ and the same holds for $\mathbf{X}'$ and $\mathbf{Z}'$. The complex input vector $\mathbf{X}'$ is bounded to the amplitude constraint $\mathcal{X}'$, i.e., $\mathbf{X}' \in \mathcal{X}' \subset \mathbb{C}^{\mathsf{N}}$. The noise vector has i.i.d. entries with zero mean and variance $2\sigma_z^2$, i.e., $\mathbf{Z}' \sim \mathcal{CN}(\mathbf{0}_{\mathsf{N}}, 2\sigma_z^2 \mathsf{I}_{\mathsf{N}})$. The channel matrix H' is an $\mathsf{N} \times \mathsf{N}$ complex-valued matrix and it is assumed to be full rank, constant throughout

channel uses, and known both at the transmitter and the receiver.

A simple diagram of the described channel model is shown in Fig. 2.1.

It is also convenient to define an equivalent real-valued channel model that can be obtained by vectorizing the complex-valued channel of Definition 2.1.1.

Definition 2.1.2 (Vectorized Fading Channel Model)

Given the complex-valued model of Definition 2.1.1, an equivalent real-valued $(2\mathsf{N}) \times (2\mathsf{N})$ channel model is

$$\mathbf{Y} = \mathsf{H}\mathbf{X} + \mathbf{Z}, \tag{2.2}$$

where the complex-valued output vector $\mathbf{Y}'$ is vectorized as $\mathbf{Y} = \Big(\mathrm{Re}\{Y'_1\}, \mathrm{Im}\{Y'_1\}, \ldots, \mathrm{Re}\{Y'_{\mathsf{N}}\}, \mathrm{Im}\{Y'_{\mathsf{N}}\}\Big)^T \in \mathbb{R}^{2\mathsf{N}}$, and similarly for $\mathbf{X}$ and $\mathbf{Z}$. The vectorized noise vector is such that $\mathbf{Z} \sim \mathcal{N}(\mathbf{0}_{2\mathsf{N}}, \sigma_z^2 \mathsf{I}_{2\mathsf{N}})$ and the equivalent real-valued channel matrix is defined as $\mathsf{H} = \mathrm{Re}\{\mathsf{H}'\} \otimes \mathsf{I}_2 + \mathrm{Im}\{\mathsf{H}'\} \otimes \left[\begin{smallmatrix} 0 & -1 \\ 1 & 0 \end{smallmatrix}\right]$, where $\otimes$ denotes the Kronecker product. Notice also that, given the complex input constraint $\mathcal{X}' \subset \mathbb{C}^{\mathsf{N}}$, we can derive the real-valued input constraint region $\mathcal{X} \subset \mathbb{R}^{2\mathsf{N}}$ by mapping each complex subspace $\mathbb{C}$ to $\mathbb{R}^2$. Given any complex number $c = a + ib \in \mathbb{C}$, where $i = \sqrt{-1}$ is the imaginary unit, the considered bijective map from $\mathbb{C}$ to $\mathbb{R}^2$ is such that $a + ib \mapsto (a, b)$ and similarly for higher order vector spaces.

The model of Definition 2.1.1 is general and accounts for fading through the channel matrix H'. It is also convenient to treat separately the *nonfading* scenario, where $\mathsf{H}' = \mathsf{I}_{\mathsf{N}}$.

Definition 2.1.3 (Nonfading Channel Model)

The $\mathsf{N} \times \mathsf{N}$ nonfading complex-valued channel model is given by

$$\mathbf{Y}' = \mathbf{X}' + \mathbf{Z}', \tag{2.3}$$

where $\mathbf{Y}' \in \mathbb{C}^{\mathsf{N}}$ is the output vector, $\mathbf{X} \in \mathcal{X}' \subset \mathbb{C}^{\mathsf{N}}$ is the amplitude-constrained input vector and $\mathbf{Z}' \sim \mathcal{CN}(\mathbf{0}_{\mathsf{N}}, 2\sigma_z^2 \mathsf{I}_{\mathsf{N}})$ is the complex Gaussian noise.

Similarly to the fading case, let us also define the vectorized nonfading channel model as follows.

Definition 2.1.4 (Vectorized Nonfading Channel Model)

Given the complex-valued model in Definition 2.1.3, an equivalent $(2\mathsf{N}) \times (2\mathsf{N})$ vectorized nonfading real-valued channel model is

$$\mathbf{Y} = \mathbf{X} + \mathbf{Z}, \tag{2.4}$$

where $\mathbf{Y} = \Big(\mathrm{Re}\{Y_1'\}, \mathrm{Im}\{Y_1'\}, \ldots, \mathrm{Re}\{Y_{\mathsf{N}}'\}, \mathrm{Im}\{Y_{\mathsf{N}}'\}\Big)^T \in \mathbb{R}^{2\mathsf{N}}$ is the output vector and similarly for $\mathbf{X}$ and $\mathbf{Z}$. The input vector is $\mathbf{X} \in \mathcal{X} \subset \mathbb{R}^{2\mathsf{N}}$, with $\mathcal{X}$ being the real-valued input constraint derived as in Definition 2.1.2. Finally, the noise vector $\mathbf{Z} \sim \mathcal{N}(\mathbf{0}_{2\mathsf{N}}, \sigma_z^2 \mathsf{I}_{2\mathsf{N}})$ is Gaussian-distributed.

Since the focus is on amplitude constraints, the Signal-to-Noise Ratio (SNR) definition used throughout this work is not the usual one and, instead, we prefer to resort to the following more convenient definition.

Definition 2.1.5 (SNR for amplitude-constrained channels)

Given the amplitude constraint $\mathcal{X}$, the SNR is defined as

$$\mathrm{SNR} \triangleq \frac{\left(r_{\max}(\mathcal{X})\right)^2}{2\mathrm{N}\sigma_z^2}, \tag{2.5}$$

where $r_{\max}(\mathcal{X})$ is the maximum radius of $\mathcal{X}$, i.e., $r_{\max}(\mathcal{X}) \triangleq \sup_{\mathbf{x}\in\mathcal{X}}\|\mathbf{x}\|$.

Furthermore, since all the considered random processes are stationary and ergodic by [53], a general definition for the channel capacity of amplitude-constrained channels is the following.

Definition 2.1.6 (Channel capacity)

The channel capacity is defined as

$$\mathrm{C}\left(\mathcal{X}, \mathsf{H}, \sigma_z^2\right) \triangleq \sup_{f_{\mathbf{X}}:\, \mathrm{supp}(f_{\mathbf{X}})\subseteq\mathcal{X}} \mathrm{I}(\mathbf{X};\mathbf{Y}) \tag{2.6}$$

$$= \sup_{f_{\mathbf{X}}:\, \mathrm{supp}(f_{\mathbf{X}})\subseteq\mathcal{X}} \mathrm{h}(\mathbf{Y}) - \mathrm{h}(\mathbf{Z}), \tag{2.7}$$

where $f_{\mathbf{X}}$ is the input distribution law and

$$\mathrm{supp}(f_{\mathbf{X}}) \triangleq \{\mathbf{x}\in\mathcal{X} :\ f_{\mathbf{X}}(\mathbf{x}) \neq 0\}, \tag{2.8}$$

is the support of $f_{\mathbf{X}}$.

Notice that the channel capacity $\mathrm{C}(\mathcal{X}, \mathsf{H}, \sigma_z^2)$ is a function of the input constrain region $\mathcal{X}$, the channel matrix H, and the noise variance σ_z^2. To ease the notation, we will often denote the channel capacity simply by C. Notice also that Definition 2.1.6 and Definition 2.1.5 hold for all of the presented channel models.

2.2 Input Amplitude Constraints

The concept of input amplitude constraint is trivial in the real-valued scalar case. The scalar input X is confined within a continuous interval $\mathcal{X} \subset \mathbb{R}$. The features of this interval are directly connected to the considered system. For instance, since free-space optical communications use intensity signals, the interval $\mathcal{X}$ can only be a subset of $\mathbb{R}_+$. Let us denote by R the amplitude constraint factor. Then, the interval $\mathcal{X}$ for the free-space optical communications could be defined as $\mathcal{X} = [0, \mathsf{R}]$. On the other hand, for microwave wireless communications this requirement is not necessary and the interval can span throughout $\mathbb{R}$. Therefore, a reasonable choice would be $\mathcal{X} = [-\mathsf{R}, \mathsf{R}]$. Whether microwave or free-space optical wireless communications are considered, the concept of amplitude constraint is clearly and unequivocally defined in the scalar case.

Let us now consider vector Gaussian channels and the associated input constraints. Let us focus on the vectorized models of Definition 2.1.2 and 2.1.4. The input vector is such that $\mathbf{X} \in \mathcal{X} \subset \mathbb{R}^{2\mathsf{N}}$. While, for the real-valued scalar case, a connected set $\mathcal{X}$ can only be an interval, for the vector case, $\mathcal{X}$ can be any constrain region in the considered vector space, i.e., any connected subset of $\mathbb{R}^{2\mathsf{N}}$. The focus of this work is on specific constraint regions $\mathcal{X}$ of practical interest.

2.3 Amplitude Constraints of Practical Interest

As mentioned in Chapter 1, to ensure that the communication system stays energy efficient, a valid design choice is to limit the peak power of the transmitted signals. This constraint is advantageous because it

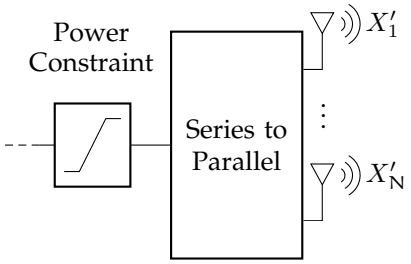

Figure 2.2: *Total Amplitude transmitter configuration.*

can bound the input signal out of the nonlinear response of the power amplifiers. Since the power constraints can be imposed on the signal fed to one or multiple antennas, there can be different transmitter configurations of practical interest. Notice that each configuration induces a different constraint region $\mathcal{X}$. Let us introduce the main constraints of practical interest, as well as the associated transmitter configurations.

2.3.1 Total Amplitude Constraint

A single power constraint, applied to the multi-dimensional signal feeding all the transmitting antennas, bounds the norm of the input vector $\mathbf{X}'$. Let us refer to this constraint as *total amplitude* constraint. The transmitted signal is constrained in its peak power (or peak amplitude) and therefore, given a constraint factor R, the norm of $\mathbf{X}'$ is such that $\|\mathbf{X}'\| \leq \mathsf{R}$. A diagram of such transmitter is shown in Fig. 2.2. The Total Amplitude (TA) transmitter configuration is relevant for any wireless system in which energy efficiency is a critical feature. Indeed, bounding the peak power of the input is clearly an effective way to reduce the overall power consumption of the system. Notice that, for the vectorized model in (2.2), the equivalent constraint on the real-valued

input vector is $\|\mathbf{X}\| \leq \mathsf{R}$. Therefore, the constraint region $\mathcal{X}$ can be interpreted as the $(2\mathsf{N})$-dimensional ball centered at the origin and of radius R. Let us define the n-dimensional closed ball of radius R as

$$\mathcal{B}_{\mathsf{R}}^{n} \triangleq \{\mathbf{x} \in \mathbb{R}^{n} : \|\mathbf{x}\| \leq \mathsf{R}\}. \tag{2.9}$$

Let us also define the n-dimensional unitary closed ball as $\mathcal{B}^{n} = \mathcal{B}_{1}^{n}$.

Definition 2.3.1 (Total Amplitude Constraint)

The TA constraint region is given by

$$\mathcal{X} = \mathcal{B}_{\mathsf{R}}^{2\mathsf{N}}, \tag{2.10}$$

where $\mathcal{B}_{\mathsf{R}}^{2\mathsf{N}}$ is the $(2\mathsf{N})$-dimensional ball of radius R centered at the origin.

Notice that, this definition of TA constraint is valid just in the case of microwave wireless communications. For free-space optical communications, the structure of $\mathcal{X}$ is different and it would be the portion of the ball lying in the positive orthant.

2.3.2 Per-Antenna Constraint

Another transmitter configuration of practical interest employs separate power constraints for each complex signal feeding each transmitting antenna [54–56]. Let us refer to the induced constraint as *per-antenna* constraint. In Fig. 2.3, it is shown a diagram of the corresponding transmitter configuration. The Per-Antenna (PA) constraint bounds the peak amplitude of each complex-valued input vector entry, i.e., $|X_i'| \leq \mathsf{R}_i$, with $i = 1, \ldots, \mathsf{N}$ and where R_i is the constraint

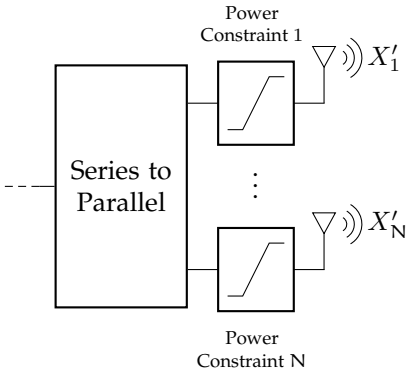

Figure 2.3: *Per-Antenna transmitter configuration.*

factor associated with each power constraint. For each entry of $\mathbf{X}'$, it holds $(\mathrm{Re}\{X'_i\}, \mathrm{Im}\{X'_i\}) \in \mathcal{B}^2_{\mathsf{R}_i} \subset \mathbb{R}^2$. Then, the PA constraint is defined as follows.

Definition 2.3.2 (Per-Antenna Constraint)

The PA constraint region for the vectorized channel of Definition 2.1.2 is the N-fold Cartesian product of 2-dimensional balls, i.e.,

$$\mathcal{X} = \mathcal{X}_1 \times \cdots \times \mathcal{X}_{\mathsf{N}}, \tag{2.11}$$

where $\mathcal{X}_i = \mathcal{B}^2_{\mathsf{R}_i}$, $\forall i$.

Remark 1. In the case of fading channels, it is always possible to consider an equivalent system with mutually identical R_i's by suitably scaling the columns of the channel matrix H', which is assumed to be known. Therefore, while we will consider arbitrary R_i's for the non-fading case, for fading channels, we will assume $\mathsf{R}_i = \mathsf{R}$, $\forall i$ without loss of generality.

Again, Definition 2.3.2 is accurate in the case of microwave wireless

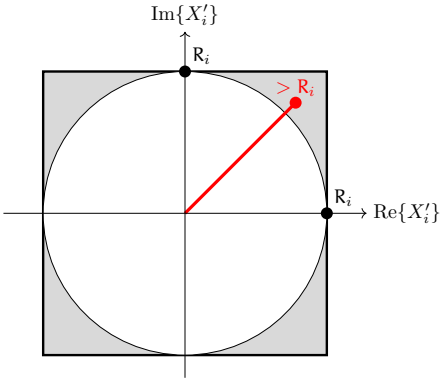

Figure 2.4: *Constraint region induced by bounding the complex input (circle) or by bounding the real and imaginary part of the input, independently (square).*

communications, where antennas can transmit/receive complex-valued signals, but not for free-space optical communications. In the latter case, each antenna transmits and receives real-valued signals, therefore the resulting constraint region would be a hyperrectangle. Fig. 2.4 intuitively shows that constraining separately the real and imaginary parts of X_i' induces a weaker constraint than $\|X_i'\| \leq \mathsf{R}_i$. In turn, this would result in an overestimation of the achievable capacity.

2.3.3 Antenna Subsets Constraint

The last examined transmitter configuration considers a hybrid solution between the previous configurations. The corresponding diagram is shown in Fig. 2.5. This transmitter configuration employs a number of power constraints, denoted by T, such that $\mathsf{T} \leq \mathsf{N}$. In general, each power constraint is applied to the signal transmitted by an arbitrary subset of the transmitting antennas. We refer to the constraint induced by this transmitter configuration as *antenna subsets* constraint. Notice

that the PA constraint can be seen as a special case of the Antenna Subsets (AS) constraint. Indeed, when $\mathsf{T} = \mathsf{N}$ each power constraint limits the peak power of the signal fed to a single transmitting antenna and we obtain again the PA constraint. In general, the AS constraint region bounds the peak amplitude of subvectors of $\mathbf{X}'$. For this reason, it is useful to subdivide $\mathbf{X}'$ in T subvectors, with each subvector associated with a single power constraint. Notice that one can always reorder the entries of the input vector. Therefore, to simplify the notation, we assume $\mathbf{X}$ to be always defined in such a way that only consecutive entries are associated with the same power constraint. As shown in Fig. 2.5, we denote by $\mathbf{X}'_i$ the ith subvector of $\mathbf{X}'$, bounded by the ith power constraint. We denote by N_i the number of entries in $\mathbf{X}'_i \in \mathbb{C}^{\mathsf{N}_i}$ and we have that $\sum_{i=1}^{\mathsf{T}} \mathsf{N}_i = \mathsf{N}$. Then, the AS constraint is such that $\|\mathbf{X}'_i\| \leq \mathsf{R}_i$, with $i = 1, \ldots, \mathsf{T}$ and where the R_i's are the constraint factors associated with the T power constraints. Let us refer once more to the vectorized model of Definition 2.1.2 and let us denote by $\mathbf{X}_i$ the vectorized version of $\mathbf{X}'_i$. Notice also that $\mathbf{X}_i$ is a $(2\mathsf{N}_i) \times 1$ vector. Like for the TA constraint, each subvector is constrained to a hyperball, i.e., $\mathbf{X}_i \in \mathcal{B}_{\mathsf{R}_i}^{2\mathsf{N}_i}$, for $i = 1, \ldots, \mathsf{T}$.

Definition 2.3.3 (Antenna Subsets Constraint)

The AS constraint is given by the following Cartesian product

$$\mathcal{X} = \mathcal{X}_1 \times \cdots \times \mathcal{X}_{\mathsf{T}}, \tag{2.12}$$

where $\mathcal{X}_i = \mathcal{B}_{\mathsf{R}_i}^{2\mathsf{N}_i}, \ \forall i$.

Similarly to Remark 1 for the PA constraint, we can assume $\mathsf{R}_i = \mathsf{R}$,

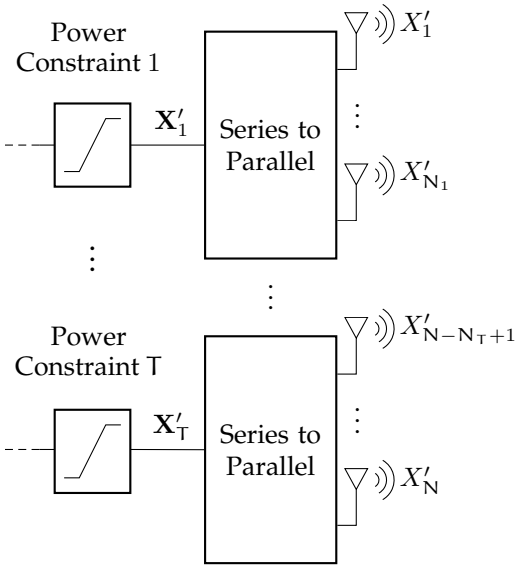

Figure 2.5: *Antenna Subsets transmitter configuration.*

$\forall i$ for the fading case, while keeping the R_i's arbitrary for nonfading channels.

Once more, the case of free-space optical wireless communications is slightly different. Similarly to the TA constraint, each subvector $\mathbf{X}_i$ would be constrained to the portion of an $(2\mathsf{N}_i)$-dimensional ball lying in the positive orthant.

PART I

Nonfading Channels

The channel model of Definition 2.1.1 accounts for both the cases of nonfading, i.e., $\mathsf{H} = \mathsf{I}_{2N}$, and fading channels, therefore, in principle treating them separately would not be necessary. Nonetheless, in this work the distinction is motivated by a crucial difference between the two cases. For nonfading channels subject to the amplitude constraints defined in Section 2.2, the structure of the capacity-achieving input PDF is either known, or it can be derived. On the other hand, this is not the case for fading channels. This crucial difference justifies the distinction between the two cases, as the methodologies adopted to investigate the capacity of these channel models will be substantially different. In the case of nonfading channels, knowing the structure of the capacity-achieving distribution will allow us to evaluate estimates of the channel capacity and of the associated optimal input distribution.

Chapter 3

The Capacity-Achieving Input Distribution

In this chapter, the main features of the capacity-achieving input distribution of nonfading amplitude-constrained channels are presented. As mentioned in Chapter 1, the first crucial results were developed for the capacity-achieving distribution of amplitude-constrained scalar channels. The author of [26] showed that the optimal input distribution is discrete, comprising of a finite number of mass points. Further results on the structure of the capacity-achieving input distribution, for the TA constraint, are derived in [27] and [28], for the quadrature and vector Gaussian channels respectively.

Let us consider the nonfading channel models defined in Section 2.1. The complex-valued channel model in Definition 2.1.3 is used for most analytical derivations. On the other hand, the vectorized channel model of Definition 2.1.4 and the TA constraint of Definition 2.3.1, will allow us to give a clear geometrical interpretation of

the input distribution. It is also useful to define the $(2\mathsf{N})$-dimensional hypersphere as

$$\mathcal{S}_{\rho}^{2\mathsf{N}} \triangleq \left\{\mathbf{x} \in \mathbb{R}^{2\mathsf{N}} : \ \|\mathbf{x}\| = \rho\right\}. \tag{3.1}$$

In [28], the authors describe the distribution of the capacity-achieving input norm to be composed of a discrete and finite number of amplitude mass points with uniformly distributed phase. Therefore, the support of the optimal input distribution is composed of concentric hyperspheres. Let us denote the capacity-achieving input distribution by $f_{\mathbf{X}^\star}$. Then, its support is such that

$$\mathrm{supp}(f_{\mathbf{X}^\star}) = \bigcup_{i=1}^{\mathsf{T}^\star} \mathcal{S}_{\rho_i^\star}^{2\mathsf{N}}, \tag{3.2}$$

where $\mathsf{T}^\star$ is the optimal number of hyperspheres and the $\rho_i^\star$'s are their radii. Since the capacity-achieving distribution $f_{\mathbf{X}^\star}$ is isotropically symmetric [28], it is always possible to fully characterize $f_{\mathbf{X}^\star}$ by the distribution of the input norm, i.e., $P_{\|\mathbf{X}^\star\|}$. In [47], we showed that, as a consequence, the maximization problem in (2.6) can be carried over mono-dimensional distributions of the input norm $P_{\|\mathbf{X}\|}$, instead of the $(2\mathsf{N})$-dimensional $f_{\mathbf{X}}$. Indeed, one can simply map $P_{\|\mathbf{X}^\star\|}$ to $f_{\mathbf{X}^\star}$ as follows

$$f_{\mathbf{X}^\star}(\mathbf{x}) = \begin{cases} \frac{P_{\|\mathbf{X}^\star\|}\left(\rho_i^\star\right)}{\mathrm{Vol}\left(\mathcal{S}_{\rho_i^\star}^{2\mathsf{N}}\right)} & \mathbf{x} : \ \|\mathbf{x}\| = \rho_i^\star \\ 0 & \text{elsewhere}, \end{cases} \tag{3.3}$$

where $\mathrm{Vol}\left(\mathcal{S}_{\rho_i^\star}^{2\mathsf{N}}\right) = 2\pi^{\mathsf{N}}(\rho_i^\star)^{2\mathsf{N}-1}/\Gamma(\mathsf{N})$ is the surface area of the ith

hypersphere. In the following, it is convenient to consider the equivalent complex-valued model of Definition 2.1.3. By a slight abuse of notation, complex-valued vectors and the equivalent vectorized real-valued vectors will be denoted by the same variables $\mathbf{Y}$, $\mathbf{X}$, and $\mathbf{Z}$ and which one is used will be made clear by the context. Notice also that (3.3) is the same for both the complex-valued and real-valued channels.

3.1 Equivalent Channel Capacity Definition

The possibility to equivalently express the capacity-achieving input distribution as a mono-dimensional Probability Mass Function (PMF), instead of a N-dimensional complex-valued PDF, can be exploited to drastically simplify the complexity of the maximization in the channel capacity definition. Let us consider the equivalent complex-valued TA constraint $\mathcal{X} = \left\{\mathbf{x} \in \mathbb{C}^{\mathsf{N}} : \|\mathbf{x}\| \leq \mathsf{R}\right\}$, the complex-valued nonfading channel model of Definition 2.1.3, and let us assume $\sigma_z^2 = 1$. Then, the channel capacity $\mathsf{C}(\mathcal{X}, \mathsf{I}_{\mathsf{N}}, 2)$ from Definition 2.1.6 can be redefined as a maximization over scalar random variables, i.e., on the input norm $\|\mathbf{X}\|$. Notice that

$$\mathsf{h}(\mathbf{Y}) \overset{(a)}{=} \mathsf{h}(\|\mathbf{Y}\|) + (2\mathsf{N}-1)\mathsf{E}[\log\|\mathbf{Y}\|] + \mathsf{h}_{\lambda}(\angle\mathbf{Y}) \tag{3.4}$$

$$\overset{(b)}{=} \mathsf{h}\big(\|\mathbf{Y}\|^2\big) + (\mathsf{N}-1)\mathsf{E}\big[\log\|\mathbf{Y}\|^2\big] + \log\frac{\pi^{\mathsf{N}}}{\Gamma(\mathsf{N})}, \tag{3.5}$$

where $\angle\mathbf{Y} \triangleq \mathbf{Y}/\|\mathbf{Y}\|$ is the *direction* of the vector $\mathbf{Y}$ and $\mathsf{h}_{\lambda}(\cdot)$ is a differential entropy-like quantity for complex-valued random vectors lying on the unit N-dimensional hypersphere [57, Lemma 6.16]. Furthermore, step (a) holds thanks to the independence between $\|\mathbf{Y}\|$ and

$\angle\mathbf{Y}$ and to [57, Lemma 6.17], while step (b) holds thanks to $\angle\mathbf{Y}$ being uniformly distributed and to [57, Lemma 6.15]. By plugging the entropy defined in (3.5) into the channel capacity definition, we obtain the following equivalent capacity expression

$$\mathsf{C}(\mathsf{R}) = \sup_{P_{\|\mathbf{X}\|}:\, \|\mathbf{X}\| \leq \mathsf{R}} \mathrm{h}\big(\|\mathbf{Y}\|^2\big) + (\mathsf{N}-1)\mathsf{E}\big[\log\|\mathbf{Y}\|^2\big] + \log\frac{\pi^{\mathsf{N}}}{\Gamma(\mathsf{N})} - \mathrm{h}(\mathbf{Z}) \tag{3.6}$$

$$= \sup_{P_{\|\mathbf{X}\|}:\, \|\mathbf{X}\| \leq \mathsf{R}} \mathrm{h}\big(\|\mathbf{Y}\|^2\big) + (\mathsf{N}-1)\mathsf{E}\big[\log\|\mathbf{Y}\|^2\big] - \log((2e)^{\mathsf{N}}\Gamma(\mathsf{N})). \tag{3.7}$$

Notice that we made explicit the dependence of the capacity on the constraint factor R, as this definition will be convenient in the next section.

The squared norm of the output vector $\mathbf{Y}$ is such that

$$\|\mathbf{Y}\|^2 = \sum_{i=1}^{\mathsf{N}} |X_i + Z_i|^2 \overset{d}{=} \Big|\|\mathbf{X}\| + Z_1\Big|^2 + \sum_{i=2}^{\mathsf{N}} |Z_i|^2, \tag{3.8}$$

where $\overset{d}{=}$ means equality in distribution. To show that the left and right-hand side of (3.8) are identically distributed, let us denote by $\chi^2_n(\xi)$ the noncentral chi-squared distribution with n degrees of freedom and noncentrality parameter ξ. Since each component of the output vector is $(Y_i \mid X_i = x_i) \sim \mathcal{CN}(x_i, 2)$, we have that $(\|\mathbf{Y}\|^2 \mid \mathbf{X} = \mathbf{x}) \sim \chi^2_{2\mathsf{N}}(\xi)$ with $\xi = \sum_{i=1}^{\mathsf{N}} |x_i|^2 = \|\mathbf{x}\|^2$. Notice that, for a given $\mathbf{X}$, the right-hand side of (3.8) is still a sum of N squared absolute values of independent complex Gaussian variables, characterized by the same variance. The only difference is that the expected values of the com-

plex Gaussian variables on the right-hand side are all zeros, except the first one, which is set to $\|\mathbf{x}\|$. Therefore, since the associated noncentrality parameter is, again, $\xi = \|\mathbf{x}\|^2$, the resulting distribution is the same of the left-hand side, i.e., the noncentral chi-squared $\chi^2_{2\mathsf{N}}(\|\mathbf{x}\|^2)$. Let us denote by $\mathbf{X}^\star$ the random vector with capacity-achieving distribution $f_{\mathbf{X}^\star}$. Given an arbitrary input PMF $P_{\|\mathbf{X}\|}$, the resulting PDF of $\|\mathbf{Y}\|^2$ is computed as follows

$$f_{\|\mathbf{Y}\|^2}(y) = \sum_{i=1}^{\mathsf{T}} p_i f_{\chi^2_{2\mathsf{N}}(\rho_i^2)}(y), \qquad y > 0, \tag{3.9}$$

where the ρ_i's are the mass point positions of $P_{\|\mathbf{X}\|}$ and the associated probabilities are $p_i = P_{\|\mathbf{X}\|}(\rho_i)$. Furthermore, $\mathsf{T} = \big|\mathrm{supp}\big(P_{\|\mathbf{X}\|}\big)\big|$ and $f_{\chi^2_n(\xi)}$ is the PDF of a $\chi^2_n(\xi)$ random variable. Given (3.9) and (3.7), let us define the information density resulting for any given $P_{\|\mathbf{X}\|}$ as

$$\begin{aligned} i(\rho; P_{\|\mathbf{X}\|}) \triangleq \int_0^\infty f_{\chi^2_{2\mathsf{N}}(\rho^2)}(y) \log \frac{y^{\mathsf{N}-1}}{\sum_{i=1}^{\mathsf{T}} p_i f_{\chi^2_{2\mathsf{N}}(\rho_i^2)}(y)} dy \\ - \log\big((2e)^{\mathsf{N}}\Gamma(\mathsf{N})\big). \end{aligned} \tag{3.10}$$

Notice that, therefore, the mutual information can be defined as follows

$$\mathrm{I}\big(\{\rho_i\}\,; P_{\|\mathbf{X}\|}\big) \triangleq \sum_{i=1}^{\mathsf{T}} p_i \cdot i(\rho_i; P_{\|\mathbf{X}\|}), \tag{3.11}$$

where $\{\rho_i\}$ is the set composed of the ρ_i's. Finally, given (3.10), by [39] it holds the following result.

Theorem 3.1.1 (KKT Conditions)

The input distribution $P_{\|\mathbf{X}^\star\|}$ is capacity-achieving if and only if

$$i(\rho; P_{\|\mathbf{X}^\star\|}) = \mathsf{C}, \qquad \rho \in \operatorname{supp}\big(P_{\|\mathbf{X}^\star\|}\big), \tag{3.12a}$$

$$i(\rho; P_{\|\mathbf{X}^\star\|}) \leq \mathsf{C}, \qquad \rho \in [0, \mathsf{R}]. \tag{3.12b}$$

3.2 Insights on the Input Distribution

In this section, further insights on the features of the capacity-achieving input distribution are presented and are derived by considering the equivalent channel capacity definition, defined in the previous section.

Theorem 3.2.1

A lower bound on the number of hyperspheres $\mathsf{T}^\star$ in $f_{\mathbf{X}^\star}$ is given by

$$\mathsf{T}^\star \geq \underline{\mathsf{T}} \triangleq \left\lceil \sqrt{\frac{\left(\mathsf{R}^2 + 2e\right)^2 + 8\pi(\mathsf{N}-1)}{8\pi e(\mathsf{N} + \mathsf{R}^2/2)}} \right\rceil. \tag{3.13}$$

Proof. Let us notice that

$$\log \mathsf{T}^\star = \log\Big|\operatorname{supp}\big(P_{\|\mathbf{X}^\star\|}\big)\Big| \tag{3.14}$$

$$= \log\Big|\operatorname{supp}\Big(P_{\|\mathbf{X}^\star\|^2}\Big)\Big| \tag{3.15}$$

$$\overset{(a)}{\geq} \mathsf{H}\big(\|\mathbf{X}^\star\|^2\big) \tag{3.16}$$

$$\overset{(b)}{\geq} \mathrm{I}\big(\|\mathbf{X}^\star\|^2; \|\mathbf{Y}^\star\|^2\big) \tag{3.17}$$

$$\overset{(c)}{\geq} \mathrm{I}\big(\|\mathbf{X}\|^2; \|\mathbf{Y}\|^2\big) \tag{3.18}$$

$$= \mathrm{h}\big(\|\mathbf{Y}\|^2\big) - \mathrm{h}\big(\|\mathbf{Y}\|^2 \mid \|\mathbf{X}\|^2\big), \tag{3.19}$$

where step (a) and (b) hold thanks to the discreteness of $\|\mathbf{X}^\star\|$ and step (c) comes from the suboptimal choice $\|\mathbf{X}\|^2 \sim \mathcal{U}[0, \mathsf{R}^2]$. Moreover, we can lower-bound $\mathrm{h}\big(\|\mathbf{Y}\|^2\big)$ as follows

$$\mathrm{h}\big(\|\mathbf{Y}\|^2\big) = \mathrm{h}\left(\left|\|\mathbf{X}\| + Z_1\right|^2 + \sum_{i=2}^{\mathsf{N}} |Z_i|^2\right) \tag{3.20}$$

$$\overset{(a)}{\geq} \frac{1}{2}\log\left(\exp\left(2\mathrm{h}\left(\left|\|\mathbf{X}\| + Z_1\right|^2\right)\right) + \exp\left(2\mathrm{h}\left(\sum_{i=2}^{\mathsf{N}} |Z_i|^2\right)\right)\right) \tag{3.21}$$

$$\overset{(b)}{\geq} \frac{1}{2}\log\big(\exp\big(2\log\big(\mathsf{R}^2 + 2e\big)\big) + \exp(\log(8\pi(\mathsf{N}-1)))\big) \tag{3.22}$$

$$= \frac{1}{2}\log\Big(\big(\mathsf{R}^2 + 2e\big)^2 + 8\pi(\mathsf{N}-1)\Big), \tag{3.23}$$

where step (a) comes from the Entropy Power Inequality (EPI), step (b) holds thanks to the following bound

$$\mathrm{h}\left(\left|\|\mathbf{X}\| + Z_1\right|^2\right) = \mathrm{h}\big(\|\mathbf{X}\|e^{j\Phi} + Z_1\big) - \log(\pi) \tag{3.24}$$

$$\overset{(a)}{\geq} \log\big(\exp\big(\mathrm{h}\big(\|\mathbf{X}\|e^{j\Phi}\big)\big) + \exp(\mathrm{h}(Z_1))\big) - \log(\pi) \tag{3.25}$$

$$= \log\big(\pi\exp\big(\mathrm{h}\big(\|\mathbf{X}\|^2\big)\big) + 2\pi e\big) - \log(\pi) \tag{3.26}$$

$$= \log\big(\exp\big(\mathrm{h}\big(\|\mathbf{X}\|^2\big)\big) + 2e\big) \tag{3.27}$$

$$= \log\big(\mathsf{R}^2 + 2e\big), \tag{3.28}$$

where the phase $\Phi \sim \mathcal{U}[0, 2\pi)$ is independent of any other variable and in step (a) we used a lower bound on the entropy of a $\chi^2_{2\mathsf{N}-2}$ variate defined in [58, Appendix C]. Notice also that the last step holds thanks

to $\mathsf{h}\big(\|\mathbf{X}\|^2\big) = \log(\mathsf{R}^2)$. As for the conditional entropy in (3.19), it holds

$$\mathsf{h}\big(\|\mathbf{Y}\|^2 \mid \|\mathbf{X}\|^2\big) \overset{(a)}{\leq} \frac{1}{2}\mathsf{E}\big[\log(8\pi e(\mathsf{N} + \|\mathbf{X}\|^2))\big] \tag{3.29}$$

$$\overset{(b)}{\leq} \frac{1}{2}\log\big(8\pi e\big(\mathsf{N} + \mathsf{E}\big[\|\mathbf{X}\|^2\big]\big)\big) \tag{3.30}$$

$$\overset{(c)}{=} \frac{1}{2}\log(8\pi e(\mathsf{N} + \mathsf{R}^2/2)), \tag{3.31}$$

where (a) holds thanks to the Gaussian maximum entropy principle, (b) thanks to Jensen's inequality, and finally (c) derives from $\mathsf{E}\big[\|\mathbf{X}\|^2\big] = \mathsf{R}^2/2$. Plugging (3.23) and (3.31) into (3.19), proves the claim. □

Some more interesting insights on the optimal input distribution can be derived by investigating the properties of the information density. Let us first consider the following result.

Lemma 1. *The derivative of the information density with respect to ρ is given by*

$$i'(\rho; P_{\|\mathbf{X}\|}) = -2\rho\,\mathsf{E}\left[\mathsf{E}\left[\frac{1}{2}\frac{\|\mathbf{X}\|}{\|\mathbf{Y}\|}\frac{I_{\mathsf{N}-2}(\|\mathbf{X}\|\|\mathbf{Y}\|)}{I_{\mathsf{N}-1}(\|\mathbf{X}\|\|\mathbf{Y}\|)} - \left(\frac{1}{2} + \frac{\mathsf{N}-1}{\|\mathbf{Y}\|^2}\right)\middle| \|\mathbf{Y}\|^2 = Q'\right]\right] \tag{3.32}$$

where $Q' \sim \chi^2_{2(\mathsf{N}+1)}(\rho^2)$ and $I_n(z)$ is the modified Bessel function of the first kind of order n and argument z.

Proof. See the proof in Section 3.8.1. □

Then, given Lemma 1, it holds the following.

Theorem 3.2.2

Given the constraint $\|\mathbf{X}\| \leq \mathsf{R}$, let us consider a PMF $P_{\|\mathbf{X}\|}$ such that its largest mass point with nonzero probability is denoted by c, i.e., for $\rho > c$ it holds that $P_{\|\mathbf{X}\|}(\|\mathbf{X}\| > c) = 0$. Let $c < \mathsf{R}$. Then, the derivative $i'(\rho; P_{\|\mathbf{X}\|})$ is lower-bounded by

$$i'(\rho; P_{\|\mathbf{X}\|}) \geq \frac{\rho}{1 + \frac{c^2(2\mathsf{N}+\rho^2)}{4(\mathsf{N}-1/2)^2}} > 0, \qquad \rho > c \tag{3.33}$$

and, therefore, the information density $i(\rho; P_{\|\mathbf{X}\|})$ is strictly increasing for any $\rho > c$.

Proof. Let us define the function

$$s_{\mathsf{N}-1}(t) = \frac{1}{t}\frac{I_{\mathsf{N}-1}(t)}{I_{\mathsf{N}-2}(t)}, \qquad t > 0. \tag{3.34}$$

The function $s_{\mathsf{N}-1}$ is decreasing in t for any $\mathsf{N} > 3/2$ [59, Lemma 2], therefore its derivative is negative. We show that this is also true for $\mathsf{N} = 1$. Notice that $I_{-1}(t) = I_1(t)$. Then, the derivative of $s_0(t)$ can be written as

$$s_0'(t) = \frac{1}{t}\left(1 - \frac{I_0^2(t)}{I_1^2(t)}\right) = \frac{1}{t}\left(1 + \frac{I_0(t)}{I_1(t)}\right)\left(1 - \frac{I_0(t)}{I_1(t)}\right). \tag{3.35}$$

The fact that $I_1(t) < I_0(t)$, for $t \geq 0$, together with (3.35), proves that $s_0'(t) < 0$ for all $t > 0$.

By (3.34), (3.35), and $P_{\|\mathbf{X}\|}(\|\mathbf{X}\| > c) = 0$, the derivative of the information density is lower-bounded by

$$i'(\rho; P_{\|\mathbf{X}\|}) \geq -2\rho\, \mathsf{E}\left[\frac{1}{2}\frac{c}{\|\mathbf{Y}\|}\frac{I_{\mathsf{N}-2}(c\|\mathbf{Y}\|)}{I_{\mathsf{N}-1}(c\|\mathbf{Y}\|)} - \frac{1}{2} - \frac{\mathsf{N}-1}{\|\mathbf{Y}\|^2}\right], \tag{3.36}$$

where $\|\mathbf{Y}\|^2 \sim \chi^2_{2(\mathsf{N}+1)}(\rho^2)$. Let us introduce the following equality, defined in [60, Eq. 9.6.26]

$$I_{\nu-1}(z) - I_{\nu+1}(z) = \frac{2\nu}{z} I_\nu(z). \tag{3.37}$$

By (3.37) and (3.36), with $\nu = \mathsf{N}-1$ and $z = c\|\mathbf{Y}\|$, we get

$$\begin{aligned}
&i'(\rho; P_{\|\mathbf{X}\|}) \\
&\geq -2\rho\, \mathsf{E}\left[\frac{\mathsf{N}-1}{\|\mathbf{Y}\|^2} \frac{I_{\mathsf{N}}(c\|\mathbf{Y}\|)}{I_{\mathsf{N}-2}(c\|\mathbf{Y}\|) - I_{\mathsf{N}}(c\|\mathbf{Y}\|)} - \frac{1}{2}\right] && (3.38)\\
&\overset{(a)}{=} -2\rho\, \mathsf{E}\left[\frac{c}{2\|\mathbf{Y}\|} \frac{I_{\mathsf{N}}(c\|\mathbf{Y}\|)}{I_{\mathsf{N}-1}(c\|\mathbf{Y}\|)} - \frac{1}{2}\right] && (3.39)\\
&= -\rho\left(\int_0^\infty \frac{c}{2\sqrt{t}} e^{-\frac{t+\rho^2}{2}} \frac{t^{\frac{\mathsf{N}}{2}}}{\rho^{\mathsf{N}}} I_N(\rho\sqrt{t}) \frac{I_{\mathsf{N}}(c\sqrt{t})}{I_{\mathsf{N}-1}(c\sqrt{t})} dt - 1\right) && (3.40)\\
&= -\rho\, \mathsf{E}\left[\frac{c}{\rho} \frac{I_{\mathsf{N}}(c\sqrt{J})}{I_{\mathsf{N}-1}(c\sqrt{J})} \frac{I_{\mathsf{N}}(\rho\sqrt{J})}{I_{\mathsf{N}-1}(\rho\sqrt{J})} - 1\right], && (3.41)
\end{aligned}$$

where in step (a) we used once more (3.37) and in the last equality we rearranged the integral by using $J \sim \chi^2_{2\mathsf{N}}(\rho^2)$. Let us also introduce the following inequality, defined in [61, Eq. (16)]

$$\frac{I_{\nu+1}(z)}{I_\nu(z)} \leq R_{\nu+1}(z) \triangleq \frac{z}{\nu + 1/2 + \sqrt{(\nu+1/2)^2 + z^2}}, \tag{3.42}$$

where $\nu \geq 0$, $z \geq 0$. By (3.42) and (3.41), we can further lower-bound the derivative of the information density as follows

$$\begin{aligned}
i'(\rho; P_{\|\mathbf{X}\|}) &\geq -\rho\, \mathsf{E}\left[cR_N\left(c\sqrt{J}\right)\frac{1}{\rho} R_N\left(\rho\sqrt{J}\right) - 1\right] && (3.43)\\
&\overset{(a)}{\geq} -\rho\, \mathsf{E}\left[R_N\left(c\sqrt{J}\right) R_N\left(c\sqrt{J}\right) - 1\right] && (3.44)
\end{aligned}$$

$$\overset{(b)}{\geq} -\rho\,\mathsf{E}\left[\frac{c^2 J}{4(\mathsf{N}-\frac{1}{2})^2 + c^2 J} - 1\right] \tag{3.45}$$

$$= \mathsf{E}\left[\frac{\rho}{1+\frac{c^2 J}{4(\mathsf{N}-\frac{1}{2})^2}}\right] \tag{3.46}$$

$$\overset{(c)}{\geq} \frac{\rho}{1+\frac{c^2\mathsf{E}[J]}{4(\mathsf{N}-\frac{1}{2})^2}} \tag{3.47}$$

$$= \frac{\rho}{1+\frac{c^2(2\mathsf{N}+\rho^2)}{4(\mathsf{N}-\frac{1}{2})^2}}, \tag{3.48}$$

where step (a) holds thanks to $\rho > c$, step (b) thanks to $J \geq 0$ in the denominator, in step (c) we used Jensen's inequality, and in the last equality $\mathsf{E}[J] = 2\mathsf{N} + \rho^2$. □

Finally, as a consequence of Theorem 3.2.2, of the Karush–Kuhn–Tucker (KKT) conditions [29, Lemma 7], and of the discreteness of the optimal input PMF, it holds the following result.

Corollary 1. *The support of the capacity-achieving input distribution* $\mathrm{supp}(f_{\mathbf{X}^\star})$ *always includes the hypersphere of radius* $\rho = \mathsf{R}$, *i.e.,* $P_{\|\mathbf{X}^\star\|}(\mathsf{R}) > 0$.

3.3 Estimation of the Input Distribution

Since the maximization in (3.7) is carried over the mono-dimensional distribution $P_{\|\mathbf{X}\|}$, it becomes computationally feasible to estimate the capacity-achieving input distribution. In Algorithm 1, we define a numerical procedure that estimates both $P_{\|\mathbf{X}^\star\|}$ and $\mathsf{C}(\mathsf{R})$. The algorithm takes in input the constraint factor R, an initial tentative input PMF $P_{\|\mathbf{X}_0\|}$, a parameter L defining the number of iterations for the main

Algorithm 1 Capacity and Input Distribution Estimation

1: **procedure** MAIN$\big(\mathsf{R}, P_{\|\mathbf{X}_0\|}, \mathsf{L}, \varepsilon\big)$
2: $(\boldsymbol{\rho}, \mathbf{p}) \leftarrow P_{\|\mathbf{X}_0\|}$
3: **repeat**
4: $k \leftarrow 0$
5: **while** $k < \mathsf{L}$ **do**
6: $k \leftarrow k + 1$
7: $\boldsymbol{\rho} \leftarrow$ GRADIENT-ASCENT$(\boldsymbol{\rho}, \mathbf{p})$
8: $\mathbf{p} \leftarrow$ BLAHUT-ARIMOTO$(\boldsymbol{\rho}, \mathbf{p})$
9: **end while**
10: $v \leftarrow$ KKT-VALIDATION$(\boldsymbol{\rho}, \mathbf{p}, \varepsilon)$
11: **if** $v = 0$ **then**
12: $(\boldsymbol{\rho}, \mathbf{p}) \leftarrow$ ADD-POINT$(\boldsymbol{\rho}, \mathbf{p})$
13: **end if**
14: **until** $v = 1$
15: $\hat{P}_{\|\mathbf{X}^\star\|} \leftarrow (\boldsymbol{\rho}, \mathbf{p})$
16: $\hat{\mathsf{C}}(\mathsf{R}) \leftarrow \mathrm{I}\Big(\boldsymbol{\rho}\,; \hat{P}_{\|\mathbf{X}^\star\|}\Big)$
17: **return** $\hat{P}_{\|\mathbf{X}^\star\|}, \hat{\mathsf{C}}(\mathsf{R})$
18: **end procedure**

loop of the Algorithm, and a tolerance factor ε that determines the precision of the capacity estimate.

First, let us provide a quick overview of each step in Algorithm 1. For any generic $P_{\|\mathbf{X}\|}$ and $\mathsf{T} = \big|\mathrm{supp}\big(P_{\|\mathbf{X}\|}\big)\big|$, let us define $\boldsymbol{\rho} = (\rho_1, \ldots, \rho_{\mathsf{T}})$, as a vector composed of the mass point positions of $P_{\|\mathbf{X}\|}$. Let us also define the vector $\mathbf{p} = (p_1, \ldots, p_{\mathsf{T}})$ comprising of the probabilities associated with $\boldsymbol{\rho}$, i.e., $p_i = P_{\|\mathbf{X}\|}(\rho_i),\ \forall i$. At line 2, the initial tentative PMF $P_{\|\mathbf{X}_0\|}$ is used to initialize the vectors $\boldsymbol{\rho}$ and $\mathbf{p}$. From line 3 to 14, the algorithm runs two nested loops. The innermost loop, from line 5 to 9, comprises of two functions that iteratively update the vectors $\boldsymbol{\rho}$ and $\mathbf{p}$ to optimize the PMF estimate. Broadly speaking, the function at line 7 uses a gradient ascent optimization to update the mass points positions based on the $\boldsymbol{\rho}$ and $\mathbf{p}$ in input. On the

other hand, the function at line 8 runs a variant of the Blahut-Arimoto algorithm [62, 63] to optimize the probabilities of the PMF. These two steps are iteratively repeated L times, with L chosen empirically in such a way that $\boldsymbol{\rho}$ and $\mathbf{p}$ can jointly reach convergence. At line 10, given ε, $\boldsymbol{\rho}$, and $\mathbf{p}$, the KKT-Validation function checks whether the KKT conditions defined in Theorem 3.1.1 are satisfied within the tolerance ε. It returns the binary variable v, which is set to 1 if the KKT conditions are satisfied and to 0 if not. If $v = 0$, the Add-Point function adds a new mass point to the PMF, resets the vectors $\boldsymbol{\rho}$ and $\mathbf{p}$, and restarts the procedure from line 4. If $v = 1$, the capacity estimate is sufficiently precise and the Algorithm stops after returning an estimate of the capacity-achieving PMF, namely $\hat{P}_{\|\mathbf{X}^\star\|}$, and an estimate of the capacity, $\hat{\mathsf{C}}(\mathsf{R})$. The PMF $\hat{P}_{\|\mathbf{X}^\star\|}$ is defined at line 15 and is given by the last values of $\boldsymbol{\rho}$ and $\mathbf{p}$. The capacity estimate is stored at line 16 as $\mathrm{I}\Big(\boldsymbol{\rho}\,; \hat{P}_{\|\mathbf{X}^\star\|}\Big)$[1], defined in (3.11).

Remark 2. Algorithm 1 optimizes separately $\boldsymbol{\rho}$ and $\mathbf{p}$. To guarantee that the independent optimizations provide joint convergence, we need to prove that the information density $i(\rho_i; P_{\|\mathbf{X}\|})$ in (3.10) is concave, differentiable, and that its gradient is Lipschitz continuous. By [64, Theorem 7] and [64, Corollary 4], we have that the mentioned properties are always satisfied in the case of amplitude-constrained Gaussian channels.

Remark 3. Peak amplitude constraints are the focus of this work, nonetheless, Algorithm 1 could be extended to joint average and peak power constraints by applying the Lagrange multipliers method to account for the average power constraint. As a result, all the functions

[1]Here, by a slight abuse of notation, the vector $\boldsymbol{\rho}$ is used equivalently to the set $\{\rho_i\}$.

in Algorithm 1 would have to be modified accordingly. For instance, a suitable implementation for the Blahut-Arimoto function, accounting for average power constraints, is derived in [65].

Let us now characterize in further details the main functions of Algorithm 1.

3.3.1 Gradient-Ascent Function

In Corollary 1, it was proved that the hypersphere of radius R is always part of the support of the capacity-achieving distribution. Therefore, R is always one of the optimal mass point positions among the $\rho_i^\star$'s. Let us consider the number of mass points T, in the input PMF, to be greater than 1. Given the definition of the mutual information in (3.11), the relative partial derivatives with respect to the ρ_i^2's are derived as

$$\frac{\partial}{\partial \rho_i^2}\mathrm{I}\big(\boldsymbol{\rho}\,;P_{\|\mathbf{X}\|}\big) = \int_0^\infty \frac{p_i}{2}\Big(f_{\chi^2_{2\mathsf{N}+2}(\rho_i^2)}(y) - f_{\chi^2_{2\mathsf{N}}(\rho_i^2)}(y)\Big) \Big(\log\big(r_i(y)y^{\mathsf{N}-1}\big) - \log\Big(f_{\chi^2_{2\mathsf{N}}(\rho_i^2)}(y)\Big)\Big)dy. \tag{3.49}$$

The $\frac{\partial}{\partial \rho_i^2}\mathrm{I}\big(\boldsymbol{\rho}\,;P_{\|\mathbf{X}\|}\big)$'s form the gradient

$$\nabla \mathrm{I}\big(\boldsymbol{\rho}\,;P_{\|\mathbf{X}\|}\big) = \left(\frac{\partial}{\partial \rho_1^2}\mathrm{I}\big(\boldsymbol{\rho}\,;P_{\|\mathbf{X}\|}\big), \ldots, \frac{\partial}{\partial \rho_{\mathsf{T}}^2}\mathrm{I}\big(\boldsymbol{\rho}\,;P_{\|\mathbf{X}\|}\big)\right). \tag{3.50}$$

Then, the gradient-ascent update is given by

$$\boldsymbol{\rho} = \sqrt{\boldsymbol{\rho}^2 + \alpha \nabla \mathrm{I}\big(\boldsymbol{\rho}\,;P_{\|\mathbf{X}\|}\big)}, \tag{3.51}$$

where α is a suitably chosen step size and where the square root and the squaring operations on the vectors are applied element-wise.

Remark 4. Each ρ_i must lie in the interval $[0, \mathsf{R}]$. Therefore, after the gradient-ascent update, any ρ_i fallen out of the interval $[0, \mathsf{R}]$ is projected back into the interval, i.e., any $\rho_i < 0$ is set to $\rho_i = 0$, while any $\rho_i > \mathsf{R}$ to $\rho_i = \mathsf{R}$.

Remark 5. Let us assume $\rho_1 = \mathsf{R}$. By Corollary 1, Theorem 3.2.2, and Remark 4, the gradient-ascent update for ρ_1 would always result in $\rho_1 = \mathsf{R}$. Therefore, the evaluation of (3.50) can be slightly simplified by setting $\frac{\partial}{\partial \rho_1^2} \mathrm{I}\big(\boldsymbol{\rho}\,; P_{\|\mathbf{X}\|}\big) = 0$.

3.3.2 Blahut-Arimoto Function

Given the number of hyperspheres T, their radii $\boldsymbol{\rho}$, and the probabilities $\mathbf{p}$, by (3.11) we have

$$\begin{aligned} &\mathrm{I}\big(\boldsymbol{\rho}\,; P_{\|\mathbf{X}\|}\big) \\ &\quad = -\log\big((2e)^{\mathsf{N}}\Gamma(\mathsf{N})\big) + \sum_{i=1}^{\mathsf{T}} p_i \int_0^\infty f_{\chi^2_{2\mathsf{N}}(\rho_i^2)}(y) \log\left(\frac{y^{\mathsf{N}-1}}{r(y, \{p_j\})}\right) dy, \end{aligned} \tag{3.52}$$

where

$$r(y, \mathbf{p}) = \sum_{j=1}^{\mathsf{T}} p_j f_{\chi^2_{2\mathsf{N}}(\rho_j^2)}(y). \tag{3.53}$$

Then, the maximization of (3.52) over $\mathbf{p}$ can be rewritten as follows

$$\begin{aligned} \max_{\mathbf{p}} \mathrm{I}\big(\boldsymbol{\rho}\,; P_{\|\mathbf{X}\|}\big) = -\log\big((2e)^{\mathsf{N}}\Gamma(\mathsf{N})\big) + \max_{\mathbf{p}} \sum_{i=1}^{\mathsf{T}} p_i \Bigg\{ \int_0^\infty f_{\chi^2_{2\mathsf{N}}(\rho_i^2)}(y) \\ \left[\log \frac{p_i f_{\chi^2_{2\mathsf{N}}(\rho_i^2)}(y) y^{\mathsf{N}-1}}{r(y, \{p_j\})} - \log(f_{\chi^2_{2\mathsf{N}}(\rho_i^2)}(y))\right] dy - \log(p_i) \Bigg\} \end{aligned} \tag{3.54}$$

$$\stackrel{(a)}{=} -\log\big((2e)^{\mathsf{N}}\Gamma(\mathsf{N})\big) + \max_{\mathbf{p}} \max_{r_i(y)} \mathrm{J}(\mathbf{p}, \{r_i(y)\}) \tag{3.55}$$

with

$$\mathrm{J}(\mathbf{p}, \{r_i(y)\}) \triangleq \sum_{i=1}^{\mathsf{T}} p_i \left\{ \int_0^\infty f_{\chi^2_{2\mathsf{N}}(\rho_i^2)}(y) \log \frac{r_i(y) y^{\mathsf{N}-1}}{f_{\chi^2_{2\mathsf{N}}(\rho_i^2)}(y)} dy - \log(p_i) \right\}, \tag{3.56}$$

where $\{r_i(y)\}_{i=1}^{\mathsf{T}}$ is a valid PMF for any given $y \in \mathbb{R}^+$ and where in step (a) we used the fact that the Kullback-Leibler divergence between $\{p_i f_{\chi^2_{2\mathsf{N}}(\rho_i^2)}(y)/r(y, \{p_j\})\}$ and $\{r_i(y)\}$ is nonnegative. Given the double maximization in (3.55), for $i = 1, \ldots, \mathsf{T}$, the inner maximization is optimized by

$$r_i(y) = \frac{p_i f_{\chi^2_{2\mathsf{N}}(\rho_i^2)}(y)}{\sum_{j=1}^{\mathsf{T}} p_j f_{\chi^2_{2\mathsf{N}}(\rho_j^2)}(y)}, \quad \forall y \in \mathbb{R}^+. \tag{3.57}$$

As for the outer maximization, each entry of $\mathbf{p}$ is optimized by

$$p_i' = \exp\left(\int_0^\infty f_{\chi^2_{2\mathsf{N}}(\rho_i^2)}(y) \log \frac{r_i(y) y^{\mathsf{N}-1}}{f_{\chi^2_{2\mathsf{N}}(\rho_i^2)}(y)} dy \right). \tag{3.58}$$

Finally, the new probabilities are evaluated by updating each entry of $\mathbf{p}$ as follows

$$p_i = \frac{p_i'}{\sum_{j=1}^{\mathsf{T}} p_j'}, \tag{3.59}$$

for $i = 1, \ldots, \mathsf{T}$. Similarly to the standard Blahut-Arimoto algorithm, the steps in (3.57), (3.58), and (3.59) are reiterated until the p_i's converge to a stable solution.

3.3.3 KKT-Validation Function

To ensure that the estimated PMF is accurate, the algorithm implements a numerical version of the KKT conditions defined in (3.12). Specifically, the KKT-Validation function sets $v = 0$ if either of the following conditions is verified

$$\left| i(\rho; \hat{P}_{\|\mathbf{X}^\star\|}) - \mathrm{I}\left(\boldsymbol{\rho}\,; \hat{P}_{\|\mathbf{X}^\star\|}\right) \right| > \varepsilon, \quad \text{for some } \rho \in \operatorname{supp}\left(\hat{P}_{\|\mathbf{X}^\star\|}\right) \tag{3.60a}$$

$$\mathrm{I}\left(\boldsymbol{\rho}\,; \hat{P}_{\|\mathbf{X}^\star\|}\right) + \varepsilon < i(\rho; \hat{P}_{\|\mathbf{X}^\star\|}), \quad \text{for some } \rho \in [0, \mathsf{R}]. \tag{3.60b}$$

On the other hand, the validation function returns $v = 1$ if neither is verified. Notice that the conditions in (3.60) are obtained by negating those in Theorem 3.1.1 and are numerically more efficient to verify. Moreover, since the true capacity C is not known, in (3.60) the mutual information $\mathrm{I}\left(\boldsymbol{\rho}\,; \hat{P}_{\|\mathbf{X}^\star\|}\right)$ is used as an estimate of C.

3.3.4 Add-Point Function

In [66, Theorem 2], the authors prove that, for R smaller than a given threshold value $\bar{\mathsf{R}}_{2\mathrm{N}}$, the optimal distribution comprises of a single hypersphere. As R and, therefore, also the SNR increase, new mass points appear in the capacity-achieving distribution $P_{\|\mathbf{X}^\star\|}$ or, equivalently, new hyperspheres are required in $\operatorname{supp}(f_{\mathbf{X}^\star})$. In [66, Theorem 4], the authors also prove that, as soon as R gets larger than $\bar{\mathsf{R}}_{2\mathrm{N}}$, a second mass point is required in the optimal PMF and it appears in 0. As the R gets even larger, we numerically observe that $i(0; P_{\|\mathbf{X}\|})$, eventually becomes larger than any $i(\rho; P_{\|\mathbf{X}\|})$, with $\rho \in (0, \mathsf{R}]$. Therefore, given an arbitrary constraint factor $\widetilde{\mathsf{R}}$ such that the corresponding capacity-

achieving PMF includes T mass points, we conjecture that for $\mathsf{R} > \widetilde{\mathsf{R}}$ the first new mass point appears in $\rho_{\mathsf{T}+1} = 0$ and also that these mass points appear one by one. Notice that whenever a new mass point is introduced in $\rho_{\mathsf{T}+1} = 0$, the probability vector has to be updated by appending a new entry $p_{\mathsf{T}+1}$ to $\mathbf{p}$. For slight SNR increments, we expect the optimal PMF to evolve slowly, therefore the new probability entry is set to zero[2].

3.4 Numerical Results

In this section, numerical results obtained through Algorithm 1 are presented. To better contextualize the derived capacity results, let us first introduce previously available upper and lower bounds on the channel capacity presented by other authors.

3.4.1 Bounds on the Channel Capacity

In [34], the authors derive two upper bounds based on a dual expression of the channel capacity. The first one is called *McKellips-Type* upper bound, a closed-form bound that extends the results of McKellips [33] to vector channels; the other upper bound has closed form expression just at low SNR, while it is evaluated numerically otherwise. The authors of [34] call it *Refined* upper bound as it is a refinement over the first one. In this work, their McKellips-Type upper bound will be denoted by $\overline{\mathsf{C}}_{\text{McK}}$ and it is defined in [34, Eq. (67)] as

$$\overline{\mathsf{C}}_{\text{McK}} \triangleq \log\left(\frac{\text{Vol}\left(\mathcal{B}_{\mathsf{R}}^{2\mathsf{N}}\right)}{(2\pi e)^{\mathsf{N}}} + \sum_{i=0}^{2\mathsf{N}-1} \binom{2\mathsf{N}-1}{i} \frac{\Gamma\left(\frac{2\mathsf{N}-i}{2}\right)}{2^{i/2}\Gamma(\mathsf{N})} \mathsf{R}^i\right), \tag{3.61}$$

[2]While not exactly zero, to avoid numerical instabilities we set $p_{\mathsf{T}+1}$ to values extremely close to zero.

where $\mathrm{Vol}(\mathcal{B}_{\mathsf{R}}^n) = \frac{\pi^{n/2}}{\Gamma\left(\frac{n}{2}+1\right)}\mathsf{R}^n$ is the volume of $\mathcal{B}_{\mathsf{R}}^n$.

Moreover, the numerical Refined bound, defined in [34, Eq. (82)], will be denoted by $\overline{\mathsf{C}}_{\text{Ref}}$.

Finally, a capacity lower bound, based on the EPI, is defined in [34, Eq. (78)] as

$$\underline{\mathsf{C}}_{\text{EPI}} \triangleq \mathsf{N}\log\left(1 + \frac{\left(\mathrm{Vol}\left(\mathcal{B}_{\mathsf{R}}^{2\mathsf{N}}\right)\right)^{1/\mathsf{N}}}{2\pi e}\right). \tag{3.62}$$

3.4.2 Optimal Input Distribution and Channel Capacity Estimates

In this section, numerical estimates of the capacity-achieving input distribution are derived. Furthermore, the resulting channel capacity estimates are compared to the capacity bounds defined in the previous section. The considered case study is characterized by $\mathsf{N} = 2$, $\varepsilon = 10^{-2}$, and SNR ranging from -5 dB to 25 dB. In Fig. 3.1, it is shown a comparison between the capacity estimate $\hat{\mathsf{C}}(\mathsf{R})$ and the bounds of Section 3.4.1. From the figure, it is clear that the Refined bound $\overline{\mathsf{C}}_{\text{Ref}}$ is very close to our capacity estimate $\hat{\mathsf{C}}(\mathsf{R})$ evaluated via Algorithm 1. On the other hand, the McKellips-Type upper bound $\overline{\mathsf{C}}_{\text{McK}}$, defined in (3.61), is significantly looser than $\overline{\mathsf{C}}_{\text{Ref}}$ and $\hat{\mathsf{C}}(\mathsf{R})$. Notice also that the EPI lower bound is loose at intermediate SNR and gets closer to the true capacity at low and at high SNR. In Fig. 3.2, it is shown the evolution of the capacity-achieving PMF estimate $\hat{P}_{\|\mathbf{X}^\star\|}$. The figure shows the positions of the mass points, normalized by R at each SNR. Moreover, the size of the circles is proportional to the associated probability measure. Note that, for the considered case and the given Definition 2.1.5, the relationship between R and SNR is $\text{SNR} = \mathsf{R}^2/(2\mathsf{N})$.

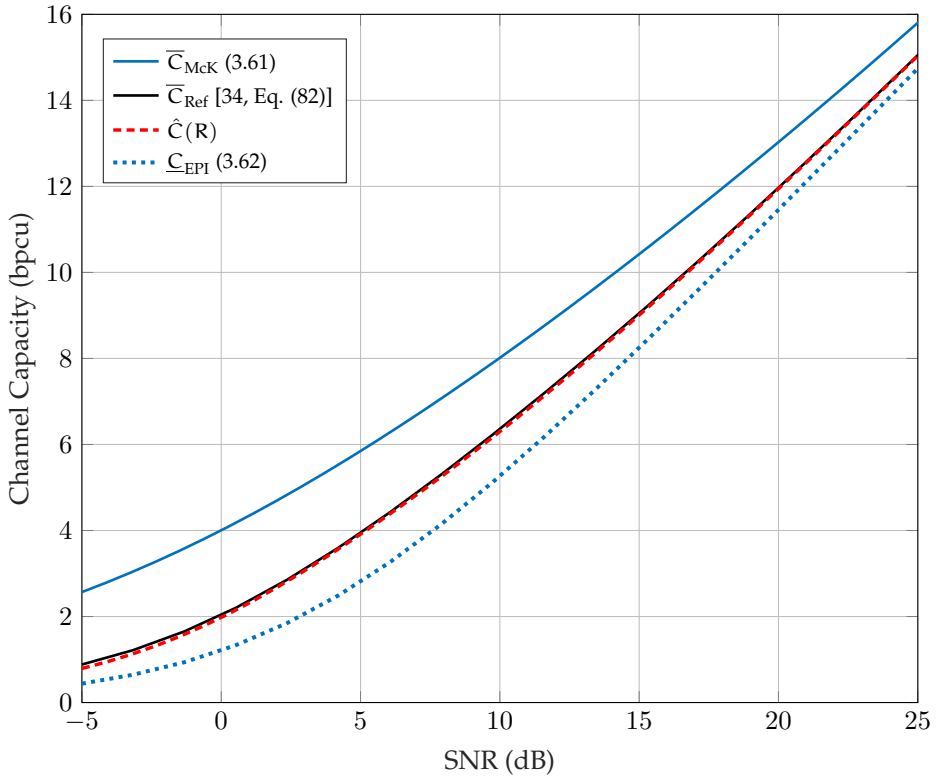

Figure 3.1: *Channel Capacity bounds and estimate versus* SNR *for* $N = 2$*, with tolerance* $\varepsilon = 10^{-2}$.

As proven in Corollary 1, the mass point in R is always optimal and indeed, it is always part of the estimate $\hat{P}_{\|\mathbf{X}^\star\|}$. Each new mass point appears in zero, with an associated probability close to zero.

Finally, Fig. 3.3 shows the estimated positions of the mass points of $\hat{P}_{\|\mathbf{X}^\star\|}$ versus R. Notice that, as N increases, each new mass point appears progressively at larger R's.

3.5 Other Constraints

The results described for the nonfading channel up to this point can be, fairly easily, extended to the case of PA and AS constraints. Let

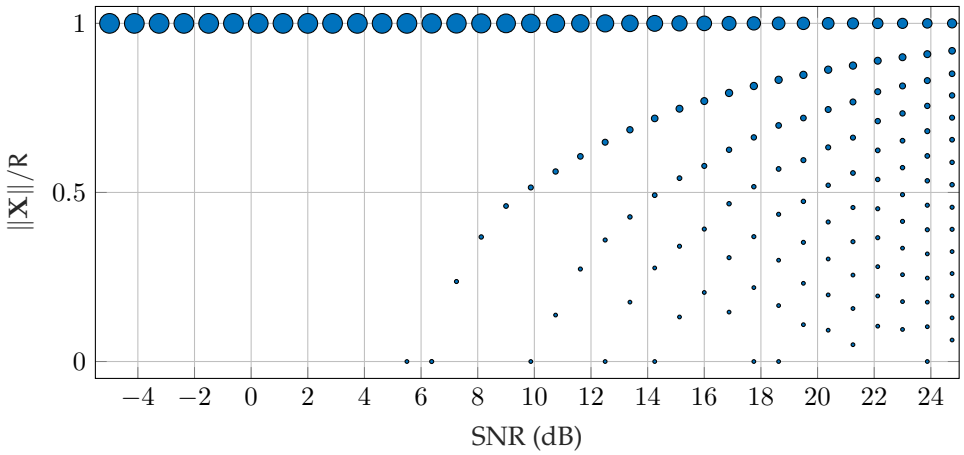

Figure 3.2: *Evolution of the numerically estimated* $\hat{P}_{\|\mathbf{X}^\star\|}$ *versus* SNR *for* $\mathsf{N} = 2$*, with tolerance* $\varepsilon = 10^{-2}$.

us start with the latter, as the PA is a special case of the AS constraint. Consider the constraint described in Definition 2.3.3. Notice that, since $\mathcal{X} = \mathcal{X}_1 \times \cdots \times \mathcal{X}_\mathsf{K}$ is given by a Cartesian product of K subspaces and since the noise $\mathbf{Z}$ has i.i.d. entries, we can decompose the nonfading channel in Definition 2.1.3 into separate subchannels. The number of subchannels K corresponds to the number of elements in the Cartesian product $\mathcal{X}$, that, in turn, is determined by the number of power constraints considered at the transmitter. Let us denote by N_i the number of complex dimensions in the ith subchannel, by $\mathbf{X}_i \in \mathcal{X}_i$ the corresponding subvector of $\mathbf{X}$, and similarly for $\mathbf{Y}_i$ and $\mathbf{Z}_i$. Then, the ith subchannel is defined as

$$\mathbf{Y}_i = \mathbf{X}_i + \mathbf{Z}_i. \tag{3.63}$$

The associated subchannel capacity is

$$\mathsf{C}_i = \sup_{f_{\mathbf{X}_i}:\, \mathbf{X}_i \in \mathcal{X}_i} \mathsf{h}(\mathbf{Y}_i) - \mathsf{h}(\mathbf{Z}_i). \tag{3.64}$$

Moreover, let us denote by $f_{\mathbf{X}_i^\star}$ the input distribution maximizing (3.64). Then, the overall channel capacity is given by

$$\mathsf{C} = \sum_{i=1}^{\mathsf{K}} \mathsf{C}_i. \tag{3.65}$$

Finally, the capacity-achieving PDF $f_{\mathbf{X}^\star}$ is such that

$$f_{\mathbf{X}^\star}(\mathbf{x}) = \prod_{i=1}^{\mathsf{K}} f_{\mathbf{X}_i^\star}(\mathbf{x}_i),\ \forall \mathbf{x} \in \mathcal{X}. \tag{3.66}$$

Let us consider the vectorized and real-valued version of each $\mathcal{X}_i$. Then, whenever $\mathcal{X}_i = \mathcal{B}_{\mathsf{R}_i}^{2\mathsf{N}_i},\ \forall i$, the subchannel capacities defined in (3.64) can be estimated again via Algorithm 1. Moreover, an estimate of the channel capacity C and of $f_{\mathbf{X}^\star}$ can be derived via (3.65) and (3.66), respectively. Note that, when the $\mathcal{X}_i$'s are not balls, one can always derive an upper bound on the capacity by substituting $\mathcal{X}_i$ with an enlarged constraint region. Let us define $r_i = r_{\max}(\mathcal{X}_i)$, i.e., the maximum radius of $\mathcal{X}_i$. Then, since $\mathcal{B}_{r_i}^{2\mathsf{N}_i} \supseteq \mathcal{X}_i$, evaluating the C_i's for $\mathbf{X}_i \in \mathcal{B}_{r_i}^{2\mathsf{N}_i} \supseteq \mathcal{X}_i$ provides and an upper bound on each subchannel capacity and, in turn, their sum upper-bounds the overall channel capacity C.

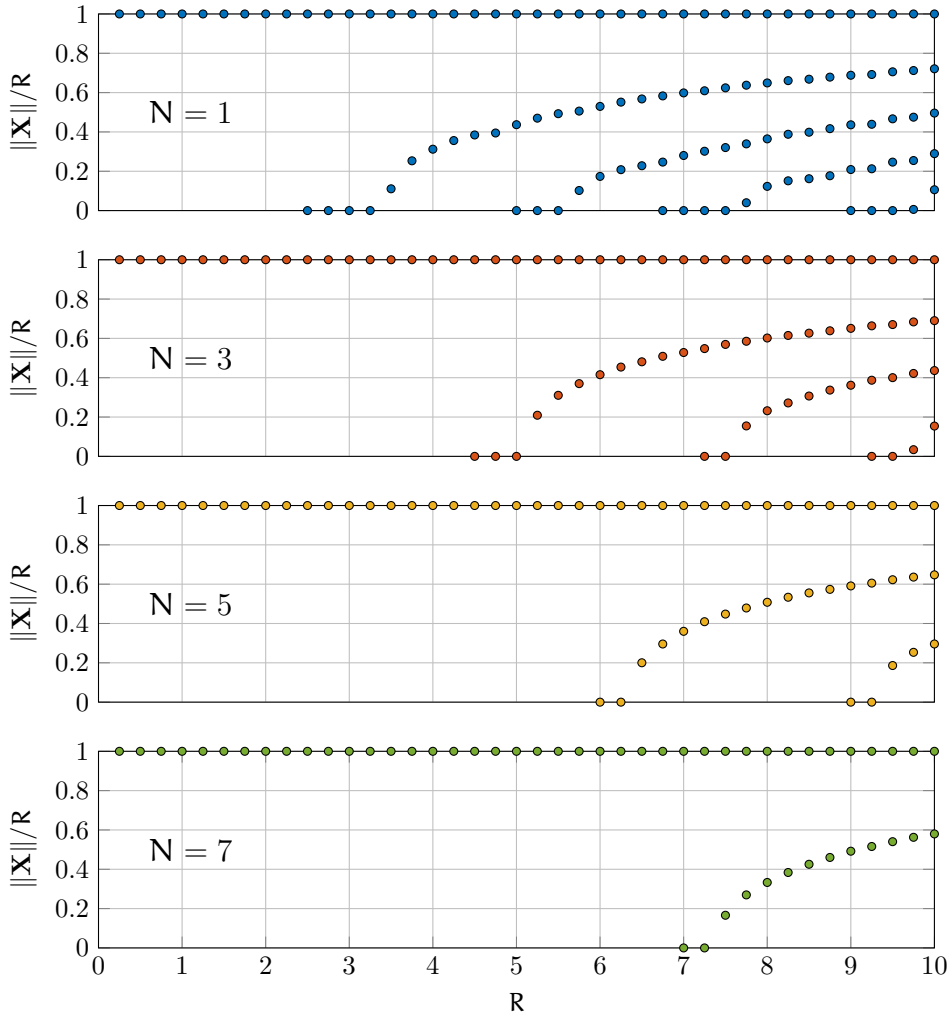

Figure 3.3: *Evolution of the numerically estimated mass points positions of* $\hat{P}_{\|\mathbf{X}^\star\|}$ *versus* R *for* $\mathsf{N} = 1, 3, 5, 7$*, with tolerance* $\varepsilon = 10^{-3}$.

3.6 Approximate Discrete Input Distribution

Practical communication systems typically employ discrete input distributions. Therefore, one might want to evaluate suboptimal, but discrete, input distributions that can be used in real life scenarios. Given the results derived in the previous sections, let us consider viable discrete approximations of the optimal PDF. Since the capacity-achieving distribution is uniform over each hypersphere belonging to $\mathrm{supp}(f_{\mathbf{X}^\star})$, one option is to consider an approximated PMF with support comprising points uniformly spaced over the hyperspheres in $\mathrm{supp}(f_{\mathbf{X}^\star})$. Notice that, for a finite number of points, in general this is not the capacity-achieving distribution, especially when few points are considered. Nonetheless, it provides a simple approximation that tends to the optimal solution as the number of considered points increases. Let us denote by $\mathbf{X}_Q$ the discrete random vector of PMF $P_{\mathbf{X}_Q}$ and by $\mathsf{K} = \left|\mathrm{supp}\big(P_{\mathbf{X}_Q}\big)\right|$ the number of mass points in the support of $\mathrm{supp}\big(P_{\mathbf{X}_Q}\big)$. Given the number of hyperspheres $\mathsf{T}^\star$ in $\mathrm{supp}(f_{\mathbf{X}^\star})$, let us also denote by K_i the number of mass points approximating the ith hypersphere, such that $\sum_{i=1}^{\mathsf{T}^\star} \mathsf{K}_i = \mathsf{K}$.

For $\mathsf{N} = 1$ complex dimension, the equivalent real-valued constraint is a circle. Therefore, $\mathrm{supp}(f_{\mathbf{X}^\star})$ is the union of concentric circumferences. Distributing evenly spaced points on a circumference is a simple task while, on the other hand, the problem is not so trivial for any $\mathsf{N} > 1$. The only known configurations of points that are evenly spread over an n-dimensional hypersphere are those defined by the vertices of convex regular polytopes. Furthermore, for $n \geq 5$ there are only 3 known regular polytopes [67]. In this work, the focus will,

therefore, be on the more tractable case of $\mathsf{N} = 1$.

Nonetheless, an interesting fact is that finding evenly spread points on a sphere is related to Thomson problem [68], that is, finding the configuration of a finite number of electrons on a sphere such that their electrostatic potential energy is minimized. In [69], the Thomson problem is generalized to higher dimensions. The electrostatic potential energy depends on the Coulomb forces acting between the electrons, therefore, in principle an approximate configuration of evenly spread points could be derived by simulation. Indeed, one could simulate the Coulomb interaction among a given a set of electrons constrained on the hypersphere. When they reach a stable configuration, the positions of the electrons can be used as a rough approximation of evenly spread points on the hypersphere.

Let us now focus on the performance that can be achieved by using approximate PMFs for $\mathsf{N} = 1$.

3.6.1 Single Hypersphere Regime

As already mentioned, in [66, Theorem 2], the authors derived the maximum radius $\bar{\mathsf{R}}_{2\mathsf{N}}$, such that the support of the optimal distribution is a single hypersphere. Let us consider first the single hypersphere regime.

We are interested in the evaluation of the information loss determined by the approximate discrete PMF over the true optimal input distribution. Let us define the information loss for the $(2\mathsf{N})$-dimensional real-valued channel of Definition 2.1.4 as

$$\mathcal{L}_{2\mathsf{N}}\big(P_{\mathbf{X}_Q}, \mathsf{K}\big) \triangleq \mathsf{C} - \mathrm{I}(\mathbf{X}_Q\,;\mathbf{Y}_Q) = \mathrm{h}(\mathbf{Y}) - \mathrm{h}(\mathbf{Y}_Q), \tag{3.67}$$

where K is, again, the number of mass points in the approximate input PMF $P_{\mathbf{X}_Q}$ and

$$\mathbf{Y}_Q = \mathbf{X}_Q + \mathbf{Z}. \tag{3.68}$$

Notice that, in the single hypersphere regime, the channel capacity can be directly evaluated and the optimization defined in Algorithm 1 is not necessary. Indeed, the resulting capacity for $\mathsf{R} \leq \bar{\mathsf{R}}_{2\mathsf{N}}$ is given by

$$\mathsf{C} = i(\mathsf{R}; P_{\|\mathbf{X}^\star\|}) \tag{3.69}$$

$$= \int_0^\infty f_{\chi^2_{2\mathsf{N}}(\mathsf{R}^2)}(y) \log \frac{y^{\mathsf{N}-1}}{f_{\chi^2_{2\mathsf{N}}(\mathsf{R}^2)}(y)} dy - \log\big((2e)^{\mathsf{N}}\Gamma(\mathsf{N})\big). \tag{3.70}$$

Let us focus on the mono-dimensional complex case. For $\mathsf{N} = 1$, the resulting equivalent 2-dimensional real-valued optimal input is distributed uniformly over a circumference of radius R, i.e., $\mathcal{S}^2_{\mathsf{R}}$. Therefore, a suitable approximate input distribution could be that composed of K evenly spaced mass points, lying on $\mathcal{S}^2_{\mathsf{R}}$ and with equal probabilities. Let us define the mass points of the approximate input distribution as

$$\mathbf{x}_{Q,k} = \mathsf{R} \cdot e^{j\frac{2\pi}{\mathsf{K}}(k-1)}, \text{ for } k = 1, \ldots, \mathsf{K}. \tag{3.71}$$

Then, the resulting PMF is

$$P_{\mathbf{X}_Q}(\mathbf{x}) = \begin{cases} \frac{1}{\mathsf{K}}, & \mathbf{x} \in \{\mathbf{x}_{Q,k},\ k = 1, \ldots, \mathsf{K}\}, \\ 0, & \text{elsewhere}, \end{cases} \tag{3.72}$$

and its support is shown in Figure 3.4. In the single hypersphere regime, the only parameter to optimize to derive $P_{\mathbf{X}_Q}$ is, therefore,

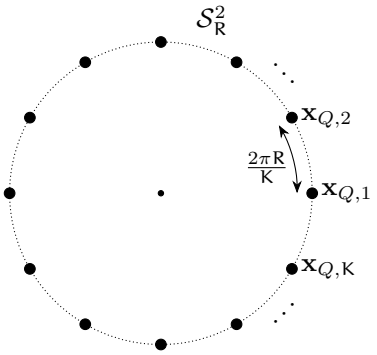

Figure 3.4: *Example of* $\mathrm{supp}\big(P_{\mathbf{X}_Q}\big)$ *for the* 2*-dimensional case and for* $\mathsf{R} \leq \bar{\mathsf{R}}_2$.

the number of mass points K. Let us denote by $\bar{\mathsf{K}}(\mathsf{R})$, the minimum number of mass points required, for each value of R, to obtain an information loss smaller than 10^{-2}, i.e., $\mathcal{L}_2\big(P_{\mathbf{X}_Q}, \bar{\mathsf{K}}(\mathsf{R})\big) \leq 10^{-2}$.

In the single hypersphere regime, it is still feasible to numerically evaluate the minimum K required to reach a given target information loss at each R. On the other hand, in the multiple hypersphere regime, the same task becomes computationally harder. Indeed, one would have to optimize simultaneously the total number of mass points K and the K_i's associated with each hypersphere. Therefore, it is convenient to derive an empirical procedure to roughly estimate the number of mass points. Let us assume that K depends just on R and on the noise variance σ_z^2. Since the mass points $\mathbf{x}_{Q,k}$'s are evenly spaced on $\mathcal{S}^2_{\mathsf{R}}$, a reasonable strategy could be to choose K in such a way that the distance between two consecutive mass points $d_{\mathsf{K}} = \|\mathbf{x}_{Q,k} - \mathbf{x}_{Q,k+1}\|$ stays more or less constant at any R. Notice that d_{K} coincides with the chord of $\mathcal{B}^2_{\mathsf{R}}$ given by an angle $2\pi/\mathsf{K}$. As K increases, the chord can be approximated by the arc $2\pi\mathsf{R}/\mathsf{K}$. Therefore, an empirical estimate of K

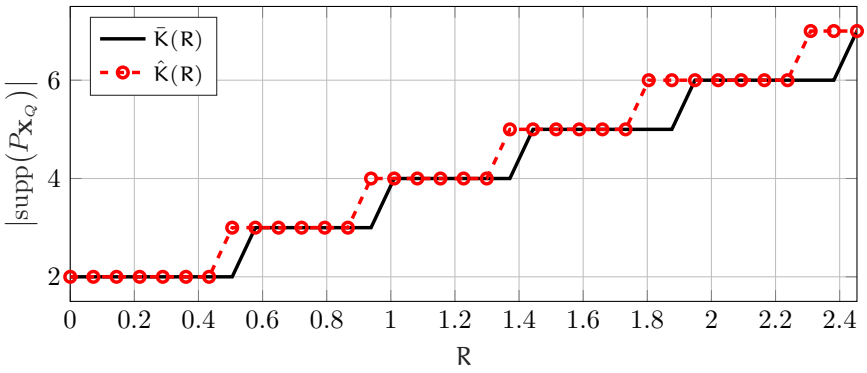

Figure 3.5: *Number of mass points in* $\mathrm{supp}\big(P_{\mathbf{X}_Q}\big)$ *versus* R *for two approximate input distributions* $P_{\mathbf{X}_Q}$.

is given by

$$\hat{\mathsf{K}}(\mathsf{R},\gamma_{\mathsf{K}}) \triangleq \left\lceil \frac{2\pi}{\gamma_{\mathsf{K}}\sigma_z}\mathsf{R} \right\rceil + 1, \tag{3.73}$$

where γ_{K} is a parameter that can be adjusted to satisfy the desired target information loss and $\lceil x \rceil$ is the ceiling function, defined as $\lceil x \rceil = \min\{n \in \mathbb{Z} : \, n \geq x\}$. Intuitively, as K increases, $P_{\mathbf{X}_Q}$ better approximates the true $P_{\mathbf{X}^\star}$. Therefore, for any γ_{K} such that $\hat{\mathsf{K}}(\mathsf{R},\gamma_{\mathsf{K}}) \geq \bar{\mathsf{K}}(\mathsf{R})$, it holds $\mathcal{L}_2(P_{\mathbf{X}_Q}, \hat{\mathsf{K}}(\mathsf{R},\gamma_{\mathsf{K}})) \leq \mathcal{L}_2\big(P_{\mathbf{X}_Q}, \bar{\mathsf{K}}\big) \leq 10^{-2}$.

A suitable value of γ_{K} for the considered target information loss can be derived numerically. Let us consider $\gamma_{\mathsf{K}} = 2\sqrt{2}$ and let us define $\hat{\mathsf{K}}(\mathsf{R}) = \hat{\mathsf{K}}(\mathsf{R}, 2\sqrt{2})$ to simplify the notation. In Fig. 3.5, it is shown the resulting empirical estimate $\hat{\mathsf{K}}(\mathsf{R})$ and $\bar{\mathsf{K}}(\mathsf{R})$, both as a function of R and and for $\sigma_z^2 = 1$. Notice that, indeed, $\hat{\mathsf{K}}(\mathsf{R}) \geq \bar{\mathsf{K}}(\mathsf{R})$ for any $\mathsf{R} \leq \bar{\mathsf{R}}_2$.

3.6.2 Multiple Hyperspheres Regime

Let us now focus on the multiple hyperspheres regime. The first difference with the previous case is that, since there are multiple hyper-

spheres, it is necessary to consider the sequence $\{\mathsf{K}_i\}$, where each K_i is the number of mass points used to approximate the ith hypersphere. Moreover, like for Algorithm 1, it is also necessary to evaluate the probabilities p_i's associated with each hyphersphere, the radii ρ_i's, and the number of hyperspheres T. The information loss for the multiple hyperspheres regime is defined as

$$\mathcal{L}_{2\mathsf{N}}\big(P_{\mathbf{X}_Q}\big) \triangleq \hat{\mathsf{C}}(\mathsf{R}) - \mathsf{I}(\mathbf{X}_Q\,;\mathbf{Y}_Q) = \mathsf{h}(\mathbf{Y}) - \mathsf{h}(\mathbf{Y}_Q), \tag{3.74}$$

where $\hat{\mathsf{C}}(\mathsf{R})$ is the capacity estimate[3] obtained via Algorithm 1.

Let us focus once more on the complex case with $\mathsf{N} = 1$. In this regime, the mass points of $P_{\mathbf{X}_Q}$ are defined as

$$\mathbf{x}_{Q,(i,k)} = \rho_i \cdot e^{j\frac{2\pi}{\mathsf{K}_i}(k-1)},\ \forall i,k, \tag{3.75}$$

where $i = 1,\ldots,\mathsf{T}$ is the index associated with each circumference and $k = 1,\ldots,\mathsf{K}_i$. Then, the resulting approximated PMF is

$$P_{\mathbf{X}_Q}(\mathbf{x}) = \begin{cases} \frac{p_i}{\mathsf{K}_i}, & \mathbf{x} \in \big\{\mathbf{x}_{Q,(i,k)},\ \forall i,k\big\} \\ 0, & \text{elsewhere.} \end{cases} \tag{3.76}$$

An example of $\mathrm{supp}\big(P_{\mathbf{X}_Q}\big)$ is shown in Fig. 3.6. Let us evaluate the information loss that can be achieved via two considered approximated PMFs, denoted by $P_{\mathbf{X}_{Q,A}}$ and $P_{\mathbf{X}_{Q,B}}$. For $P_{\mathbf{X}_{Q,A}}$, the ρ_i's, p_i's, and T used are those of the PMF estimate $\hat{P}_{\|\mathbf{X}\|}$ obtained via Algorithm 1. The number of mass points K_i used to approximate each circumference can be estimated via (3.73). Therefore, let us consider $\mathsf{K}_i = \hat{\mathsf{K}}(\rho_i)$

[3]The capacity estimate in (3.74) is evaluated with a tolerance factor $\varepsilon = 10^{-4}$.

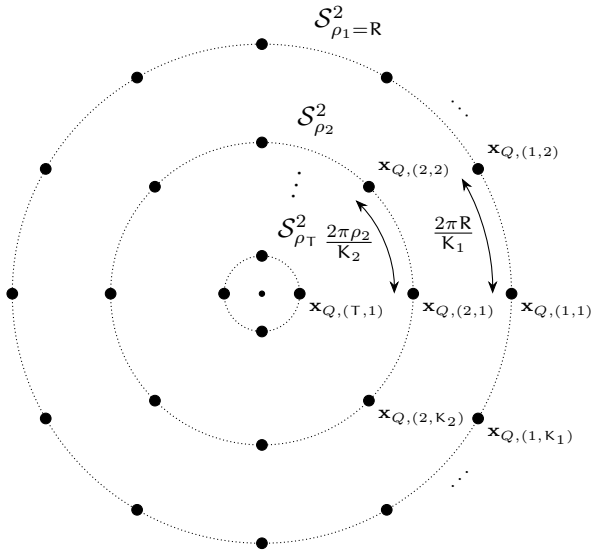

Figure 3.6: *Example of* $\mathrm{supp}\big(P_{\mathbf{X}_Q}\big)$ *for the* 2*-dimensional case and* $\mathsf{R} > \bar{\mathsf{R}}_2$.

for all i and a total number of mass points $\mathsf{K} = \sum_{i=1}^{\mathsf{T}} \mathsf{K}_i$. Fig. 3.7 shows the information rate resulting from $P_{\mathbf{X}_{Q,A}}$ and the capacity estimate $\hat{\mathsf{C}}(\mathsf{R})$ given by Algorithm 1. Moreover, the blue dashed line shows $\log_2 \mathsf{K}$. Since $\mathsf{I}(\mathbf{X}_Q\,;\mathbf{Y}_Q) \leq \mathsf{H}(\mathbf{X}_Q) \leq \log_2 \mathsf{K}$, the blue dashed line gives us a rough indication on how appropriate is the considered K at each SNR level. Roughly speaking, the fact that $\log_2 \mathsf{K}$ scales similarly to the channel capacity indicates that the number of mass points K, chosen according to the empirical estimate (3.73), is reasonable. Fig. 3.8 shows that the information loss, in the considered SNR range, is $\mathcal{L}_2(P_{\mathbf{X}_{Q,A}}) \leq 10^{-2}$. Notice that, naturally, one can always improve the accuracy of the approximation by considering a larger number of mass points K. Nonetheless, the goal of the approximation is to define an input distribution that can be practically implemented by keeping the K as small as possible. The considered target, i.e., $\mathcal{L}_2(P_{\mathbf{X}_Q}) \leq 10^{-2}$, provides a good trade off between the information loss and the number

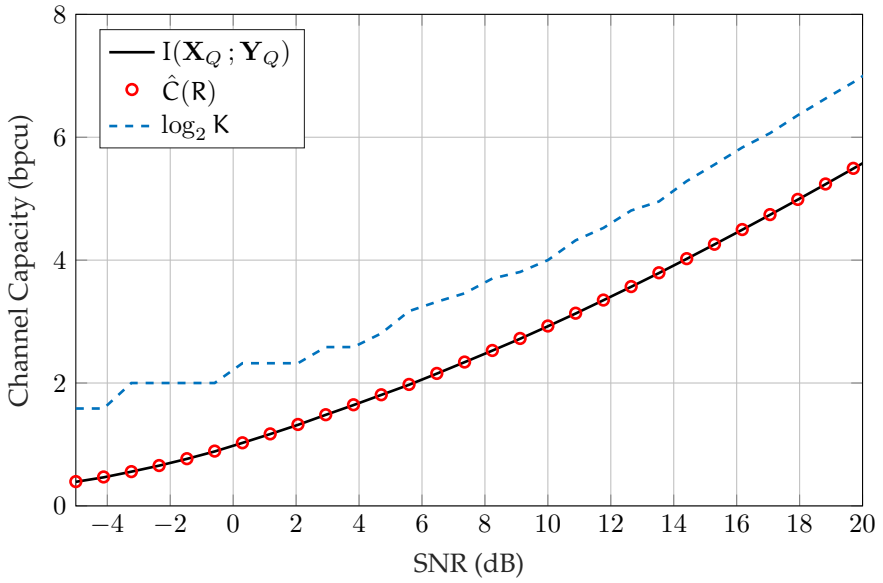

Figure 3.7: *Capacity results for the approximate input distribution $P_{\mathbf{X}_{Q,A}}$ versus SNR and for* $\mathsf{N} = 1$.

of mass points required K. Notice that, $P_{\mathbf{X}_{Q,A}}$ relies on the derivation of the optimal positions ρ_i's and probabilities p_i's via Algorithm 1. A coarser approximation can be derived by noticing that, roughly speaking, the ρ_i's tend to be evenly spaced as the SNR grows and the associated probabilities p_i's tend to be proportional to $\mathrm{Vol}\big(\mathcal{S}_{\rho_i}^{2\mathsf{N}}\big)$. Let us denote this coarser approximated PMF by $P_{\mathbf{X}_{Q,B}}$. Then, let us define the radii used in $P_{\mathbf{X}_{Q,B}}$ as

$$\rho_i = \rho_{i-1} - \Delta\rho, \quad i = 2, \ldots, \mathsf{T}, \tag{3.77}$$

where $\rho_1 = \mathsf{R}$, $\Delta\rho$ is the spacing between each ρ_i and ρ_{i+1} that has to be adjusted empirically, and $\mathsf{T} = \lceil \mathsf{R}/\Delta\rho \rceil$. A suitable radii spacing, empirically derived for the considered target information loss, is $\Delta\rho =$

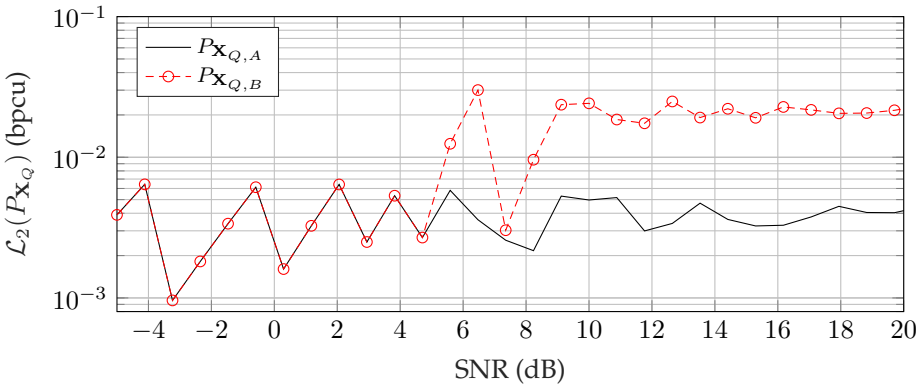

Figure 3.8: *Comparison of the information losses versus SNR obtained via the approximate distributions $P_{\mathbf{X}_{Q,A}}$ and $P_{\mathbf{X}_{Q,B}}$, with $\Delta\rho = 3$.*

$3\sigma_z = 3$. Furthermore, the associated probabilities can be defined as

$$p_i = \frac{\mathrm{Vol}\left(\mathcal{S}^2_{\rho_i}\right)}{\sum_{j=1}^{\mathsf{T}} \mathrm{Vol}\left(\mathcal{S}^2_{\rho_j}\right)}, \quad i = 1, \ldots, \mathsf{T}. \tag{3.78}$$

The K_i's are, again, chosen as $\mathsf{K}_i = \hat{\mathsf{K}}(\rho_i)$. In Fig. 3.8, it is shown a comparison between the information loss given by $P_{\mathbf{X}_{Q,A}}$ and $P_{\mathbf{X}_{Q,B}}$. Notice that, at low SNR, the resulting information losses coincide. Indeed, for $\mathsf{R} \leq \bar{\mathsf{R}}_2$ we are in the single hypersphere regime and, therefore, $P_{\mathbf{X}_{Q,A}} = P_{\mathbf{X}_{Q,B}}$, with $\rho_1 = \mathsf{R}$ and $p_1 = 1$. On the other hand, as the SNR increases, it is noticeable that the coarser definition of $P_{\mathbf{X}_{Q,B}}$ determines a worse performance compared to $P_{\mathbf{X}_{Q,A}}$. For $P_{\mathbf{X}_{Q,B}}$, one cannot improve the resulting information loss simply by increasing the number of mass points K, as it is possible for $P_{\mathbf{X}_{Q,A}}$. Indeed, because of the suboptimal choice of the ρ_i's and p_i's, a larger number of mass point K does not provide a significant improvement in terms of the resulting information loss. Nonetheless, for the number of mass points $\mathsf{K}_i = \hat{\mathsf{K}}(\rho_i),\ \forall i$, the information loss obtained via $P_{\mathbf{X}_{Q,B}}$ is still compa-

rable to that of $P_{\mathbf{X}_{Q,A}}$ and, therefore, might be a viable low-complexity option.

Finally, notice that, by Section 3.5, the presented results on the approximate input distributions can be extend also to MIMO systems subject to a PA constraint. Indeed, for any N-dimensional complex-valued MIMO system subject to the PA constraint, $\mathsf{N}_i = 1$ for $i = 1, \ldots, \mathsf{N}$. Therefore, each $f_{\mathbf{X}_i^\star}$ can be approximated via the techniques described in this section and the overall approximate discrete input distribution can be evaluated via (3.66).

3.7 Application to Wireless Wiretap Channels

The results derived for the nonfading channels can also be easily adapted to another interesting scenario, namely that of wireless wiretap channels. The definition of wiretap channel was proposed by Wyner in [70], that described it as a channel model in which a malicious user can gain access to the transmitted information. If the malicious user is assumed to perceive a noisier channel than the legitimate user, then one can introduce also the concept of secrecy-capacity. It is defined as the maximum rate at which information can be reliably and privately transmitted to the legitimate user, in presence of an eavesdropper [70]. The definition of wiretap channel and secrecy capacity were further generalized to the case of Gaussian channels in [71], where the authors proved that the secrecy capacity-achieving distribution under average power constraints is Gaussian. The case of multi-antenna legitimate transmission and of a single antenna malicious receiver is investigated in [72]. The Gaussianity of the optimal

input distribution for MIMO AWGN channels under average power constraints is proved both in [73] and in [74]. Further results on MIMO wiretap channels are presented in [75–77]. For more information on wiretap channels, see [78–82]. In this section, we will focus on the secrecy capacity for nonfading channels. For further detail on wiretap channels subject to fading, see [83–86].

Like in the case of the traditional channel capacity, less is known in the case of wiretap channel under amplitude constraints if compared to average power constraints. One of the main results for the scalar case is introduced in [87]. Other important results about the optimal input distribution are presented in [88–90].

The main result that is used in this work is that derived in [90]. Like for the capacity-achieving distribution in the nonfading standard case, the authors of [90] prove that the support of the optimal input distribution for the nonfading vector wiretap channel under peak amplitude constraints comprises of a finite number of concentric spheres.

Let us describe the channel model. A diagram of such channel is shown in Fig. 3.9. The input-output relationships are similar to Definition 2.1.3 and are given by

$$\mathbf{Y}_{\mathrm{B}} = \mathbf{X} + \mathbf{Z}_{\mathrm{B}}, \tag{3.79a}$$

$$\mathbf{Y}_{\mathrm{E}} = \mathbf{X} + \mathbf{Z}_{\mathrm{E}}, \tag{3.79b}$$

where $\mathbf{Z}_{\mathrm{B}} \sim \mathcal{CN}(\mathbf{0}_{\mathrm{N}}, 2\sigma_{\mathrm{B}}^2 \mathsf{I}_{\mathrm{N}})$ and $\mathbf{Z}_{\mathrm{E}} \sim \mathcal{CN}(\mathbf{0}_{\mathrm{N}}, 2\sigma_{\mathrm{E}}^2 \mathsf{I}_{\mathrm{N}})$, with $\sigma_{\mathrm{E}}^2 > \sigma_{\mathrm{B}}^2$. The secrecy capacity is defined as

$$\mathrm{C}_s = \max_{f_{\mathbf{X}}:\, \mathbf{X}\in\mathcal{X}} \mathrm{I}(\mathbf{X}\,;\mathbf{Y}_{\mathrm{B}}) - \mathrm{I}(\mathbf{X}\,;\mathbf{Y}_{\mathrm{E}}), \tag{3.80}$$

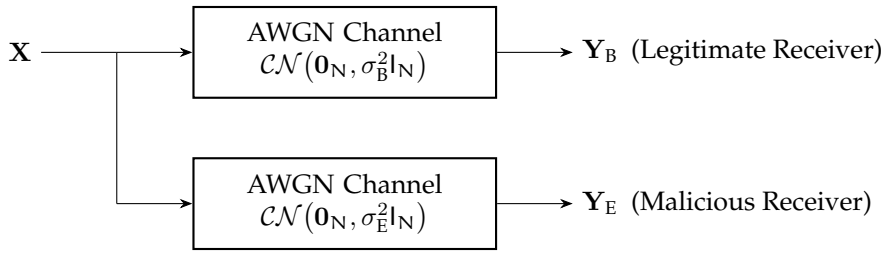

Figure 3.9: *Diagram of the wireless vector Gaussian wiretap channel.*

where $\mathcal{X} = \left\{\mathbf{x} \in \mathbb{C}^{\mathsf{N}} : \ \|\mathbf{x}\| \leq \mathsf{R}\right\}$ is the input constraint region and $\mathsf{R} \in \mathbb{R}^{+}$ is, again, the constraint factor. Notice also that, thanks to [90], we know that the structure of the optimal input distribution is the same as that described in Section 3.1. Therefore, we can rewrite $\mathrm{I}(\mathbf{X}\,;\mathbf{Y}_{\mathrm{B}})$ and $\mathrm{I}(\mathbf{X}\,;\mathbf{Y}_{\mathrm{E}})$ as function of the mono-dimensional distribution of the input norm $P_{\|\mathbf{X}\|}$ defined in (3.3). As a consequence, we can also adapt the numerical procedure in Algorithm 1 to the wiretap channel with a few minor changes.

Let us define the secrecy density as

$$i_s(\rho; P_{|\mathbf{X}|}) \triangleq i_{\mathrm{B}}(\rho; P_{|\mathbf{X}|}) - i_{\mathrm{E}}(\rho; P_{|\mathbf{X}|}), \tag{3.81}$$

where $i_{\mathrm{B}}(\rho; P_{|\mathbf{X}|})$ and $i_{\mathrm{E}}(\rho; P_{|\mathbf{X}|})$ are, respectively, the information densities associated with (3.79a) and (3.79b). Notice that the information density definition is slightly different than that of (3.10), where we assumed the noise variance to be unitary. For the general case of Definition 2.1.3, the information density is defined as

$$\begin{aligned} i(\rho; P_{\|\mathbf{X}\|}) \triangleq \int_0^{\infty} f_{\chi^2_{2\mathsf{N}}(\rho^2/\sigma_z^2)}(y) \log \frac{y^{\mathsf{N}-1}}{\sum_{k=1}^{\mathsf{T}} p_k f_{\chi^2_{2\mathsf{N}}(\rho_k^2/\sigma_z^2)}(y)} dy \\ - \log\big((2e)^{\mathsf{N}} \Gamma(\mathsf{N})\big). \end{aligned} \tag{3.82}$$

Therefore, we can use (3.82) to evaluate both $i_{\mathrm{B}}(\rho; P_{|\mathbf{X}|})$ and $i_{\mathrm{E}}(\rho; P_{|\mathbf{X}|})$. Furthermore, similarly to (3.11), we define the secrecy information as

$$\mathrm{I}_s\big(\boldsymbol{\rho}\,; P_{\|\mathbf{X}\|}\big) \triangleq \sum_{i=1}^{\mathsf{T}} p_i \cdot i_s(\rho_i; P_{\|\mathbf{X}\|}). \tag{3.83}$$

Then, the changes required to adapt Algorithm 1 to the wiretap channel are the following.

In the gradient-ascent function, we have to evaluate the gradient of the secrecy information in (3.83). It holds

$$\frac{\partial}{\partial \rho_i^2}\mathrm{I}_s\big(\boldsymbol{\rho}\,; P_{\|\mathbf{X}\|}\big) = \frac{\partial}{\partial \rho_i^2}\sum_{i=1}^{\mathsf{T}} p_i \cdot i_s(\rho_i; P_{\|\mathbf{X}\|}) \tag{3.84}$$

$$= \frac{\partial}{\partial \rho_i^2}\sum_{i=1}^{\mathsf{T}} p_i \cdot i_{\mathrm{B}}(\rho_i; P_{\|\mathbf{X}\|}) - \frac{\partial}{\partial \rho_i^2}\sum_{i=1}^{\mathsf{T}} p_i \cdot i_{\mathrm{E}}(\rho_i; P_{\|\mathbf{X}\|}), \tag{3.85}$$

where both partial derivatives are evaluated as in Section 3.8.2. Then, similarly to that of Section 3.3.1, the gradient is

$$\nabla \mathrm{I}_s\big(\boldsymbol{\rho}\,; P_{\|\mathbf{X}\|}\big) = \left(\frac{\partial}{\partial \rho_1^2}\mathrm{I}_s\big(\boldsymbol{\rho}\,; P_{\|\mathbf{X}\|}\big), \ldots, \frac{\partial}{\partial \rho_{\mathsf{T}}^2}\mathrm{I}_s\big(\boldsymbol{\rho}\,; P_{\|\mathbf{X}\|}\big)\right), \tag{3.86}$$

and the gradient-ascent update is

$$\boldsymbol{\rho} = \sqrt{\boldsymbol{\rho}^2 + \alpha \nabla \mathrm{I}_s\big(\boldsymbol{\rho}\,; P_{\|\mathbf{X}\|}\big)}, \tag{3.87}$$

where α is, again, a suitably chosen step size.

For the Blahut-Arimoto function of Section 3.3.2, the probability up-

dates are defined as

$$p'_i = p_i \exp\big(i_s(\rho_i; P_{\|\mathbf{X}\|})\big). \tag{3.88}$$

For the KKT-Validation function of Section 3.3.3 and the Add-Point function of Section 3.3.4, the only required change is to use the secrecy density $\mathrm{I}_s\Big(\boldsymbol{\rho}\,; \hat{P}_{\|\mathbf{X}\|}\Big)$ of (3.83) and $i_s(\rho_i; P_{\|\mathbf{X}\|})$ of (3.81), instead of $\mathrm{I}\Big(\boldsymbol{\rho}\,; \hat{P}_{\|\mathbf{X}\|}\Big)$ and $i(\rho_i; P_{\|\mathbf{X}\|})$, respectively.

Finally, line 15 of Algorithm 1 is unchanged and line 16 is used to estimate the secrecy capacity $\hat{\mathsf{C}}_s(\mathsf{R}) = \mathrm{I}_s\Big(\boldsymbol{\rho}\,; \hat{P}_{\|\mathbf{X}^*\|}\Big)$.

3.8 Appendix

3.8.1 Proof of Lemma 1

Proof. Let us consider two values ρ_1, ρ_2 such that $\rho_1 > \rho_2$ and the following definition of information density

$$\begin{aligned} i(\rho; P_{\|\mathbf{X}\|}) \triangleq & \int_0^\infty f_{\chi^2_{2\mathsf{N}}(\rho^2)}(y) \log \frac{y^{\mathsf{N}-1}}{\int_0^{\mathsf{R}} f_{\chi^2_{2\mathsf{N}}(t^2)}(y) dP_{\|\mathbf{X}\|}(t)} dy \\ & - \log\big((2e)^{\mathsf{N}}\Gamma(\mathsf{N})\big). \end{aligned} \tag{3.89}$$

Then, it holds the following

$$\begin{aligned} & i(\rho_1; P_{\|\mathbf{X}\|}) - i(\rho_2; P_{\|\mathbf{X}\|}) \\ & = \int_0^\infty \Big(f_{\chi^2_{2\mathsf{N}}(\rho_1^2)}(y) - f_{\chi^2_{2\mathsf{N}}(\rho_2^2)}(y)\Big) \log \frac{y^{\mathsf{N}-1}}{f_{\|\mathbf{Y}\|^2}(y; P_{\|\mathbf{X}\|})} dy \qquad (3.90) \\ & = -\int_0^\infty \Big(F_{\chi^2_{2\mathsf{N}}(\rho_2^2)}(y) - F_{\chi^2_{2\mathsf{N}}(\rho_1^2)}(y)\Big) \frac{d}{dy} \log \frac{f_{\|\mathbf{Y}\|^2}(y; P_{\|\mathbf{X}\|})}{y^{\mathsf{N}-1}} dy \qquad (3.91) \end{aligned}$$

where we used integration by parts. Let us also notice that

$$\int_0^\infty \Big(F_{\chi^2_{2\mathsf{N}}(\rho_2^2)}(y) - F_{\chi^2_{2\mathsf{N}}(\rho_1^2)}(y)\Big)dy = \rho_1^2 - \rho_2^2, \tag{3.92}$$

and that, since $\chi^2_{2\mathsf{N}}(\rho_1^2)$ is statistically dominant compared to $\chi^2_{2\mathsf{N}}(\rho_2^2)$, the integrand function in (3.92) is always positive. Furthermore, let us also define an auxiliary output random variable Q with PDF

$$f_Q(y;\rho_1,\rho_2) = \frac{F_{\chi^2_{2\mathsf{N}}(\rho_2^2)}(y) - F_{\chi^2_{2\mathsf{N}}(\rho_1^2)}(y)}{\rho_1^2 - \rho_2^2}, \qquad y > 0. \tag{3.93}$$

Given (3.93), the integral in (3.91) can be rewritten as

$$\begin{aligned} &i(\rho_1; P_{\|\mathbf{X}\|}) - i(\rho_2; P_{\|\mathbf{X}\|}) \\ &\quad = -(\rho_1^2 - \rho_2^2)\int_0^\infty f_Q(y;\rho_1,\rho_2)\frac{d}{dy}\log\frac{f_{\|\mathbf{Y}\|^2}(y; P_{\|\mathbf{X}\|})}{y^{\mathsf{N}-1}}dy. \end{aligned} \tag{3.94}$$

The derivative in (3.94) is such that

$$\frac{d}{dy}\log\frac{f_{\|\mathbf{Y}\|^2}(y; P_{\|\mathbf{X}\|})}{y^{\mathsf{N}-1}} \tag{3.95}$$

$$\overset{(a)}{=} \frac{y^{\mathsf{N}-1}}{f_{\|\mathbf{Y}\|^2}(y; P_{\|\mathbf{X}\|})}\int_0^{\mathsf{R}} \frac{d}{dy}\frac{f_{\chi^2_{2\mathsf{N}}(\rho^2)}(y)}{y^{\mathsf{N}-1}}dP_{\|\mathbf{X}\|}(\rho) \tag{3.96}$$

$$\overset{(b)}{=} \int_0^{\mathsf{R}} \left(\frac{f_{\chi^2_{2(\mathsf{N}-1)}(\rho^2)}(y)}{2y^{\mathsf{N}-1}} - \left(\frac{1}{2}+\frac{\mathsf{N}-1}{y}\right)\frac{f_{\chi^2_{2\mathsf{N}}(\rho^2)}(y)}{y^{\mathsf{N}-1}}\right)dP_{\|\mathbf{X}\|}(\rho) \\ \frac{y^{\mathsf{N}-1}}{f_{\|\mathbf{Y}\|^2}(y; P_{\|\mathbf{X}\|})} \tag{3.97}$$

$$= \mathsf{E}\left[\frac{1}{2}\frac{f_{\chi^2_{2(\mathsf{N}-1)}(\|\mathbf{X}\|^2)}(\|\mathbf{Y}\|^2)}{f_{\chi^2_{2\mathsf{N}}(\|\mathbf{X}\|^2)}(\|\mathbf{Y}\|^2)} - (\frac{1}{2}+\frac{\mathsf{N}-1}{\|\mathbf{Y}\|^2}) \mid \|\mathbf{Y}\|^2 = y\right] \tag{3.98}$$

$$= \mathsf{E}\left[\frac{1}{2}\frac{\|\mathbf{X}\|}{\|\mathbf{Y}\|}\frac{I_{\mathsf{N}-2}(\|\mathbf{X}\|\|\mathbf{Y}\|)}{I_{\mathsf{N}-1}(\|\mathbf{X}\|\|\mathbf{Y}\|)} - (\frac{1}{2}+\frac{\mathsf{N}-1}{\|\mathbf{Y}\|^2}) \mid \|\mathbf{Y}\|^2 = y\right] \tag{3.99}$$

where step (a) holds thanks to $f_{\|\mathbf{Y}\|^2}(y; P_{\|\mathbf{X}\|}) = \int_0^{\mathsf{R}} f_{\chi^2_{2\mathsf{N}}(\rho^2)}(y) dP_{\|\mathbf{X}\|}(\rho)$ and step (b) to

$$\frac{d}{dy} f_{\chi^2_{2\mathsf{N}}(\rho^2)}(y) = \frac{1}{2} f_{\chi^2_{2(\mathsf{N}-1)}(\rho^2)}(y) - \frac{1}{2} f_{\chi^2_{2\mathsf{N}}(\rho^2)}(y). \tag{3.100}$$

By plugging (3.99) into (3.94), we obtain

$$\begin{aligned} &i(\rho_1; P_{\|\mathbf{X}\|}) - i(\rho_2; P_{\|\mathbf{X}\|}) = \\ &- (\rho_1^2 - \rho_2^2) \mathsf{E}\left[\mathsf{E}\left[\frac{1}{2} \frac{\|\mathbf{X}\|}{\|\mathbf{Y}\|} \frac{I_{\mathsf{N}-2}(\|\mathbf{X}\|\|\mathbf{Y}\|)}{I_{\mathsf{N}-1}(\|\mathbf{X}\|\|\mathbf{Y}\|)} - (\frac{1}{2} + \frac{\mathsf{N}-1}{\|\mathbf{Y}\|^2}) \mid \|\mathbf{Y}\|^2 = Q\right]\right]. \end{aligned} \tag{3.101}$$

Let us now evaluate the derivative of the information density as follows

$$\begin{aligned} &i'(\rho; P_{\|\mathbf{X}\|}) \\ &= \lim_{h \to 0} \frac{i(\rho + h; P_{\|\mathbf{X}\|}) - i(\rho; P_{\|\mathbf{X}\|})}{h} \end{aligned} \tag{3.102}$$

$$= -2\rho\, \mathsf{E}\left[\mathsf{E}\left[\frac{1}{2} \frac{\|\mathbf{X}\|}{\|\mathbf{Y}\|} \frac{I_{\mathsf{N}-2}(\|\mathbf{X}\|\|\mathbf{Y}\|)}{I_{\mathsf{N}-1}(\|\mathbf{X}\|\|\mathbf{Y}\|)} - (\frac{1}{2} + \frac{\mathsf{N}-1}{\|\mathbf{Y}\|^2}) \mid \|\mathbf{Y}\|^2 = Q'\right]\right] \tag{3.103}$$

where $Q' \sim \chi^2_{2(\mathsf{N}+1)}(\rho^2)$, see the following Lemma. □

Lemma 2. *We have*

$$\lim_{h \to 0} f_Q(y; \rho + h, \rho) = f_{\chi^2_{2(\mathsf{N}+1)}(\rho^2)}(y), \qquad y > 0. \tag{3.104}$$

Proof. Given (3.93), it holds

$$\lim_{h \to 0} f_Q(y; \rho + h, \rho) \tag{3.105}$$

$$= \lim_{h\to 0} \frac{F_{\chi^2_{2\mathsf{N}}(\rho^2)}(y) - F_{\chi^2_{2\mathsf{N}}((\rho+h)^2)}(y)}{h(2\rho+h)} \tag{3.106}$$

$$= \lim_{h\to 0} \frac{1}{h(2\rho+h)} \int_0^y \Big(f_{\chi^2_{2\mathsf{N}}(\rho^2)}(t) - f_{\chi^2_{2\mathsf{N}}((\rho+h)^2)}(t) \Big) dt \tag{3.107}$$

$$= \frac{1}{2\rho} \int_0^y \sum_{i=0}^{\infty} \lim_{h\to 0} \frac{1}{h} \left(\frac{e^{-\rho^2/2}(\rho^2/2)^i}{i!} - \frac{e^{-(\rho+h)^2/2}((\rho+h)^2/2)^i}{i!} \right) \tag{3.108}$$

$$f_{\chi^2_{2\mathsf{N}+2i}}(t)dt$$

$$= \frac{1}{2\rho} \int_0^y \sum_{i=0}^{\infty} \frac{d}{d\rho} \left(\frac{e^{-\rho^2/2}(\rho^2/2)^i}{i!} \right) f_{\chi^2_{2\mathsf{N}+2i}}(t)dt \tag{3.109}$$

$$= \frac{1}{2} \int_0^y \sum_{i=0}^{\infty} \left(-\frac{e^{-\rho^2/2}(\rho^2/2)^i}{i!} + \frac{e^{-\rho^2/2}(\rho^2/2)^{i-1}}{(i-1)!} \mathbb{1}(i \geq 1) \right) f_{\chi^2_{2\mathsf{N}+2i}}(t)dt \tag{3.110}$$

$$= \frac{1}{2} \int_0^y \Big(-f_{\chi^2_{2\mathsf{N}}(\rho^2)}(t) + f_{\chi^2_{2(\mathsf{N}+1)}(\rho^2)}(t) \Big) dt \tag{3.111}$$

$$= \int_0^y \frac{d}{dt} f_{\chi^2_{2(\mathsf{N}+1)}(\rho^2)}(t)dt \tag{3.112}$$

$$= f_{\chi^2_{2(\mathsf{N}+1)}(\rho^2)}(y), \tag{3.113}$$

where $\mathbb{1}(\cdot)$ is the indicator function. □

3.8.2 Partial Derivatives of the Secrecy Information

Let us consider the information density $i(\,\cdot\,; P_{\|\mathbf{X}\|})$ for the channel model of Definition 2.1.3 defined in (3.82). The derivative of the non-central chi square PDF is given by

$$\begin{aligned} &\frac{\partial}{\partial \rho^2} \Big[f_{\chi^2_{2\mathsf{N}}(\rho^2/\sigma_z^2)}(z) \Big] \\ &= \frac{\partial}{\partial \rho^2} \frac{1}{2} e^{-\frac{1}{2}(z + \frac{\rho^2}{\sigma_z^2})} \left(\frac{z}{\rho^2} \sigma_z^2 \right)^{\frac{\mathsf{N}-1}{2}} I_{\mathsf{N}-1}\Big(\frac{\rho}{\sigma} \sqrt{z} \Big) \end{aligned} \tag{3.114}$$

$$
\begin{aligned}
&= -\frac{1}{2}e^{-\frac{1}{2}(z+\frac{\rho^2}{\sigma_z^2})}\left(\frac{z}{\rho^2}\sigma_z^2\right)^{\frac{\mathsf{N}-1}{2}} I_{\mathsf{N}-1}\left(\frac{\rho}{\sigma}\sqrt{z}\right)\cdot\frac{1}{2\sigma_z^2} \\
&\quad -\frac{1}{2}e^{-\frac{1}{2}(z+\frac{\rho^2}{\sigma_z^2})}\left(\frac{z}{\rho^2}\sigma_z^2\right)^{\frac{\mathsf{N}-1}{2}} I_{\mathsf{N}-1}\left(\frac{\rho}{\sigma}\sqrt{z}\right)\cdot 2\frac{\mathsf{N}-1}{2\rho^2} \qquad (3.115) \\
&\quad +\frac{1}{2}e^{-\frac{1}{2}(z+\frac{\rho^2}{\sigma_z^2})}\left(\frac{z}{\rho^2}\sigma_z^2\right)^{\frac{\mathsf{N}-2}{2}} I_{\mathsf{N}-2}\left(\frac{\rho}{\sigma}\sqrt{z}\right)\cdot\left(\frac{z}{2\rho^2}\right) \\
&= \left(\frac{1-\mathsf{N}}{\rho^2}-\frac{1}{2\sigma_z^2}\right) f_{\chi^2_{2\mathsf{N}}(\rho^2/\sigma_z^2)}(z) + \left(\frac{z}{2\rho^2}\right) f_{\chi^2_{2\mathsf{N}-2}(\rho^2/\sigma_z^2)}(z). \qquad (3.116)
\end{aligned}
$$

Furthermore, given that

$$
\frac{\partial}{\partial\rho_j^2}\left[\log\frac{z^{\mathsf{N}-1}}{\sum_{i=1}^{\mathsf{K}} p_i f_{\chi^2_{2\mathsf{N}}(\rho_i^2/\sigma_z^2)}(z)}\right] = -p_j\frac{\frac{\partial}{\partial\rho_j^2}\left[f_{\chi^2_{2\mathsf{N}}(\rho_j^2/\sigma_z^2)}(z)\right]}{\sum_{i=1}^{\mathsf{K}} p_i f_{\chi^2_{2\mathsf{N}}(\rho_i^2/\sigma_z^2)}(z)}, \qquad (3.117)
$$

we obtain

$$
\begin{aligned}
&\frac{\partial}{\partial\rho_j^2}\left[f_{\chi^2_{2\mathsf{N}}(\rho_j^2/\sigma_z^2)}(z)\log\frac{z^{\mathsf{N}-1}}{\sum_{i=1}^{\mathsf{K}} p_i f_{\chi^2_{2\mathsf{N}}(\rho_i^2/\sigma_z^2)}(z)}\right] = \\
&\qquad \log\left(\frac{z^{\mathsf{N}-1}}{\sum_{i=1}^{\mathsf{K}} p_i f_{\chi^2_{2\mathsf{N}}(\rho_i^2/\sigma_z^2)}(z)}\right)\frac{\partial}{\partial\rho_j^2}\left[f_{\chi^2_{2\mathsf{N}}(\rho_j^2/\sigma_z^2)}(z)\right] \qquad (3.118) \\
&\qquad -p_j\frac{f_{\chi^2_{2\mathsf{N}}(\rho_j^2/\sigma_z^2)}(z)}{\sum_{i=1}^{\mathsf{K}} p_i f_{\chi^2_{2\mathsf{N}}(\rho_i^2/\sigma_z^2)}(z)}\frac{\partial}{\partial\rho_j^2}\left[f_{\chi^2_{2\mathsf{N}}(\rho_j^2/\sigma_z^2)}(z)\right].
\end{aligned}
$$

Finally, we have that

$$
\begin{aligned}
&\frac{\partial}{\partial\rho_j^2}\sum_{k=1}^{\mathsf{K}} p_k\cdot i(\rho_k;P_{\|\mathbf{x}\|}) \\
&\qquad = \sum_{k=1}^{\mathsf{K}} p_k\int_0^\infty\frac{\partial}{\partial\rho_j^2}\left[f_{\chi^2_{2\mathsf{N}}(\rho_k^2/\sigma_z^2)}(z)\log\frac{z^{\mathsf{N}-1}}{\sum_{i=1}^{\mathsf{K}} p_i f_{\chi^2_{2\mathsf{N}}(\rho_i^2/\sigma_z^2)}(z)}\right]dz
\end{aligned} \qquad (3.119)
$$

$$= p_j \int_0^\infty \frac{\partial}{\partial \rho_j^2} \left[f_{\chi^2_{2\mathsf{N}}(\rho_j^2/\sigma_z^2)}(z) \log \frac{z^{\mathsf{N}-1}}{\sum_{i=1}^{\mathsf{K}} p_i f_{\chi^2_{2\mathsf{N}}(\rho_i^2/\sigma_z^2)}(z)} \right] dz$$
$$+ \sum_{k \neq j}^{\mathsf{K}} p_k \int_0^\infty f_{\chi^2_{2\mathsf{N}}(\rho_k^2/\sigma_z^2)}(z) \frac{\partial}{\partial \rho_j^2} \left[\log \frac{z^{\mathsf{N}-1}}{\sum_{i=1}^{\mathsf{K}} p_i f_{\chi^2_{2\mathsf{N}}(\rho_i^2/\sigma_z^2)}(z)} \right] dz. \tag{3.120}$$

PART II

Fading Channels

Let us now consider fading channels. The immediate consequence is that our channel model will also include a channel matrix H. The results derived in the following part are valid for any full rank channel matrix. The fading is characterized by a channel matrix H, which is random, but known and fixed throughout the considered channel uses. While for nonfading channel the structure of the capacity-achieving input distribution is known, this is not the case for fading channels. Therefore, the focus in this part will be on the derivation of bounds on the channel capacity.

Chapter 4

Capacity Bounds

In this chapter, upper bounds based on the capacity of amplitude-constrained fading channels are introduced. The channel model used throughout this chapter is that of Definition 2.1.2. The first bound is based on a sphere packing argument and it can be adapted to any convex constraint region $\mathcal{X}$ and, therefore, also those introduced in Chapter 2. The second upper bound uses an entirely different approach and targets specifically the AS and PA constraints. To better contextualize these bounds, let us first introduce the main results that were available in the literature prior to both the presented upper bounds.

4.1 Literature Review

One of the main contribution in the investigation of the channel capacity for fading amplitude-constrained channels is presented in [39]. The authors of [39] develop both capacity upper and lower bounds. Given the constraint region $\mathcal{X}$, let us refer to $\mathsf{H}\mathcal{X}$ as output constraint region. They derive duality upper bounds by considering an enlarged output

constraint region $\mathcal{D} \supset \mathsf{H}\mathcal{X}$. This approach, although suboptimal, is viable for any convex constraint region $\mathcal{X}$. Note that there exist special cases for which one can still use a duality approach tailored on $\mathsf{H}\mathcal{X}$, see [41], but they only apply to specific $\mathcal{X}$. The enlarged constraint region $\mathcal{D}$ is designed to make the derivation of an upper bound feasible. The techniques presented in [39] consider $\mathcal{D}$ to be either a ball or a box, specifically, the smallest ball or box containing the original output constraint region $\mathsf{H}\mathcal{X}$. Let us denote by $\mathcal{D}_1$ the $(2\mathsf{N})$-dimensional ball of radius $d_1 = r_{\max}(\mathsf{H}\mathcal{X})$ and by $\mathcal{D}_2$ the smallest box containing $\mathsf{H}\mathcal{X}$. The resulting duality upper bounds derived in [39, Theorem 10] are

$$\mathsf{C} \leq \overline{\mathsf{C}}_{\mathrm{D},1} \triangleq \log\left(c_{2\mathsf{N}}(d_1) + \frac{\mathrm{Vol}_{2\mathsf{N}}(\mathcal{D}_1)}{(2\pi e\sigma_z^2)^{\mathsf{N}}}\right), \tag{4.1}$$

where $c_{2\mathsf{N}}(d_1) = \sum_{j=0}^{2\mathsf{N}-1} \binom{2\mathsf{N}-1}{j} \frac{\Gamma(\mathsf{N}-j/2)}{2^{j/2}\Gamma(\mathsf{N})} (d_1/\sigma_z)^j$ and

$$\mathsf{C} \leq \overline{\mathsf{C}}_{\mathrm{D},2} \triangleq \sum_{j=1}^{2\mathsf{N}} \log\left(1 + \frac{d_{2,j}}{\sqrt{2\pi e\sigma_z^2}}\right), \tag{4.2}$$

where $d_{2,j}$ is the jth side length of the box $\mathcal{D}_2$. Although introducing $\mathcal{D}$ makes the upper bound fairly general, the main drawback comes from the fact that the more $\mathcal{D}$ differs from $\mathsf{H}\mathcal{X}$ the less accurate the bounds become. Loosely speaking, better results than those in [39] can be achieved if one is able to derive an upper bound that depends on a more suitable constraint region $\mathcal{S}$ such that $\mathcal{D} \supset \mathcal{S} \supseteq \mathsf{H}\mathcal{X}$.

As for the lower bound, the main result is given by the generalization to fading channels and any constraint region $\mathcal{X}$ of the EPI lower bound defined in (3.62) for the nonfading case. By following the derivation in [39, Theorem 12], we define the EPI lower bound for

amplitude-constrained fading channels as

$$\mathsf{C} \geq \underline{\mathsf{C}}_{\text{EPI}} \triangleq \mathsf{N} \log\left(1 + \frac{\det(\mathsf{H})^{1/\mathsf{N}} \mathrm{Vol}_{2\mathsf{N}}(\mathcal{X})^{1/\mathsf{N}}}{2\pi e \sigma_z^2}\right). \tag{4.3}$$

In [49], we introduce a slightly improved variant of the EPI lower bound, which is defined as follows. Let λ_i be the ith singular value of H. Whenever even just a single $\lambda_i \approx 0$, we have that $\underline{\mathsf{C}}_{\text{EPI}} \approx 0$. Intuitively, since all the other singular values are nonvanishing, the capacity should not be vanishing as well. The EPI lower bound is not able to, roughly speaking, exclude the vanishing singular value because of the term $\det(\mathsf{H}) = \prod_{i=1}^{2\mathsf{N}} \lambda_i$. Let us assume that the MIMO channel is rearranged in such a way that $\lambda_1 \geq \cdots \geq \lambda_{2\mathsf{N}}$. Then, if a given λ_i is vanishing, then all $\lambda_{i+1}, \ldots, \lambda_{2\mathsf{N}}$ will be vanishing as well. Let us introduce a variant of the EPI lower bound and refer to it as Piecewise Entropy Power Inequality (P-EPI) lower bound. By EPI and data processing inequality, for any $k = 1, \ldots, 2\mathsf{N}$, it holds

$$\mathsf{C} \geq \sup_{f_{\mathbf{X}_1^k} \colon \mathbf{X}_1^k \in \mathcal{X}_1^k} \mathrm{I}\big(\mathbf{X}_1^k ; \mathbf{Y}_1^k\big) \tag{4.4}$$

$$\geq \frac{k}{2} \log\left(1 + \frac{\left(\prod_{i=1}^{k} \lambda_i^{2/k}\right) \mathrm{Vol}_k\big(\mathcal{X}_1^k\big)^{2/k}}{2\pi e \sigma_z^2}\right), \tag{4.5}$$

where $f_{\mathbf{X}_1^k}$ is the input distribution of $\mathbf{X}_1^k = (X_1, \ldots, X_k)^T$ and the vector $\mathbf{Y}_1^k$ is defined similarly to $\mathbf{X}_1^k$. Moreover, $\mathcal{X}_1^k$ is the projection of $\mathcal{X}$ onto the subspace $\mathbb{R}^k$. Then, we define the P-EPI lower bound as

follows

$$\mathsf{C} \geq \underline{\mathsf{C}}_{\text{P-EPI}} \triangleq \max_{k} \frac{k}{2} \log \left(1 + \frac{\left(\prod_{i=1}^{k} \lambda_i^{2/k} \right) \mathrm{Vol}_k \left(\mathcal{X}_1^k \right)^{2/k}}{2\pi e \sigma_z^2} \right), \tag{4.6}$$

where $k = 1, \ldots, 2\mathsf{N}$. Notice that the maximization is carried out separately at each SNR level.

4.2 Sphere Packing Upper Bound

Let us now focus on the derivation of the sphere packing bound. Similarly to the duality upper bounds in [39], the sphere packing bound can be applied to any convex constraint region and for any full rank channel matrix. Furthermore, the sphere packing bound converges asymptotically to the capacity as the SNR goes to infinity. The proposed bound heavily relies on concepts of convex geometry and in particular with functionals associated with a convex set, called *intrinsic volumes*. Therefore, the next section provides a brief introduction to the most relevant geometrical concepts for the definition of the bound.

4.2.1 Convex Geometry Preliminaries

Let $\mathcal{K}$ be a convex body in $\mathbb{R}^n$. The Lebesgue measure of $\mathcal{K}$, i.e., its n-dimensional volume, is denoted by $\mathrm{Vol}_n(\mathcal{K})$. In convex geometry, the well known n-volume is one of the important geometric functionals that can be associated with a given set $\mathcal{K}$. These functionals are called intrinsic volumes. Let us denote by $\mathrm{V}_j(\mathcal{K})$ the jth intrinsic volume of $\mathcal{K}$, with $j = 0, \ldots, n$. Intrinsic volumes are nonnegative, homogeneous, and monotonic functionals and represent a fundamental

measure of content for a convex body [91]. The jth intrinsic volume is obtained by rotating uniformly at random the set $\mathcal{K}$, projecting it onto a j-dimensional subspace and evaluating the average j-dimensional volume of the rotated projections of $\mathcal{K}$. Formally, let us denote by P_j an $n \times n$ orthogonal matrix, projecting any point onto a given j-dimensional subspace of $\mathbb{R}^n$. Furthermore, let us denote by Q an $n \times n$ random rotation matrix drawn uniformly from the Haar measure[1] on the compact, homogeneous group of $n \times n$ orthogonal matrices with determinant one.

Definition 4.2.1 (Intrinsic Volumes)

The jth intrinsic volume of a convex set $\mathcal{K}$ is defined as

$$\mathrm{V}_j(\mathcal{K}) \triangleq \binom{n}{j} \frac{\kappa_n}{\kappa_j \kappa_{n-j}} \mathsf{E}[\mathrm{Vol}_j(\mathsf{P}_j \mathsf{Q} \mathcal{K})], \quad j = 0, \ldots, n, \tag{4.7}$$

where the expectation is taken with respect to the random rotation matrix Q and where $\kappa_i \triangleq \pi^{\frac{i}{2}} / \Gamma\left(\frac{i}{2} + 1\right)$ is the volume of the i-dimensional unit ball.

Notice that the nth intrinsic volume of $\mathcal{K}$ is the volume $\mathrm{Vol}_n(\mathcal{K})$. Moreover, the surface area of $\mathcal{K}$ can be evaluated as $2\mathrm{V}_{n-1}(\mathcal{K})$, while $2\mathrm{V}_1(\mathcal{K})\kappa_{n-1}/(n\kappa_n)$ is the mean width, and $\mathrm{V}_0(\mathcal{K}) = 1$ is the Euler characteristic [93]. Let us consider a simple example to better understand Definition 4.2.1. Let $\mathcal{K}$ be a cube. In Fig. 4.1, it is given a graphical representation of the steps required in the evaluation of $\mathrm{Vol}_j(\mathsf{P}_j \mathsf{Q} \mathcal{K})$ in (4.7), for the intrinsic volume $\mathrm{V}_2(\mathcal{K})$. The random matrix Q rotates the cube, while P_2 projects it onto a plane. Then, the volume $\mathrm{Vol}_2(\mathsf{P}_2 \mathsf{Q} \mathcal{K})$ corresponds to the measure of the gray area in Fig. 4.1.

[1] A rigorous definition of the Haar measure can be found in [92].

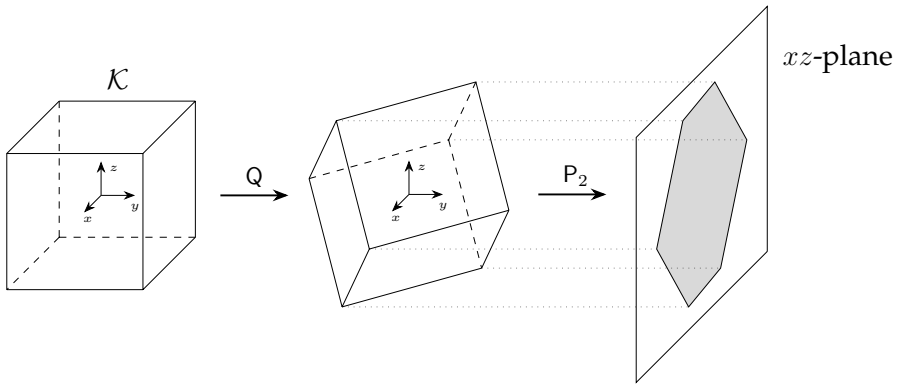

Figure 4.1: *Example of rotation and projection of a cube $\mathcal{K}$ for the evaluation of the 2nd intrinsic volume $\mathrm{V}_2(\mathcal{K})$.*

Averaging this area over random rotations Q and scaling it by the factor $\binom{n}{j}\frac{\kappa_n}{\kappa_j\kappa_{n-j}}$ provides $\mathrm{V}_2(\mathcal{K})$.

To better characterize these functionals, it is also useful to present their most important properties. They are nonnegative

$$\mathrm{V}_j(\mathcal{K}) \geq 0, \quad \forall j. \tag{4.8}$$

As mentioned, intrinsic volumes are also homogeneous functionals. Then, given $\mathsf{R} \in \mathbb{R}_+$ we have

$$\mathrm{V}_j(\mathsf{R}\mathcal{K}) = \mathsf{R}^j \mathrm{V}_j(\mathcal{K}), \quad \forall j. \tag{4.9}$$

Given a set $\mathcal{K}$ such that $\mathcal{K} \supset \mathcal{R}$, thanks to their monotonicity it holds

$$\mathrm{V}_j(\mathcal{K}) \geq \mathrm{V}_j(\mathcal{R}), \ \forall j. \tag{4.10}$$

Another relevant application of the intrinsic volumes in the field of convex geometry is Steiner's formula [94, Theorem 4]. Let us first introduce an operator called Minkowski sum. Let $\mathcal{K}$ and $\mathcal{R}$ two convex

subsets of a vector space. The operator $\oplus$ denotes the Minkowski sum and summing the subsets $\mathcal{K}$ and $\mathcal{R}$ results in a new subset obtained by adding each vector in $\mathcal{K}$ to each vector in $\mathcal{R}$

$$\mathcal{K} \oplus \mathcal{R} \triangleq \{\mathbf{k} + \mathbf{r} \mid \mathbf{k} \in \mathcal{K},\ \mathbf{r} \in \mathcal{R}\}. \tag{4.11}$$

Steiner's formula [94, Theorem 4] is another notable result from convex geometry that closely ties the concept of intrinsic volumes to the Minkowski sum and it is given by

$$\mathrm{Vol}_n(\mathcal{K} \oplus \mathcal{B}_\delta^n) = \sum_{j=0}^{n} \mathrm{V}_j(\mathcal{K}) \mathrm{Vol}_{n-j}\left(\mathcal{B}_\delta^{n-j}\right), \tag{4.12}$$

where $\delta \geq 0$. Since the right-hand side of (4.12) is a convolution, it is convenient to define the (logarithmic) generating function of the intrinsic volumes of $\mathcal{K}$ as [94, Theorem 8]

$$G_{\mathcal{K}}(t) = \log\left(\sum_{j=0}^{n} \mathrm{V}_j(\mathcal{K}) e^{jt}\right). \tag{4.13}$$

A property of these generating functions, defined in [91] and relevant in the derivation of the sphere packing bound, is that, given two sets $\mathcal{K}$ and $\mathcal{R}$, it holds

$$G_{\mathcal{K}\times\mathcal{R}}(t) = G_{\mathcal{K}}(t) + G_{\mathcal{R}}(t),\ \forall t \in \mathbb{R}. \tag{4.14}$$

Finally, it is also convenient to provide a definition for the convex conjugate of a function. Let $\mathcal{T}$ be a topological vector space and $\mathcal{T}^*$ be the corresponding dual vector space, i.e., the set of all linear forms on $\mathcal{T}$. Given a function $f : \mathcal{T} \to \mathbb{R} \cup \{-\infty, +\infty\}$, by [95] the convex conjugate

of f is defined as $f^* : \mathcal{T}^* \to \mathbb{R} \cup \{-\infty, +\infty\}$ such that

$$f^*(t^*) \triangleq \sup_{t \in \mathcal{T}} \{t \cdot t^* - f(t)\}. \tag{4.15}$$

4.2.2 Main Upper Bound Definition

In this section, the Sphere Packing (SP) upper bound is introduced. The capacity of Gaussian scalar channels, subject to both average and peak power constraints, is investigated via an SP argument in [94]. The upper bound provided in their work has been the starting point in the definition of the SP upper bound that we proposed in [50]. Let us first introduce the idea behind the bound in [94]. The authors consider $n \to \infty$ channel uses and, therefore, they define the corresponding n-dimensional input constraint region $\mathcal{K}$. Then, thanks to the SP argument, they claim that, roughly speaking and as the SNR increases, the number of noise balls that can be packed into $\mathcal{K}$ is $\approx \mathrm{Vol}_n(\mathcal{K})/\mathrm{Vol}_n(\mathcal{B}_\delta^n)$, where $\mathcal{B}_\delta^n$ is the noise ball. On the other hand, at finite SNR levels, the number of balls cannot be approximated just by considering the mentioned ratio. Nonetheless, it is possible to derive an upper bound as $\mathrm{Vol}_n(\mathcal{K} \oplus \mathcal{B}_\delta^n)/\mathrm{Vol}_n(\mathcal{B}_\delta^n)$, where $\mathcal{K} \oplus \mathcal{B}_\delta^n$ is the Minkowski sum between the input signal space $\mathcal{K}$ and the noise ball $\mathcal{B}_\delta^n$. Notice that the Minkowski sum $\mathcal{K} \oplus \mathcal{B}_\delta^n$ is given by the union of an infinitely many replicas of the noise ball $\mathcal{B}_\delta^n$, centered at each point of $\mathcal{K}$. Let us look at a simple example for a finite value of n. In Fig. 4.2, the red dashed hollow circle represents $\mathcal{K} = \mathcal{B}^2$, the light gray circles are the noise balls, and the dark gray circle is the Minkowski sum between $\mathcal{K}$ and a single noise ball. Therefore, Fig. 4.2 intuitively shows why $\mathrm{Vol}_n(\mathcal{K} \oplus \mathcal{B}_\delta^n)/\mathrm{Vol}_n(\mathcal{B}_\delta^n)$ is an upper bound on the number of balls that

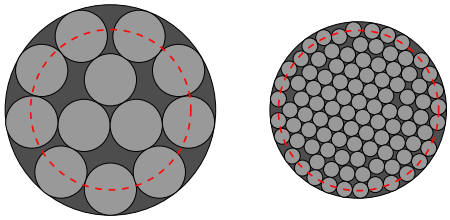

Figure 4.2: *Two sphere packing examples under an amplitude constraint and different SNR values. For both cases, the red dashed circle delimits the border of the input signal space $\mathcal{K} = \mathcal{B}^2$. The dark gray circle is given by the Minkowski sum between $\mathcal{K}$ and the noise ball. The light gray circles represent the noise balls at low SNR, on the left side, at higher SNR, on the right side.*

can be packed in the output signal space. Notice also that Fig. 4.2 shows intuitively how, as the SNR increases, the difference in volume between the dark gray circle and the red dashed hollow circle becomes negligible, i.e., $\lim_{\delta\to 0} \mathrm{Vol}_n(\mathcal{K} \oplus \mathcal{B}_\delta^n) = \mathrm{Vol}_n(\mathcal{K})$. In [94], the authors use this SP argument to define a capacity upper bound as $\limsup_{n\to\infty} \frac{1}{n} \log(\mathrm{Vol}_n(\mathcal{K} \oplus \mathcal{B}_\delta^n)/\mathrm{Vol}_n(\mathcal{B}_\delta^n))$, where $\delta = \sqrt{n\sigma_z^2}$. In [50], we extend their results to amplitude-constrained MIMO fading channels.

Let $n = 2\mathsf{N} \cdot \mathsf{M}$. Then, the n channel uses can be seen as M uses of a $(2\mathsf{N})$-dimensional MIMO channel, with $\mathsf{M} \to \infty$. Moreover, each MIMO channel use is independent of the other and, therefore, the constraint region $\mathcal{K}$ is an M-fold Cartesian product of the output signal space for a single channel use, i.e., $\mathcal{K} = [\mathsf{H}\mathcal{X}]^{\times \mathsf{M}}$. Then, an upper bound on the capacity of MIMO channels can be derived as follows [50].

Theorem 4.2.1

The SP bound is defined as

$$\mathsf{C} \leq \overline{\mathsf{C}}_{\mathsf{SP}} \triangleq \ell(\sigma_z^2) - \mathsf{N} \log\left(2\pi e \sigma_z^2\right), \tag{4.16}$$

where $\ell(\sigma_z^2)$ is

$$\ell(\sigma_z^2) = \sup_{\theta\in[0,1]} \left\{ -2\mathsf{N} \sup_t \left\{ \theta t - \frac{1}{2\mathsf{N}} \log\left(\sum_{j=0}^{2\mathsf{N}} \mathrm{V}_j(\mathsf{H}\mathcal{X}) e^{jt} \right) \right\} + (1-\theta)\mathsf{N} \log \frac{2\pi e \sigma_z^2}{1-\theta} \right\}. \tag{4.17}$$

Proof. See Appendix 4.4.1. □

Notice that, since $\mathsf{h}(\mathbf{Z}) = \mathsf{N}\log(2\pi e\sigma_z^2)$, by (4.16) and (2.6) the term $\ell(\sigma_z^2)$ in Theorem 4.2.1 is an upper bound on the output signal entropy, i.e.,

$$\sup_{F_{\mathbf{X}}:\, \mathrm{supp}(F_{\mathbf{X}})\subseteq\mathcal{X}} \mathsf{h}(\mathbf{Y}) \le \ell(\sigma_z^2). \tag{4.18}$$

Moreover, the SP bound asymptotically converges to the capacity.

Proposition 1. *The capacity gap between the SP bound of Theorem 4.2.1 and the EPI lower bound in* (4.3) *is asymptotically vanishing.*

$$g_{\mathrm{SP}} \triangleq \lim_{\sigma_z^2\to 0} \overline{\mathsf{C}}_{\mathrm{SP}} - \underline{\mathsf{C}}_{\mathrm{EPI}} = 0. \tag{4.19}$$

Proof. See Appendix 4.4.2. □

Notice that the results of Theorem 4.2.1 and Proposition 1 hold for any full rank channel matrix H, any MIMO dimension $2\mathsf{N}$, and any convex constraint region $\mathcal{X}$.

4.2.3 Generalized Sphere Packing

Although, in principle, the SP can be applied to any convex constraint region $\mathcal{X}$, in practice, to compute the term $\ell(\sigma_z^2)$ in Theorem 4.2.1 one has to also evaluate the intrinsic volumes $\mathrm{V}_j(\mathsf{H}\mathcal{X})$, for $j = 0, \ldots, 2\mathsf{N}$. While $\mathrm{V}_0(\mathsf{H}\mathcal{X})$ and $\mathrm{V}_{2\mathsf{N}}(\mathsf{H}\mathcal{X})$ are trivial to evaluate, the other intrinsic volumes can be problematic. They are known just for simple geometric *shapes*. Specifically, for balls and boxes, in closed form, while the intrinsic volumes of ellipsoids can be evaluated numerically [91, 96]. Moreover, even if the intrinsic volumes of $\mathcal{X}$ were known, it would not be trivial to evaluate the intrinsic volumes of $\mathsf{H}\mathcal{X}$. A solution is given by the Generalized Sphere Packing (G-SP) upper bound, defined in [50]. The G-SP approach derives a further upper bound on $\overline{\mathsf{C}}_{\mathrm{SP}}$.

The fundamental concept is similar, in essence, to that of [39]. The authors derive their upper bounds by considering a larger constraint region $\mathcal{D} \supset \mathsf{H}\mathcal{X}$. Since intrinsic volumes describe geometric measures of a set, the same strategy can be applied to the SP bound. Indeed, thanks to (4.10), by considering a larger region $\mathcal{D}$ one can upper-bound the intrinsic volumes of $\mathsf{H}\mathcal{X}$ with those of $\mathcal{D}$. Furthermore, one does not have to choose a single $\mathcal{D}$ for all of the intrinsic volumes, as all of them can be bounded independently. The G-SP approach, that we defined in [50], uses (4.10) to upper-bound each intrinsic volume in the most efficient way possible. One crucial feature of the G-SP approach is that it allows us to keep the last intrinsic volume unaltered. Notice that, as mentioned, $\mathrm{V}_{2\mathsf{N}}(\mathsf{H}\mathcal{X})$ is trivial to evaluate, i.e., $\mathrm{V}_{2\mathsf{N}}(\mathsf{H}\mathcal{X}) = \mathrm{Vol}_{2\mathsf{N}}(\mathsf{H}\mathcal{X}) = \det(\mathsf{H})\mathrm{Vol}_{2\mathsf{N}}(\mathcal{X})$. Moreover, $\mathrm{V}_0(\mathcal{K}) = 1$ for any convex region $\mathcal{K}$. For each $j = 1, \ldots, 2\mathsf{N} - 1$, let $\mathcal{S}_j$ be a convex constraint

region, such that $\mathcal{S}_j \supset \mathsf{H}\mathcal{X}$. Then, the intrinsic volumes of $\mathsf{H}\mathcal{X}$ can be upper-bounded as follows

$$\mathrm{V}_j(\mathsf{H}\mathcal{X}) \leq \overline{\mathrm{V}}_j \triangleq \begin{cases} 1, & j = 0, \\ \mathrm{V}_j(\mathcal{S}_j), & j = 1, \ldots, 2\mathsf{N}-1, \\ \det(\mathsf{H})\mathrm{Vol}_{2\mathsf{N}}(\mathcal{X}), & j = 2\mathsf{N}. \end{cases} \tag{4.20}$$

The $\mathcal{S}_j$'s are chosen among those sets that are the closest to $\mathsf{H}\mathcal{X}$, while still having known intrinsic volumes. By the G-SP approach, let us define the following result.

Lemma 3. *Consider the upper bounds $\overline{\mathrm{V}}_j$ on the intrinsic volumes of $\mathsf{H}\mathcal{X}$ defined in* (4.20)*. The G-SP upper bound is defined as*

$$\mathsf{C} \leq \overline{\mathsf{C}}_{\text{G-SP}} \triangleq \ell_{\mathrm{G}}(\sigma_z^2) - \mathsf{N}\log\big(2\pi e\sigma_z^2\big), \tag{4.21}$$

where $\ell_{\mathrm{G}}(\sigma_z^2)$ is

$$\ell_{\mathrm{G}}(\sigma_z^2) \triangleq \sup_{\theta\in[0,1]} \left\{ -2\mathsf{N}\sup_t \left\{ \theta t - \frac{1}{2\mathsf{N}}\log\left(\sum_{j=0}^{2\mathsf{N}} \overline{\mathrm{V}}_j e^{jt}\right)\right\} + (1-\theta)\mathsf{N}\log\frac{2\pi e\sigma_z^2}{1-\theta}\right\}. \tag{4.22}$$

Proof. The proof follows the same steps of that of Theorem 4.2.1. Aside from the upper bounds $\overline{\mathrm{V}}_j$ on the intrinsic volumes of $\mathsf{H}\mathcal{X}$, the SP and G-SP have the same formulation. Notice that the logarithm is a monotonic increasing function. Moreover, we already mentioned that the intrinsic volumes are always nonnegative. Since each $\mathrm{V}_j(\mathsf{H}\mathcal{X})$ acts as the coefficient of the jth exponential term in the sum of (4.17), upper-

bounding each intrinsic volume via $\overline{\mathrm{V}}_j$ determines a further upper bound on the whole (4.17). In other words, $\ell_{\mathrm{G}}(\sigma_z^2) \geq \ell(\sigma_z^2)$ and, in turn, $\mathsf{C} \leq \overline{\mathsf{C}}_{\text{SP}} \leq \overline{\mathsf{C}}_{\text{G-SP}}$. □

Moreover, keeping the $(2\mathrm{N})$th intrinsic volume unaltered, determines the following results.

Proposition 2. *The capacity gap between the G-SP bound of Lemma 3 and the EPI lower bound in* (4.3) *is asymptotically vanishing.*

$$g_{\text{G-SP}} \triangleq \lim_{\sigma_z^2 \to 0} \overline{\mathsf{C}}_{\text{G-SP}} - \underline{\mathsf{C}}_{\text{EPI}} = 0. \tag{4.23}$$

Proof. As mentioned, beside the intrinsic volumes definition, the formulations of $\ell_{\mathrm{G}}(\sigma_z^2)$ in Lemma 3 and of $\ell(\sigma_z^2)$ in Theorem 4.2.1 are identical. Therefore, as σ_z^2 decreases, similarly to $\ell(\sigma_z^2)$ in (4.103), also $\ell_{\mathrm{G}}(\sigma_z^2)$ tends asymptotically to be equal to $\log(\overline{\mathrm{V}}_{2\mathrm{N}})$. Moreover, since $\overline{\mathrm{V}}_{2\mathrm{N}} = \mathrm{V}_{2\mathrm{N}}(\mathsf{H}\mathcal{X})$, the same result of (4.19) applies also to $g_{\text{G-SP}}$. □

4.2.4 Piecewise Sphere Packing

Let us define another variant based on the SP bound, namely the Piecewise Sphere Packing (P-SP) upper bound. Notice that both the SP and G-SP bounds are asymptotically tight as proven in Proposition 1 and 2. Nonetheless, they can become loose in the low SNR regime. Indeed, as the SNR decreases, the tightness of the SP and, even more so, of the G-SP bounds get worse. The reduced accuracy is due to the Minkowski sum in (4.67). The sum of $[\mathsf{H}\mathcal{X}]^{\times \mathrm{M}}$ with the noise ball $\mathcal{B}_\delta^n$ gives a result that, roughly speaking, is equivalent to the support of a convolution of the noise ball $\mathcal{B}_\delta^n$ over a uniform distribution on $[\mathsf{H}\mathcal{X}]^{\times \mathrm{M}}$. While close to optimal as the SNR goes

to infinity, at low SNR this is far from ideal. Specifically, a true sphere packing argument considers nonoverlapping noise balls, while the Minkowski sum uniformly distributes these balls over $[\mathsf{H}\mathcal{X}]^{\times \mathsf{M}}$. As already mentioned, indeed Fig. 4.2 shows graphically that the Minkowski sum becomes an accurate approximation of the output signal space determined by a true sphere packing only as the SNR increases and the noise balls get smaller. Therefore, let us now define the family of P-SP upper bounds from [50] that provides better results than the SP and G-SP approaches in the low SNR regime.

Lemma 4. *Let us denote the maximum radius of $\mathcal{X}$ by $r \triangleq r_{max}(\mathcal{X})$. Moreover, let us use the singular value decomposition of $\mathsf{H} = \mathsf{U}\Lambda\mathsf{V}^T$. Finally, let $\lambda_1, \ldots, \lambda_{2\mathsf{N}}$ be the diagonal elements of Λ, such that*

$$\lambda_1 \geq \lambda_2 \geq \cdots \geq \lambda_{2\mathsf{N}}. \tag{4.24}$$

Notice that, without loss of generality, we can assume that (4.24) *is always satisfied since this can be achieved by simply rearranging accordingly the MIMO subspaces. Let u and l be any pair of positive integers such that $u + l = 2\mathsf{N}$. The P-SP bound is defined as*

$$\mathsf{C} \leq \overline{\mathsf{C}}_{\text{P-SP}} \triangleq \min_{\substack{u: \\ u+l=2\mathsf{N}}} \sup_{\alpha\in[0,1]} \{\ell_U(\alpha) + \ell_L(\alpha)\} - \mathsf{N}\log(2\pi e\sigma_z^2), \tag{4.25}$$

with $\ell_U(\alpha)$ given by

$$\ell_U(\alpha) \triangleq \sup_{\theta\in[0,1]} \left\{ -u \sup_t \left\{ \theta t - \frac{1}{u}\log\sum_{j=0}^{u} \mathrm{V}_j(\Lambda_U\mathcal{X}_U)e^{jt} \right\} + (1-\theta)\frac{u}{2}\log\frac{2\pi e\sigma_z^2}{1-\theta} \right\}, \tag{4.26}$$

where Λ_U *is the* $u \times u$ *submatrix of* Λ *of diagonal elements* $\lambda_1, \ldots, \lambda_u$ *and* $\mathcal{X}_U = \mathcal{B}^u_{r\sqrt{1-\alpha^2}}$. *Furthermore,* $\ell_L(\alpha)$ *is given by*

$$\ell_L(\alpha) \triangleq \sum_{k=1}^{l} \frac{1}{2} \log\big(2\pi e\big(\lambda^2_{u+k}\mathsf{P}_k(\alpha) + \sigma_z^2\big)\big), \tag{4.27}$$

where $\mathsf{P}_k(\alpha)$ *is the power allocation determined via the water-filling algorithm, for* l *parallel channels and a total power* $\alpha^2 r^2$ *allocated according to* $\sigma_z^2/\lambda^2_{u+1}, \ldots, \sigma_z^2/\lambda^2_{2\mathsf{N}}$.

Proof. See Appendix 4.4.3. □

Remark 6. In general, the asymptotic gap between the P-SP upper bound in Lemma 4 and the EPI lower bound in (4.3) never vanishes, even as the SNR goes to infinity. The only special case for which the capacity gap goes to zero is that of $\mathcal{X}$ being a ball. Notice that, in this special case, for $u = 2\mathsf{N}$ the P-SP formulation is equivalent to that of the standard SP approach and, therefore, by Proposition 1 the P-SP bound converges to the capacity.

4.3 Quasi Parallel Channels Upper Bound

Let us now introduce another upper bound that is particularly relevant for those input constraints that can be decomposed as a Cartesian product of subregions, like the PA and the AS constraints. The idea is to exploit the Cartesian features of the input constraint region and define an upper bound that is given by a sum of *approximately independent* capacity contributions. Indeed, the name Quasi Parallel Channels (QPC) refers to the fact that the bound depends on the sum of the subchannels capacities corresponding to the subspaces in which each

$\mathcal{X}_i$ lies. The term *quasi* stands for the fact that, other than the sum of capacities, the bound depends on a residual nonnegative logarithmic term that, roughly speaking, quantifies how far the subchannels are from being truthfully parallel.

The QPC upper bound is defined as the compound bound given by the minimum between two contributions. The first one is suitable for the high SNR regime and, as mentioned, approximates the capacity as a sum of independent terms plus a distortion term. On the other hand, for the low SNR regime, a similar approach to that of the P-SP is used, based on a Gaussian maximum entropy argument.

Let us start with the high SNR regime.

4.3.1 High SNR Regime

Given the vectorized channel of Definition 2.1.2, it is convenient to consider the equivalent channel model multiplied by the inverse of the channel matrix H. Note that since H is known and full rank it is always possible to evaluate its inverse. Therefore, the equivalent channel is defined as

$$\mathsf{H}^{-1}\mathbf{Y} = \mathsf{H}^{-1}\mathsf{H}\cdot\mathbf{X} + \mathsf{H}^{-1}\mathbf{Z} \tag{4.28}$$

$$= \mathbf{X} + \mathsf{H}^{-1}\mathbf{Z} \tag{4.29}$$

$$= \mathbf{X} + \mathbf{Z}_{\mathsf{D}}, \tag{4.30}$$

where $\mathbf{Z}_{\mathsf{D}} = \mathsf{H}^{-1}\mathbf{Z}$ is such that $\mathbf{Z}_{\mathsf{D}} \sim \mathcal{N}(\mathbf{0}_{2\mathsf{N}}, \mathsf{D})$ with covariance matrix $\mathsf{D} = \sigma_z^2\mathsf{H}^{-1}\mathsf{H}^{-T}$. Let us consider the AS constraint region $\mathcal{X}$ of Definition 2.3.3. Moreover, let $\mathsf{D}_{k,l}$ denote the element (k,l) of D and let D_i be

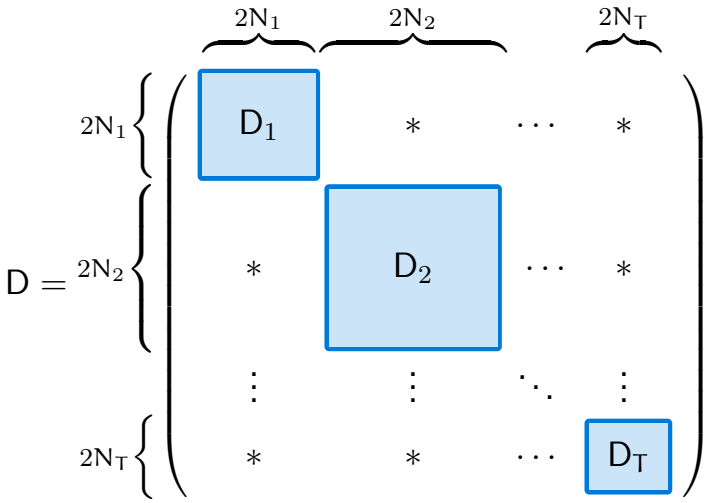

Figure 4.3: *Diagram of the block diagonal submatrices of* D.

the block submatrices, on the main-diagonal of D, given by

$$\mathsf{D}_i \triangleq [\mathsf{D}_{k,l}]_{k,l=m_i+1}^{m_i+2\mathsf{N}_i}, \quad i = 1, \ldots, \mathsf{T}, \tag{4.31}$$

where $m_i = \sum_{j=1}^{i-1} 2\mathsf{N}_j$ and $m_1 = 0$. See Figure 4.3 for a more intuitive graphical representation. Finally, let $\mathbf{X}_i$ be the $2\mathsf{N}_i \times 1$ subvector of $\mathbf{X}$ such that $\mathbf{X}_i = (X_{m_i+1}, X_{m_i+2}, \ldots, X_{m_i+2\mathsf{N}_i})^T$ and

$$\mathbf{X} = \Big(\overbrace{X_1, \ldots, X_{2\mathsf{N}_1}}^{\mathbf{X}_1 \in \mathbb{R}^{2\mathsf{N}_1}}, \ \ldots \ , \overbrace{X_{m_\mathsf{T}+1}, \ldots, X_{2\mathsf{N}}}^{\mathbf{X}_\mathsf{T} \in \mathbb{R}^{2\mathsf{N}_\mathsf{T}}} \Big)^T \tag{4.32}$$

$$= (\mathbf{X}_1, \ldots, \mathbf{X}_\mathsf{T})^T. \tag{4.33}$$

Consider also a similar partition of the vector $\mathbf{Z}_\mathsf{D}$ into the subvectors $\mathbf{Z}_{\mathsf{D},i} \in \mathbb{R}^{2\mathsf{N}_i}$.

Theorem 4.3.1 (Quasi Parallel Channels: High SNR)

Given a constraint region $\mathcal{X}$ that can be decomposed in a Cartesian

product of subregions, as defined in (2.12), an upper bound on the channel capacity is given by

$$\mathsf{C} \leq \overline{\mathsf{C}}_1 \triangleq \left(\sum_{i=1}^{\mathsf{T}} \mathsf{C}_i \right) + \frac{1}{2} \log \frac{\prod_{j=1}^{\mathsf{T}} \det(\mathsf{D}_j)}{\det(\mathsf{D})}, \tag{4.34}$$

where

$$\mathsf{C}_i \triangleq \max_{f_{\mathbf{X}_i} \colon \mathbf{X}_i \in \mathcal{X}_i} \mathsf{h}(\mathbf{X}_i + \mathbf{Z}_{\mathsf{D},i}) - \mathsf{h}(\mathbf{Z}_{\mathsf{D},i}) \tag{4.35}$$

and $\mathbf{Z}_{\mathsf{D},i} \sim \mathcal{N}(\mathbf{0}_{2\mathsf{N}_i}, \mathsf{D}_i)$.

Proof.

$$\begin{aligned}
\mathsf{C} &= \max_{f_{\mathbf{X}} \colon \mathbf{X} \in \mathcal{X}} \mathrm{I}(\mathbf{X}\,; \mathsf{H}\mathbf{X} + \mathbf{Z}) && (4.36)\\
&= \max_{f_{\mathbf{X}} \colon \mathbf{X} \in \mathcal{X}} \mathrm{I}(\mathbf{X}\,; \mathbf{X} + \mathbf{Z}_{\mathsf{D}}) && (4.37)\\
&= \max_{f_{\mathbf{X}} \colon \mathbf{X} \in \mathcal{X}} \mathsf{h}(\mathbf{X} + \mathbf{Z}_{\mathsf{D}}) - \mathsf{h}(\mathbf{Z}_{\mathsf{D}}) && (4.38)\\
&\overset{(a)}{\leq} \left(\max_{f_{\mathbf{X}} \colon \mathbf{X} \in \mathcal{X}} \sum_{i=1}^{\mathsf{T}} \mathsf{h}(\mathbf{X}_i + \mathbf{Z}_{\mathsf{D},i}) \right) + \frac{1}{2} \log \frac{1}{\det(\mathsf{D})} \\
&\quad - \mathsf{N} \log(2\pi e) && (4.39)\\
&= \left(\sum_{i=1}^{\mathsf{T}} \max_{f_{\mathbf{X}_i} \colon \mathbf{X}_i \in \mathcal{X}_i} \mathsf{h}(\mathbf{X}_i + \mathbf{Z}_{\mathsf{D},i}) \right) + \frac{1}{2} \log \frac{1}{\det(\mathsf{D})} \\
&\quad - \mathsf{N} \log(2\pi e) + \frac{1}{2} \log \frac{\prod_{j=1}^{\mathsf{T}} \det(\mathsf{D}_j)}{\prod_{k=1}^{\mathsf{T}} \det(\mathsf{D}_k)} && (4.40)\\
&= \left(\sum_{i=1}^{\mathsf{T}} \max_{f_{\mathbf{X}_i} \colon \mathbf{X}_i \in \mathcal{X}_i} \mathsf{h}(\mathbf{X}_i + \mathbf{Z}_{\mathsf{D},i}) - \mathsf{h}(\mathbf{Z}_{\mathsf{D},i}) \right) \\
&\quad + \frac{1}{2} \log \frac{\prod_{j=1}^{\mathsf{T}} \det(\mathsf{D}_j)}{\det(\mathsf{D})}, && (4.41)
\end{aligned}$$

where the step (a) derives from the subadditivity of the differential entropy, while $\mathbf{Z}_{\mathsf{D},i}$ is the result of the marginalization of $\mathbf{Z}_{\mathsf{D}}$ on the ith subspace to which $\mathcal{X}_i$ belongs. Since $\mathbf{Z}_{\mathsf{D}}$ is multivariate Gaussian-distributed with zero mean and covariance matrix D, the result of the marginalization is $\mathbf{Z}_{\mathsf{D},i} \sim \mathcal{N}(\mathbf{0}_{2\mathsf{N}_i}, \mathsf{D}_i)$. Moreover, since $\mathcal{X}$ is a Cartesian product, the capacity-achieving distribution $f_{\mathbf{X}}$ will be a product distribution of the T terms $f_{\mathbf{X}_i}$. Therefore, the maximization in (4.39) can be decomposed and carried out into T independent subspaces, one for each subchannel. Since the maximization is carried over independent subspaces, it is also possible to invert the order of the sum and the maximization in (4.39) without making the bound looser. In (4.40), the logarithmic term $\frac{1}{2}\log\prod_i \det(\mathsf{D}_i)$ is added and subtracted. Finally, the subtracted term is combined with the noise entropy to derive the $\mathrm{h}(\mathbf{Z}_{\mathsf{D},i})$'s in (4.41). □

Remark 7. Since the C_i's depend on the maximization over the $f_{\mathbf{X}_i}$'s, $\overline{\mathsf{C}}_1$ is defined implicitly and requires additional step to be evaluated. Nonetheless, it is possible to evaluate upper bounds on the C_i's via any given suitable technique. For instance, the SP bounds in Section 4.2 can be used for any convex constraint $\mathcal{X}$. Then, the upper bounds on the subchannel capacities C_i's can be used in (4.34) to derive an explicit upper bound on $\overline{\mathsf{C}}_1$. Notice also that, whenever the subregion $\mathcal{X}_i$ is a ball and D_i is a scalar matrix, then we can also apply the upper bounds of [34], defined in Section 4.1, or also the capacity estimate given by Algorithm 1 from Chapter 3.

Remark 8. Using the SP approach on the subchannel capacities C_i's to derive an upper bound on C_1 via the QPC is fundamentally different

than directly applying the SP upper bound to the capacity of the entire channel. Both approaches are viable and yield to different results.

Remark 9. Since D is a covariance matrix, it is positive-semidefinite and by Fischer's inequality [97], it holds that $\det(\mathsf{D}) \leq \prod_{j=1}^{\mathsf{T}} \det(\mathsf{D}_j)$. Then, we have also that

$$\log \frac{\prod_{j=1}^{\mathsf{T}} \det(\mathsf{D}_j)}{\det(\mathsf{D})} \geq 0. \tag{4.42}$$

Remark 10. Loosely speaking, the logarithmic term in (4.34) quantifies the inaccuracy induced by the marginalization of $\mathbf{Z}_{\mathsf{D}}$ on each of the T subspaces. This intuitive interpretation is supported by the fact that, whenever D is block diagonal and has zero off-diagonal elements, $\det(\mathsf{D}) = \prod_{i=1}^{\mathsf{T}} \det(\mathsf{D}_i)$ and, therefore, the logarithmic term $\log \frac{\det(\mathsf{D})}{\prod_j \det(\mathsf{D}_j)}$ vanishes. In this special case, the upper bound in (4.34) becomes the true capacity. Notice that, therefore, the sum $\sum_{i=1}^{\mathsf{T}} \mathsf{C}_i$ accounts for the contribution due to the diagonal submatrices D_i, while the logarithmic term accounts for the *distortion* induced by the off-diagonal terms of D.

As for the SP bounds, the capacity gap given by the difference between $\overline{\mathsf{C}}_1$ and the EPI lower bound in (4.3) goes to zero as the SNR increases.

Lemma 5. *Let $\sigma_z^2 \to 0$. The resulting capacity gap is*

$$\lim_{\sigma_z^2 \to 0} \overline{\mathsf{C}}_1 - \underline{\mathsf{C}} = 0. \tag{4.43}$$

Proof. The mutual information for the ith subchannel is defined as $\mathsf{I}(\mathbf{X}_i\,;\mathbf{X}_i + \mathbf{Z}_{\mathsf{D},i}) = \mathsf{h}(\mathbf{X}_i + \mathbf{Z}_{\mathsf{D},i}) - \mathsf{h}(\mathbf{Z}_{\mathsf{D},i})$. Let M_i denote the $(2\mathsf{N}_i) \times (2\mathsf{N}_i)$ matrix for which $\mathsf{D}_i = \sigma_z^2 \mathsf{M}_i^{-1} \mathsf{M}_i^{-T}$. Again, since D_i is a covari-

ance matrix it is also positive-semidefinite, therefore the matrix M_i can always be computed. Then, we can equivalently express the mutual information as

$$\mathrm{I}(\mathbf{X}_i\,;\mathbf{X}_i+\mathbf{Z}_{\mathsf{D},i})=\mathrm{I}(\mathbf{X}_i\,;\mathsf{M}_i\mathbf{X}_i+\mathbf{Z}_i), \tag{4.44}$$

where $\mathbf{Z}_i\sim\mathcal{N}(\mathbf{0}_{2\mathsf{N}_i},\sigma_z^2\mathsf{I}_{2\mathsf{N}_i})$. Moreover, it holds

$$\lim_{\sigma_z^2\to 0}\sum_{i=1}^{\mathsf{T}}\mathsf{C}_i=\sum_{i=1}^{\mathsf{T}}\max_{f_{\mathbf{X}_i}:\,\mathbf{X}_i\in\mathcal{X}_i}\mathsf{h}(\mathsf{M}_i\mathbf{X}_i)-\lim_{\sigma_z^2\to 0}\mathsf{h}(\mathbf{Z}_i) \tag{4.45}$$

$$=\left(\sum_{i=1}^{\mathsf{T}}\log\mathrm{Vol}_{2\mathsf{N}_i}(\mathsf{M}_i\mathcal{X}_i)\right)-\lim_{\sigma_z^2\to 0}\mathsf{h}(\mathbf{Z}) \tag{4.46}$$

$$=\left(\sum_{i=1}^{\mathsf{T}}\log\det(\mathsf{M}_i)\mathrm{Vol}_{2\mathsf{N}_i}(\mathcal{X}_i)\right)-\lim_{\sigma_z^2\to 0}\mathsf{h}(\mathbf{Z}), \tag{4.47}$$

where (4.46) holds because the uniform distribution over $\mathcal{X}_i$ maximizes the entropy term $\mathsf{h}(\mathsf{M}_i\mathbf{X}_i)$. Notice that

$$\lim_{\sigma_z^2\to 0}\frac{1}{2}\log\frac{\prod_{i=1}^{\mathsf{T}}\det(\mathsf{D}_i)}{\det(\mathsf{D})}=\lim_{\sigma_z^2\to 0}\frac{1}{2}\log\frac{\prod_{i=1}^{\mathsf{T}}\det\left(\sigma_z^2\mathsf{M}_i^{-1}\mathsf{M}_i^{-T}\right)}{\det(\sigma_z^2\mathsf{H}^{-1}\mathsf{H}^{-T})} \tag{4.48}$$

$$=\log\det(\mathsf{H})-\sum_{i=1}^{\mathsf{T}}\log\det(\mathsf{M}_i), \tag{4.49}$$

where we used the following property of the determinant $\det(\mathsf{H}^{-1}\mathsf{H}^{-T})=(\det(\mathsf{H}^{-1}))^2=1/(\det(\mathsf{H}))^2$ for both H and the M_i's.

Given the EPI lower bound, we have that

$$\lim_{\sigma_z^2\to 0}\underline{\mathsf{C}}=\lim_{\sigma_z^2\to 0}\mathsf{N}\log\left(\frac{(\mathrm{Vol}_{2\mathsf{N}}(\mathsf{H}\mathcal{X}))^{\frac{1}{\mathsf{N}}}}{2\pi e\sigma_z^2}\right) \tag{4.50}$$

$$=\lim_{\sigma_z^2\to 0}\log(\mathrm{Vol}_{2\mathsf{N}}(\mathsf{H}\mathcal{X}))-\mathsf{h}(\mathbf{Z}) \tag{4.51}$$

$$= \lim_{\sigma_z^2 \to 0} \log\det(\mathsf{H}) + \log\left(\prod_{i=1}^{\mathsf{T}} \mathrm{Vol}_{\mathsf{N}_i}(\mathcal{X}_i)\right) - \mathrm{h}(\mathbf{Z}). \tag{4.52}$$

Since $\mathcal{X}$ is a Cartesian product, we can evaluate its volume as $\mathrm{Vol}_{2\mathsf{N}}(\mathcal{X}) = \prod_i \mathrm{Vol}_{2\mathsf{N}_i}(\mathcal{X}_i)$.

By putting everything together all these results we obtain the claim

$$\lim_{\sigma_z^2 \to 0} \overline{\mathsf{C}}_1 - \underline{\mathsf{C}} = 0. \tag{4.53}$$

□

Remark 11. In Remark 7, we mentioned that one has to resort to upper bounds on the C_i's to get an explicit formulation for $\overline{\mathsf{C}}_1$. Nonetheless, whenever the upper bounds used on the C_i's converge to the true capacity as the SNR increases, then Lemma 5 is valid also for the resulting upper bounds on $\overline{\mathsf{C}}_1$.

4.3.2 Low SNR Regime

In Remark 9, we already mentioned that the Theorem 4.3.1 is loose in the low SNR regime. Indeed, unless the M_i's are scalar matrices (see Remark 10), $\overline{\mathsf{C}}_1$ never goes to zero as the SNR decreases. Like for the P-SP bound in Section 4.2.4, we derive in an equivalent fashion an upper bound based on a Gaussian maximum entropy argument. Compared to the P-SP approach, in this case we do not adopt a piecewise approach. We either consider all the MIMO dimensions to be at high SNR and, therefore, rely on Theorem 4.3.1, or we consider the noise to be dominant for all MIMO dimensions and use the following Gaussian

maximum entropy argument.

Given the singular value decomposition of the channel matrix H, i.e., $\mathsf{H} = \mathsf{U}\Lambda\mathsf{V}^T$, consider the following equivalent definition.

$$\Lambda^{-1}\bar{\mathbf{Y}} = \bar{\mathbf{X}} + \Lambda^{-1}\bar{\mathbf{Z}} \tag{4.54}$$

$$= \bar{\mathbf{X}} + \bar{\mathbf{Z}}_{\bar{\mathsf{D}}}, \tag{4.55}$$

where $\bar{\mathbf{Y}} = \mathsf{U}^{-1}\mathbf{Y}$, the input is $\bar{\mathbf{X}} = \mathsf{V}^T\mathbf{X}$, and the noise vector is $\bar{\mathbf{Z}}_{\bar{\mathsf{D}}} = \Lambda^{-1}\bar{\mathbf{Z}} = \Lambda^{-1}\mathsf{U}^{-1}\mathbf{Z}$. Once more, since $\mathbf{Z}$ is isotropically distributed, it holds $\bar{\mathbf{Z}} \sim \mathcal{N}(\mathbf{0}_{2\mathsf{N}}, \sigma_z^2\mathsf{I}_{2\mathsf{N}})$ and $\bar{\mathbf{Z}}_{\bar{\mathsf{D}}} \sim \mathcal{N}\big(\mathbf{0}_{2\mathsf{N}}, \bar{\mathsf{D}}\big)$ with $\bar{\mathsf{D}} = \sigma_z^2\Lambda^{-1}\Lambda^{-T}$.

Theorem 4.3.2

Given the constraint region $\mathcal{X}$ defined in (2.12), we derive the following upper bound via a Gaussian maximum entropy argument

$$\mathsf{C} \leq \overline{\mathsf{C}}_2 \triangleq \left(\sum_{i=1}^{2\mathsf{N}} \frac{1}{2}\log(\mathsf{P}_i + \lambda_i(\mathsf{D}))\right) - \frac{1}{2}\log\det(\mathsf{D}), \tag{4.56}$$

where P_i is the power allocation obtained via the water-filling principle, for a total available power $\mathsf{P}_{\text{av}} = (r_{\max}(\mathcal{X}))^2$ and for the noise variances $\lambda_i(\mathsf{D})$'s, with $\lambda_i(\mathsf{D})$ being the ith singular value of D.

Proof. Notice that the proof is mostly the same of that devised in Section 4.4.3. Given the input constraint $\mathcal{X}$ in (2.12) and the looser average power constraint $\mathsf{E}\big[\mathbf{X}^T\mathbf{X}\big] \leq \mathsf{P}_{\text{av}}$, an upper bound on the channel capacity is given by

$$\mathsf{C} = \max_{f_{\mathbf{X}}:\, \mathbf{X}\in\mathcal{X}} \mathrm{I}(\mathbf{X}\,;\mathsf{H}\mathbf{X} + \mathbf{Z}) \tag{4.57}$$

$$= \max_{\substack{f_{\mathbf{X}}:\, \mathbf{X}\in\mathcal{X},\\ \mathsf{E}\left[\mathbf{X}^T\mathbf{X}\right]\leq \mathsf{P}_{\text{av}}}} \mathrm{I}(\mathbf{X}\,;\mathsf{H}\mathbf{X}+\mathbf{Z}) \tag{4.58}$$

$$\leq \max_{f_{\mathbf{X}}:\, \mathsf{E}[\mathbf{X}^T\mathbf{X}]\leq \mathsf{P}_{\text{av}}} \mathrm{I}(\mathbf{X}\,;\mathsf{H}\mathbf{X}+\mathbf{Z}) \tag{4.59}$$

$$= \max_{f_{\bar{\mathbf{X}}}:\, \mathsf{E}\left[\bar{\mathbf{X}}^T\bar{\mathbf{X}}\right]\leq \mathsf{P}_{\text{av}}} \mathrm{I}\big(\bar{\mathbf{X}}\,;\bar{\mathbf{X}}+\bar{\mathbf{Z}}_{\bar{\mathsf{D}}}\big) \tag{4.60}$$

$$= \max_{f_{\bar{\mathbf{X}}}:\, \mathsf{E}\left[\bar{\mathbf{X}}^T\bar{\mathbf{X}}\right]\leq \mathsf{P}_{\text{av}}} \mathsf{h}\big(\Lambda^{-1}\bar{\mathbf{Y}}\big) - \mathsf{h}\big(\bar{\mathbf{Z}}_{\bar{\mathsf{D}}}\big) \tag{4.61}$$

$$\leq \max_{f_{\bar{\mathbf{X}}}:\, \mathsf{E}\left[\bar{\mathbf{X}}^T\bar{\mathbf{X}}\right]\leq \mathsf{P}_{\text{av}}} \mathsf{h}\Big(\widetilde{\mathbf{Y}}\Big) - \mathsf{h}\big(\bar{\mathbf{Z}}_{\bar{\mathsf{D}}}\big) \tag{4.62}$$

$$\leq \max_{f_{\bar{\mathbf{X}}}:\, \mathsf{E}\left[\bar{\mathbf{X}}^T\bar{\mathbf{X}}\right]\leq \mathsf{P}_{\text{av}}} \sum_{i=1}^{2\mathsf{N}} \frac{1}{2}\log\Big(2\pi e\Big(\mathsf{E}\Big[\big|\bar{X}_i\big|^2\Big] + \lambda_i\big(\bar{\mathsf{D}}\big)\Big)\Big) - \frac{1}{2}\log\det\big(2\pi e\bar{\mathsf{D}}\big) \tag{4.63}$$

$$= \left(\sum_{i=1}^{2\mathsf{N}} \frac{1}{2}\log(\mathsf{P}_i + \lambda_i(\mathsf{D}))\right) - \frac{1}{2}\log\det(\mathsf{D}), \tag{4.64}$$

where the upper bound in (4.59) is obtained by removing the constraint $\mathcal{X}$ and in (4.60) we introduced an equivalent formulation based on the model in (4.55). Notice that V^T is a unitary matrix, therefore $\mathsf{E}\big[\mathbf{X}^T\mathbf{X}\big] = \mathsf{E}\big[\bar{\mathbf{X}}^T\bar{\mathbf{X}}\big]$. Let $\widetilde{\mathbf{Y}} \sim \mathcal{N}(\mathbf{0}_{2\mathsf{N}}, \Sigma)$ be a Gaussian-distributed vector, with $\Sigma = \mathsf{E}\big[\bar{\mathbf{X}}\bar{\mathbf{X}}^T\big] + \bar{\mathsf{D}}$. By the Gaussian maximum entropy bound $\mathsf{h}\big(\Lambda^{-1}\bar{\mathbf{Y}}\big) \leq \mathsf{h}(\widetilde{\mathbf{Y}})$, we obtain (4.62), while (4.63) holds by noticing that $\mathsf{h}(\widetilde{\mathbf{Y}}) \leq \sum_i \mathsf{h}(\widetilde{Y}_i)$. Finally, (4.64) is obtained thanks to $\lambda_i\big(\bar{\mathsf{D}}\big) = \lambda_i(\mathsf{D})$ for each i and by applying the water-filling principle. □

Remark 12. It is easy to show that the upper bound $\overline{\mathsf{C}}_2$ is vanishing for $\sigma_z^2 \to \infty$, i.e.,

$$\lim_{\sigma_z^2\to\infty} \overline{\mathsf{C}}_2 = 0. \tag{4.65}$$

Indeed, since the $\lambda_i(\mathsf{D})$ are proportional to σ_z^2, as $\sigma_z^2 \to \infty$ the power allocation terms P_i disappear in the limit. Therefore,

$$\lim_{\sigma_z^2 \to \infty} \overline{\mathsf{C}}_2 = \lim_{\sigma_z^2 \to \infty} \left(\sum_{i=1}^{2\mathsf{N}} \frac{1}{2} \log(\lambda_i(\mathsf{D})) \right) - \frac{1}{2} \log\det(\mathsf{D}) = 0. \tag{4.66}$$

4.4 Appendix

4.4.1 Proof of Theorem 4.2.1

Given an arbitrarily large number, M, of independent channel uses, for $\mathsf{M} \to \infty$ and by [94, Theorem 3], it holds

$$\begin{aligned}
\mathsf{C} &\leq \limsup_{\mathsf{M}\to\infty} \frac{1}{\mathsf{M}} \log \frac{\mathrm{Vol}_n\big([\mathsf{H}\mathcal{X}]^{\times \mathsf{M}} \oplus \mathcal{B}_\delta^n\big)}{\mathrm{Vol}_n(\mathcal{B}_\delta^n)} && (4.67)\\
&= \limsup_{\mathsf{M}\to\infty} \frac{1}{\mathsf{M}} \log \mathrm{Vol}_n\big([\mathsf{H}\mathcal{X}]^{\times \mathsf{M}} \oplus \mathcal{B}_\delta^n\big) - \lim_{\mathsf{M}\to\infty} \frac{1}{\mathsf{M}} \log \mathrm{Vol}_n(\mathcal{B}_\delta^n) && (4.68)\\
&= \limsup_{\mathsf{M}\to\infty} \frac{1}{\mathsf{M}} \log \mathrm{Vol}_n\big([\mathsf{H}\mathcal{X}]^{\times \mathsf{M}} \oplus \mathcal{B}_\delta^n\big) - \mathsf{N} \log\big(2\pi e \sigma_z^2\big), && (4.69)
\end{aligned}$$

where $n = 2\mathsf{N}\mathsf{M}$ and $\delta = \sqrt{n\sigma_z^2}$. Notice that $[\mathsf{H}\mathcal{X}]^{\times \mathsf{M}} \oplus \mathcal{B}_\delta^n$ in (4.69) is a convolution. Then, it useful to define the limiting normalized generating function of $\mathrm{V}_j(\mathsf{H}\mathcal{X})$. Let us ease the notation and define $\mathcal{K} = [\mathsf{H}\mathcal{X}]^{\times \mathsf{M}}$. Then, the corresponding generating function is defined as

$$\begin{aligned}
f(t) &\triangleq \lim_{\mathsf{M}\to\infty} \frac{1}{2\mathsf{N}\mathsf{M}} G_{\mathcal{K}}(t) && (4.70)\\
&= \lim_{\mathsf{M}\to\infty} \frac{1}{2\mathsf{N}\mathsf{M}} G_{[\mathsf{H}\mathcal{X}]^{\times \mathsf{M}}}(t) && (4.71)\\
&\overset{(4.14)}{=} \lim_{\mathsf{M}\to\infty} \frac{\mathsf{M}}{2\mathsf{N}\mathsf{M}} G_{\mathsf{H}\mathcal{X}}(t) && (4.72)
\end{aligned}$$

$$= \frac{1}{2\mathsf{N}} \log \left(\sum_{j=0}^{2\mathsf{N}} \mathrm{V}_j(\mathsf{H}\mathcal{X}) e^{jt} \right), \tag{4.73}$$

where (4.72) holds thanks to (4.14). Note that $\mathsf{H}\mathcal{X}$ is a bounded and convex constraint region and, therefore, its intrinsic volumes exist and are finite. As a consequence, the limit in (4.70) exists as well. By (4.12), we also show that

$$\mathrm{Vol}_n\big([\mathsf{H}\mathcal{X}]^{\times \mathsf{M}} \oplus \mathcal{B}_\delta^n\big) = \sum_{j=0}^{n} \mathrm{V}_j(\mathcal{K}) \mathrm{Vol}_{n-j}\big(\mathcal{B}_\delta^{n-j}\big). \tag{4.74}$$

Furthermore, notice that, as done in [94], the Steiner's formula can be decomposed as a sum of exponentials. Let us define the functions $a_n(\theta)$ and $b_n(\theta)$ with support $\theta \in [0,1]$. The first function, $a_n(\theta)$, is given by the linear interpolation of

$$a_n(j/n) = \frac{1}{n} \log \mathrm{V}_j(\mathcal{K}), \quad j = 0, \ldots, n. \tag{4.75}$$

Then, we can also define the sequence of measures

$$\widetilde{\mathrm{V}}_n(\theta) \triangleq e^{n a_n(\theta)}, \quad \theta \in [0,1]. \tag{4.76}$$

On the other hand, the second function, $b_n(\theta)$, is

$$b_n(\theta) = \frac{1}{n} \log \frac{\pi^{n(1-\theta)/2}}{\Gamma(n(1-\theta)/2+1)} \delta^{n(1-\theta)}, \quad \theta \in [0,1]. \tag{4.77}$$

These two functions account for each of the two terms in the Minkowski sum of (4.74). Specifically, $a_n(\theta)$ is related to the intrinsic volumes of $\mathsf{H}\mathcal{X}$, while $b_n(\theta)$ to the volume of the noise ball

$\mathrm{Vol}_{n-j}\big(\mathcal{B}_\delta^{n-j}\big)$. Let us consider the function $v_n : [0,1] \to \mathbb{R}$ defined as

$$v_n(\theta) \triangleq a_n(\theta) + b_n(\theta). \tag{4.78}$$

Then, the Steiner's formula in (4.74) is equivalent to

$$\mathrm{Vol}_n\big([\mathsf{H}\mathcal{X}]^{\times \mathsf{M}} \oplus \mathcal{B}_\delta^n\big) = \sum_{j=0}^{n} e^{n v_n(j/n)}. \tag{4.79}$$

Let us verify that v_n converges as M goes to infinity. Notice that to guarantee the convergence of v_n we just need to prove that both a_n and b_n converge. Let use denote by f^* the convex conjugate of f in (4.70), defined according to (4.15). Given a closed set $I \subseteq \mathbb{R}$ and an open set $F \subseteq \mathbb{R}$, by [94, Lemma 14] the authors prove the following large deviation bounds. The upper bound

$$\limsup_{n\to\infty} \frac{1}{n} \log \widetilde{\mathrm{V}}_n(I) = \limsup_{n\to\infty} a_n(I) \leq -\inf_{t\in I} f^*(t), \tag{4.80}$$

and the lower bound

$$\limsup_{n\to\infty} \frac{1}{n} \log \widetilde{\mathrm{V}}_n(F) = \limsup_{n\to\infty} a_n(F) \geq -\inf_{t\in F} f^*(t). \tag{4.81}$$

Notice that, moreover, a requirement to ensure that these bounds are valid is to guarantee that the limit $f(t)$ exists for any $t \in \mathbb{R}$ and that $f(0) < \infty$. In our case these conditions are always satisfied thanks to (4.73). Furthermore, the concavity of $a_n(\cdot)$ for each n [94, Lemma 13], (4.80), and (4.81) ensure that

$$\lim_{n\to\infty} a_n(\theta) = -f^*(\theta). \tag{4.82}$$

See [94, Lemma 15] for a more detailed proof. Notice that the convergence of b_n can be easily proven as follows

$$\lim_{n\to\infty} b_n(\theta) = \frac{1-\theta}{2}\log\frac{2\pi e\sigma_z^2}{1-\theta}. \tag{4.83}$$

Therefore, putting everything together we can show that v_n converges

$$v(\theta) \triangleq \lim_{n\to\infty} v_n(\theta) = -f^*(\theta) + \frac{1-\theta}{2}\log\frac{2\pi e\sigma_z^2}{1-\theta}. \tag{4.84}$$

Let us define the value of θ for which $v_n(\theta)$ is maximized as

$$\hat{\theta}_n = \arg\max_{\theta} v_n(\theta). \tag{4.85}$$

Thanks to (4.79) and to the monotonicity of logarithmic functions, we define the following inequalities

$$\frac{\log\left(e^{nv_n(\hat{\theta}_n)}\right)}{\mathsf{M}} \leq \frac{\log \mathrm{Vol}_n\left([\mathsf{H}\mathcal{X}]^{\times\mathsf{M}} \oplus \mathcal{B}_\delta^n\right)}{\mathsf{M}} \leq \frac{\log\left((n+1)e^{nv_n(\hat{\theta}_n)}\right)}{\mathsf{M}}. \tag{4.86}$$

Notice that, by [94, Lemma 17], it holds that

$$\lim_{n\to\infty} v_n\left(\hat{\theta}_n\right) = \sup_{\theta} v(\theta). \tag{4.87}$$

Therefore, given the fact that

$$\lim_{\mathsf{M}\to\infty} \frac{1}{\mathsf{M}}\log\left(e^{nv_n(\hat{\theta}_n)}\right) = \lim_{\frac{n}{2\mathsf{N}}\to\infty} 2\mathsf{N}v_n\left(\hat{\theta}_n\right) \tag{4.88}$$

$$= 2\mathsf{N}\lim_{n\to\infty} v_n\left(\hat{\theta}_n\right), \tag{4.89}$$

the limit for $\mathsf{M} \to \infty$ of (4.86) is bounded on both sides by

$$2\mathsf{N} \sup_{\theta} v(\theta) \leq \lim_{\mathsf{M}\to\infty} \frac{1}{\mathsf{M}} \log \mathrm{Vol}_n\big([\mathsf{H}\mathcal{X}]^{\times \mathsf{M}} \oplus \mathcal{B}_\delta^n\big) \leq 2\mathsf{N} \sup_{\theta} v(\theta). \quad (4.90)$$

Finally, for $\sigma_z^2 > 0$ and by (4.90), the limit superior in (4.69) is given by

$$\begin{aligned}
\ell(\sigma_z^2) &\triangleq \limsup_{\mathsf{M}\to\infty} \frac{1}{\mathsf{M}} \log \mathrm{Vol}_n\big([\mathsf{H}\mathcal{X}]^{\times \mathsf{M}} \oplus \mathcal{B}_\delta^n\big) && (4.91)\\
&\overset{(4.90)}{=} \sup_{\theta\in[0,1]} 2\mathsf{N} \cdot v(\theta) && (4.92)\\
&\overset{(4.84)}{=} \sup_{\theta\in[0,1]} \left\{ -2\mathsf{N} f^*(\theta) + (1-\theta)\mathsf{N} \log \frac{2\pi e \sigma_z^2}{1-\theta} \right\} && (4.93)\\
&\overset{(4.15)}{=} \sup_{\theta\in[0,1]} \left\{ -2\mathsf{N} \sup_t \{\theta t - f(t)\} + (1-\theta)\mathsf{N} \log \frac{2\pi e \sigma_z^2}{1-\theta} \right\} && (4.94)\\
&\overset{(4.73)}{=} \sup_{\theta\in[0,1]} \left\{ -2\mathsf{N} \sup_t \left\{ \theta t - \frac{1}{2\mathsf{N}} \log \left(\sum_{j=0}^{2\mathsf{N}} \mathrm{V}_j(\mathsf{H}\mathcal{X}) e^{jt} \right) \right\} \right. \\
&\qquad \left. + (1-\theta)\mathsf{N} \log \frac{2\pi e \sigma_z^2}{1-\theta} \right\}. && (4.95)
\end{aligned}$$

This concludes the proof.

4.4.2 Proof of Proposition 1

Let us define the value of θ maximizing $v(\theta)^2$ as

$$\theta^*(\sigma_z^2) = \arg\max_{\theta} v(\theta). \quad (4.96)$$

By [94, Lemma 18], it holds that

$$\limsup_{\sigma_z^2 \to 0} \theta^*(\sigma_z^2) = 1. \quad (4.97)$$

[2]Note that the notation used in this work is different to that of [94] and θ of [94] is equivalent to $1-\theta$.

Therefore, we also have that

$$\lim_{\sigma_z^2 \to 0} \ell(\sigma_z^2) = -2\mathsf{N} f^*(1) \tag{4.98}$$

$$= -2\mathsf{N} \sup_t \left\{ t - \frac{1}{2\mathsf{N}} \log\left(\sum_{j=0}^{2\mathsf{N}} \mathrm{V}_j(\mathsf{H}\mathcal{X}) e^{jt} \right) \right\} \tag{4.99}$$

$$= \inf_t \left\{ \log\left(\sum_{j=0}^{2\mathsf{N}} \mathrm{V}_j(\mathsf{H}\mathcal{X}) e^{(j-2\mathsf{N})t} \right) \right\} \tag{4.100}$$

$$= \log\left(\inf_t \left\{ \sum_{j=0}^{2\mathsf{N}} \mathrm{V}_j(\mathsf{H}\mathcal{X}) e^{(j-2\mathsf{N})t} \right\} \right) \tag{4.101}$$

$$= \log\left(\mathrm{V}_{2\mathsf{N}}(\mathsf{H}\mathcal{X}) + \inf_t \left\{ \sum_{j=0}^{2\mathsf{N}-1} \mathrm{V}_j(\mathsf{H}\mathcal{X}) e^{(j-2\mathsf{N})t} \right\} \right) \tag{4.102}$$

$$= \log(\mathrm{Vol}_{2\mathsf{N}}(\mathsf{H}\mathcal{X})), \tag{4.103}$$

where: i) (4.99) derives from (4.15) and (4.73); ii) (4.101) is due to the monotonicity of logarithmic functions; iii) (4.102) holds thanks to the fact that $\mathrm{V}_j(\mathsf{H}\mathcal{X}) e^{(j-2\mathsf{N})t}$ is independent of t for $j = 2\mathsf{N}$; iv) as for (4.103), since the argument of the infimum in (4.102) is a sum of exponentials and since each exponential is scaled by nonnegative coefficients, the infimum is zero and it is given by $t \to \infty$. Finally, we conclude the proof by showing that, therefore, the asymptotic gap is

$$g_{\text{SP}} = \lim_{\sigma_z^2 \to 0} \overline{\mathsf{C}}_{\text{SP}} - \underline{\mathsf{C}}_{\text{EPI}} \tag{4.104}$$

$$= \lim_{\sigma_z^2 \to 0} \ell(\sigma_z^2) - \mathsf{N} \log\Big((\mathrm{Vol}_{2\mathsf{N}}(\mathsf{H}\mathcal{X}))^{\frac{1}{\mathsf{N}}} \Big) = 0. \tag{4.105}$$

4.4.3 Proof of Lemma 4

It is convenient to decompose the MIMO channel into two independent subchannels. Let us upper-bound the capacity of the one subchannel by the SP upper bound and the other subchannel by a Gaussian maximum entropy argument. Let $\mathsf{H} = \mathsf{U}\Lambda\mathsf{V}^T$ be the singular value decomposition of H and let $\widetilde{\mathbf{Y}} = \mathsf{U}^{-1}\mathbf{Y}$, $\widetilde{\mathbf{X}} = \mathsf{V}^T\mathbf{X}$, and $\widetilde{\mathbf{Z}} = \mathsf{U}^{-1}\mathbf{Z}$ with $\widetilde{\mathbf{Z}} \sim \mathcal{N}(\mathbf{0}_{2\mathsf{N}}, \sigma_z^2 \mathsf{I}_{2\mathsf{N}})$. Notice that the entropy in (2.6) is upper-bounded by

$$\sup_{F_{\mathbf{X}}:\, \mathbf{X}\in\mathcal{X}} \{\mathrm{h}(\mathbf{Y})\} = \sup_{F_{\mathbf{X}}:\, \mathbf{X}\in\mathcal{X}} \left\{\mathrm{h}\left(\widetilde{\mathbf{Y}}\right)\right\} \tag{4.106}$$

$$= \sup_{F_{\mathbf{X}}:\, \mathbf{X}\in\mathcal{X}} \{\mathrm{h}(\mathbf{Y}_U, \mathbf{Y}_L)\} \tag{4.107}$$

$$\leq \sup_{F_{\mathbf{X}}:\, \mathbf{X}\in\mathcal{X}} \{\mathrm{h}(\mathbf{Y}_U) + \mathrm{h}(\mathbf{Y}_L)\}, \tag{4.108}$$

where $\widetilde{\mathbf{Y}} = \left(\begin{smallmatrix}\mathbf{Y}_U \\ \mathbf{Y}_L\end{smallmatrix}\right)$, with

$$\mathbf{Y}_U = \begin{pmatrix}\widetilde{Y}_1 \\ \vdots \\ \widetilde{Y}_u\end{pmatrix} \in \mathbb{R}^u, \quad \mathbf{Y}_L = \begin{pmatrix}\widetilde{Y}_{u+1} \\ \vdots \\ \widetilde{Y}_{u+l}\end{pmatrix} \in \mathbb{R}^l, \quad u + l = 2\mathsf{N}. \tag{4.109}$$

Moreover, it holds $\widetilde{\mathbf{X}} = \left(\begin{smallmatrix}\mathbf{X}_U \\ \mathbf{X}_L\end{smallmatrix}\right)$, with $\mathbf{X}_U$ and $\mathbf{X}_L$ defined analogously to $\mathbf{Y}_U$ and $\mathbf{Y}_L$. We want to separate the contributions of $\mathrm{h}(\mathbf{Y}_U)$ and $\mathrm{h}(\mathbf{Y}_L)$ and apply tailored bounding techniques to each of them. By (4.24) and since

$$\mathrm{V}_j(\mathsf{H}\mathcal{X}) = \mathrm{V}_j(\Lambda\mathcal{X}), \quad \forall j, \tag{4.110}$$

the subchannel of $\mathbf{Y}_U$ is characterized by larger singular values and perceives a higher SNR. On the other hand, the relative singular values for the subchannel of the vector $\mathbf{Y}_L$ are smaller and the noise is more predominant. Therefore, SP upper bound is a suitable bounding technique for $\mathrm{h}(\mathbf{Y}_U)$, while the Gaussian maximum entropy argument provides a better bound for $\mathrm{h}(\mathbf{Y}_L)$. Let us start with the subchannel where the noise is the dominant component and define $\overline{\mathbf{Y}}_L \sim \mathcal{N}(\mathbf{0}_l, \Sigma_L)$, with $\Sigma_L = \Lambda_L \mathsf{E}\big[\mathbf{X}_L \mathbf{X}_L^T\big] \Lambda_L + \sigma_z^2 \mathsf{I}_l$ and with Λ_L being the $l \times l$ submatrix of Λ of diagonal elements $\lambda_{u+1}, \ldots, \lambda_{2\mathsf{N}}$. Furthermore, let us reformulate the input constraint in such a way that the two differential entropy in (4.108) can be maximized independently. For now, let us assume $\mathcal{X}$ to be a ball and let $r = r_{\max}(\mathcal{X})$ be its radius. It holds that

$$\|\mathbf{X}\|^2 = \|\mathbf{X}_U\|^2 + \|\mathbf{X}_L\|^2 \leq r^2. \tag{4.111}$$

Let us decompose r^2 in the sum of two terms as $r^2(1-\alpha^2) + r^2\alpha^2$ with $\alpha \in [0,1]$. Then, the constraint $\|\mathbf{X}\| \leq r$ is equivalent to

$$\bigcup_{\alpha \in [0,1]} \Big\{ F_{\mathbf{X}} : \ \|\mathbf{X}_U\| \leq r\sqrt{1-\alpha^2}, \ \|\mathbf{X}_L\| \leq r\alpha \Big\}. \tag{4.112}$$

By plugging (4.112) into (4.108), we have that

$$\sup_{F_{\mathbf{X}}:\, \mathbf{X} \in \mathcal{X}} \{\mathrm{h}(\mathbf{Y}_U) + \mathrm{h}(\mathbf{Y}_L)\} \tag{4.113}$$

$$= \sup_{\alpha \in [0,1]} \left\{ \sup_{F_{\mathbf{X}}: \begin{cases} \|\mathbf{X}_U\| \leq r\sqrt{1-\alpha^2} \\ \|\mathbf{X}_L\| \leq r\alpha \end{cases}} \{\mathrm{h}(\mathbf{Y}_U) + \mathrm{h}(\mathbf{Y}_L)\} \right\} \tag{4.114}$$

$$= \sup_{\alpha\in[0,1]} \left\{ \sup_{F_{\mathbf{X}_U}\colon \|\mathbf{X}_U\|\le r\sqrt{1-\alpha^2}} \{\mathsf{h}(\mathbf{Y}_U)\} + \sup_{F_{\mathbf{X}_L}\colon \|\mathbf{X}_L\|\le r\alpha} \{\mathsf{h}(\mathbf{Y}_L)\} \right\}. \tag{4.115}$$

Then, by applying the SP upper bound in (4.18) to the subchannel of $\mathbf{Y}_U$ we obtain the following upper bound

$$\sup_{F_{\mathbf{X}_U}\colon \|\mathbf{X}_U\|\le r\sqrt{1-\alpha^2}} \{\mathsf{h}(\mathbf{Y}_U)\} \le \ell_U(\alpha). \tag{4.116}$$

As for the differential entropy of $\mathbf{Y}_L$, we have that

$$\sup_{F_{\mathbf{X}_L}\colon \|\mathbf{X}_L\|\le r\alpha} \mathsf{h}(\mathbf{Y}_L) \tag{4.117}$$

$$\le \sup_{F_{\mathbf{X}_L}\colon \|\mathbf{X}_L\|\le r\alpha} \mathsf{h}\big(\overline{\mathbf{Y}}_L\big) \tag{4.118}$$

$$\overset{(a)}{\le} \sup_{F_{\mathbf{X}_L}\colon \mathsf{E}\left[\|\mathbf{X}_L\|^2\right]\le r^2\alpha^2} \mathsf{h}\big(\overline{\mathbf{Y}}_L\big) \tag{4.119}$$

$$\overset{(b)}{\le} \sup_{F_{\mathbf{X}_L}\colon \mathsf{E}\left[\|\mathbf{X}_L\|^2\right]\le r^2\alpha^2} \sum_{k=1}^{l} \frac{1}{2}\log\big(2\pi e\big(\lambda_{u+k}^2 \mathsf{E}\left[|X_{L,k}|^2\right] + \sigma_z^2\big)\big) \tag{4.120}$$

$$= \sum_{k=1}^{l} \frac{1}{2}\log\big(2\pi e\big(\lambda_{u+k}^2 \mathsf{P}_k(\alpha) + \sigma_z^2\big)\big), \tag{4.121}$$

where in (a) we introduced the looser average power constraint $\mathsf{E}[\|\mathbf{X}_L\|^2] \le r^2\alpha^2$ and where (b) holds thanks to $\mathsf{h}\big(\overline{\mathbf{Y}}_L\big) \le \sum_k \mathsf{h}\big(\overline{Y}_{L,k}\big)$, with $\overline{Y}_{L,k}$ being the kth component of the vector $\overline{\mathbf{Y}}_L$. As for $\overline{Y}_{L,k}$, let $X_{L,k}$ denote the kth component of the vector $\mathbf{X}_L$. Then, given the constraint $\mathsf{E}[\|\mathbf{X}_L\|^2] \le r^2\alpha^2$, we define $\mathsf{P}_k(\alpha)$ as the power allocation obtained to maximize (4.120) by applying the water-filling principle. Notice that, even if we assumed $\mathcal{X}$ to be a ball, we can extend the same technique to any input constraint region. Indeed, one can trivially

consider the enlarged constraint $\mathcal{B}^{2\mathsf{N}}_{r_{\max}(\mathcal{X})} \supset \mathcal{X}$ instead of $\mathcal{X}$ and still obtain a valid upper bound.

Chapter 5

Applications to Common Case Studies

In this chapter, the SP and the QPC upper bounds are applied to the case studies defined in Section 2.3.

5.1 Total Amplitude Constraint

Let us evaluate the SP upper bound of Theorem 4.2.1 for the TA constraint defined in Definition 2.3.1. Notice that, to compute the bound $\overline{\mathsf{C}}_{\mathrm{SP}}$, we first need to evaluate the intrinsic volumes $\mathrm{V}_j(\mathsf{H}\mathcal{X})$, for $j = 0, \dots, 2\mathrm{N}$. Since the TA constraint region $\mathcal{X}$ is a $(2\mathrm{N})$-dimensional ball, by (4.110) in Appendix 4.4.3 it holds

$$\mathrm{V}_j(\mathsf{H}\mathcal{X}) = \mathrm{V}_j(\Lambda\mathcal{X}), \quad \forall j. \tag{5.1}$$

Notice that $\Lambda\mathcal{X}$ is an ellipsoid and [96] provides the following formulation, that is useful to numerically evaluate the intrinsic volumes of

an ellipsoid. Let us define the ellipsoid as

$$\mathcal{E} = \Big\{ \mathbf{x} = (x_1, \dots, x_{2\mathsf{N}})^T \in \mathbb{R}^{2\mathsf{N}} : \mathbf{x}^T \Sigma^{-1} \mathbf{x} \leq 1 \Big\}. \tag{5.2}$$

Let $\mathbf{Q}_1, \dots, \mathbf{Q}_j \sim \mathcal{N}(\mathbf{0}_{2\mathsf{N}}, \Sigma)$ be j independent and identically distributed random vectors and let $\mathsf{Q} = (\mathbf{Q}_1, \dots, \mathbf{Q}_j)$ be the random matrix with columns equal to the $\mathbf{Q}_i$'s. Then, the jth intrinsic volume of the ellipsoid $\mathcal{E}$ defined in (5.2) is

$$\mathrm{V}_j(\mathcal{E}) = \frac{(2\pi)^{j/2}}{j!} \mathsf{E}\Big[\sqrt{\det(\mathsf{Q}^T \cdot \mathsf{Q})} \Big]. \tag{5.3}$$

Let us consider vectors $\mathbf{Q}_i$'s such that their covariance matrix is $\Sigma = \Lambda^2$. Then, the intrinsic volumes $\mathrm{V}_j(\mathsf{H}\mathcal{X})$ are given by

$$\mathrm{V}_j(\mathsf{H}\mathcal{X}) \overset{(4.9)}{=} \mathrm{V}_j(\mathcal{E}) \mathsf{R}^j, \qquad j = 0, \dots, 2\mathsf{N}. \tag{5.4}$$

Thanks to (5.4), it is possible to numerically evaluate the intrinsic volumes of the ellipsoid $\mathsf{H}\mathcal{X}$. Therefore, the TA constraint is one of the few special cases for which the intrinsic volumes of $\mathsf{H}\mathcal{X}$ are known. Notice also that the resulting $\mathcal{X}$, for the TA constraint, is a ball and, therefore, the P-SP upper bound outperforms the standard SP bound at each SNR level, see Remark 6.

5.1.1 Capacity Gap and Performance

Let us derive some numerical results on the capacity for the TA constraint. To determine the tightness of the SP bound, let us evaluate the associated capacity gap defined as

$$g_{\mathrm{TA}} \triangleq \overline{\mathsf{C}}_{\mathrm{TA}} - \underline{\mathsf{C}}_{\mathrm{TA}}, \tag{5.5}$$

where $\overline{\mathsf{C}}_{\text{TA}}$ is given by the P-SP upper bound in Lemma 4, applied to the TA constraint and $\underline{\mathsf{C}}_{\text{TA}}$ is the P-EPI lower bound in (4.6). The gap g_{TA} is evaluated numerically by Monte Carlo simulation for $\mathsf{N} = 2, \ldots, 10$ and over random realizations of the channel matrix. The entries of H' in (2.2) are complex Gaussian-distributed, i.e., $\mathsf{H}'_{i,j} \sim \mathcal{CN}(0, 2),\ \forall i, j$.

The numerical results for the capacity gap in (5.5) are shown in Figs. 5.1–5.3. Fig. 5.1a shows a scatter plot of the gap over the random channel realizations and, with solid curves, the resulting average gap. The gap realizations and the resulting averages are shown versus SNR and each color corresponds to a different MIMO dimension N. Fig. 5.1b shows the associated standard deviation. Thanks to the P-SP approach, as the SNR decreases the gap goes to zero. Indeed, in the low SNR regime, the P-SP upper bound is minimized by $u = 0$, i.e., the noise is the dominant component for all MIMO dimensions. Then, in this regime the upper bound depends just on the term $\ell_L(\alpha)$ of (4.25), which is the one based on a Gaussian maximum entropy argument and gives accurate results at low SNR. Moreover, also at high SNR the gap decreases and eventually reaches zero, as stated in Remark 6, via Proposition 1. Fig. 5.2 shows that the average ratio between the capacity gap and the P-SP upper bound improves as both N and the SNR increase. In Fig. 5.3, it is shown the average gap per complex dimension N, solid curves, and the one resulting from the duality upper bounds of [39], dashed curves, defined in (4.1) and (4.2). Notice that, given $\overline{\mathsf{C}}_{\text{D,TA}} \triangleq \min\big(\overline{\mathsf{C}}_{\text{D},1}, \overline{\mathsf{C}}_{\text{D},2}\big)$, the capacity gap for the duality upper

bounds is defined as

$$g_{\mathrm{D,TA}} \triangleq \overline{\mathrm{C}}_{\mathrm{D,TA}} - \underline{\mathrm{C}}_{\mathrm{TA}}. \tag{5.6}$$

Therefore, the dashed lines in Fig. 5.3 are given by $\mathsf{E}[g_{\mathrm{D,TA}}]/\mathsf{N}$ averaged over random channel realizations. Notice that the $\mathsf{E}[g_{\mathrm{D,TA}}]/\mathsf{N}$ is looser than $\mathsf{E}[g_{\mathrm{TA}}]/\mathsf{N}$ for any N and at any SNR level. Finally, Fig. 5.4 shows the bounds resulting from a random channel realization for $\mathsf{N} = 10$ and shows that the P-SP bound is a substantial improvement compared to duality bounds of [39].

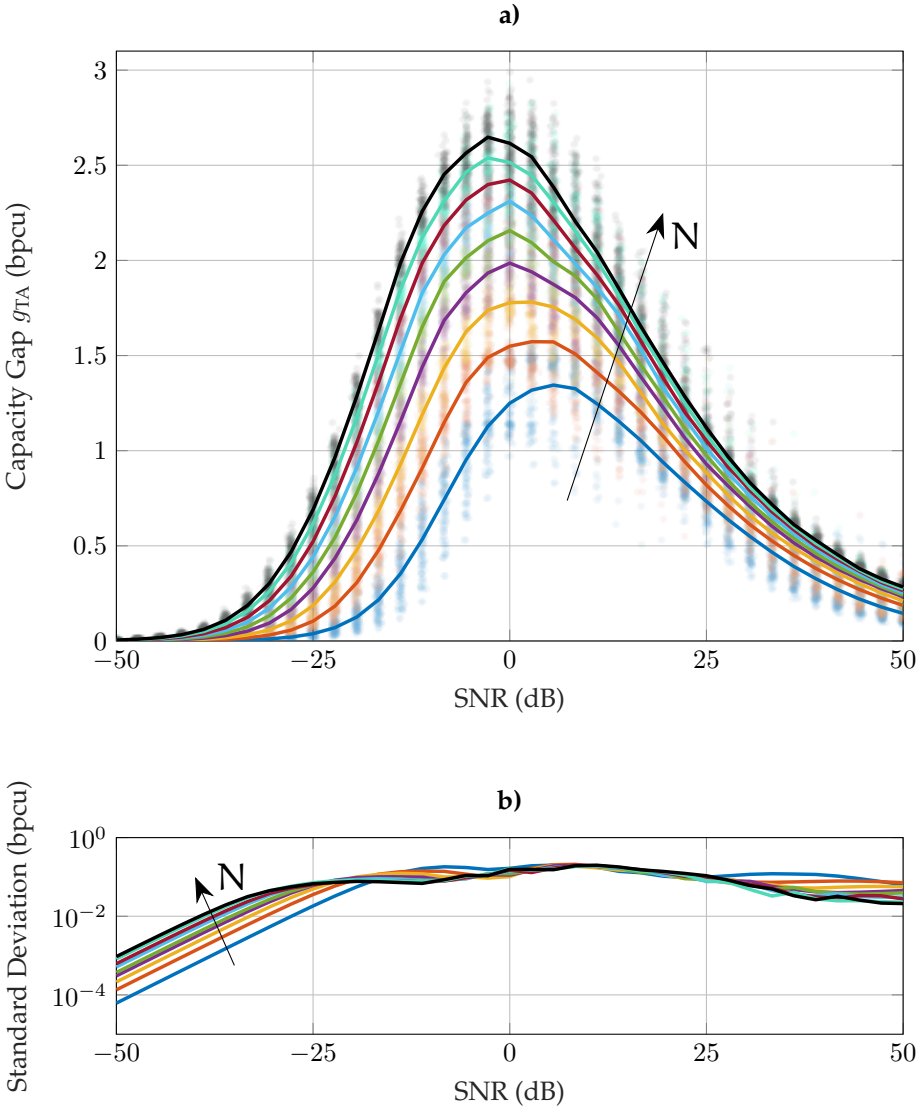

Figure 5.1: ***a)*** *Numerical evaluation of the capacity gap g_{TA}, defined in* (5.5)*, in bit per channel use (bpcu) versus SNR, for $\mathsf{N} = 2, \ldots, 10$. For all values of N, each filled circle shows the gap resulting from a random channel realization. The solid curves show the averaged behavior.* ***b)*** *Numerical evaluation of the standard deviation of g_{TA} in bpcu versus SNR, for $\mathsf{N} = 2, \ldots, 10$.*

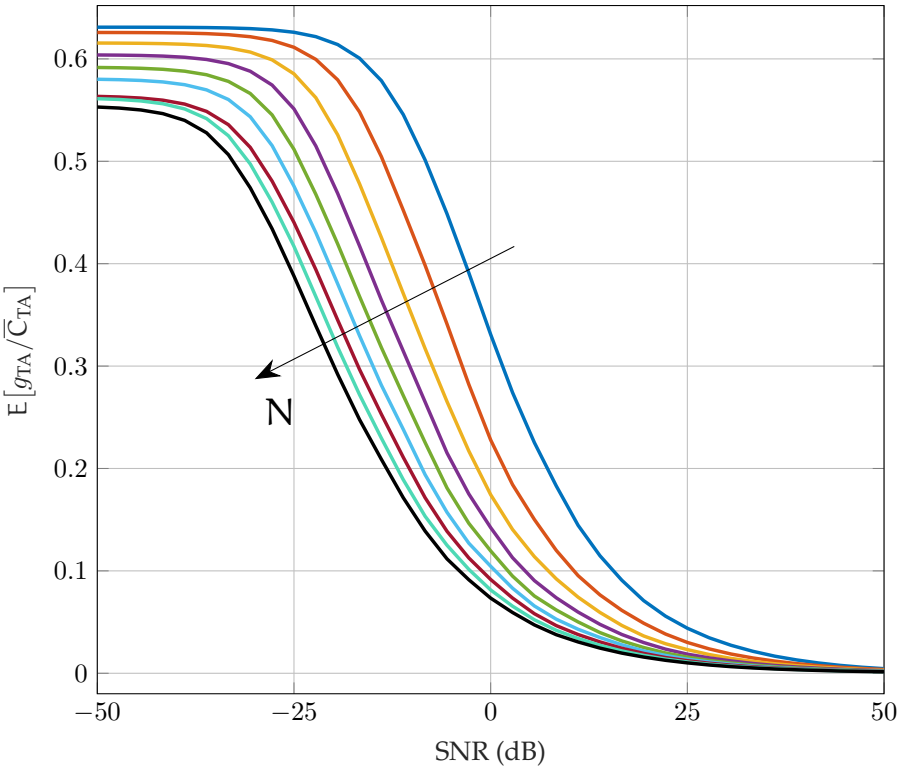

Figure 5.2: *Numerical evaluation of the average ratio between the capacity gap g_{TA}, defined in* (5.5)*, and the upper bound $\overline{C}_{TA}$, derived from* (4.25)*. The average ratio is plotted versus the SNR and for $N = 2, \ldots, 10$.*

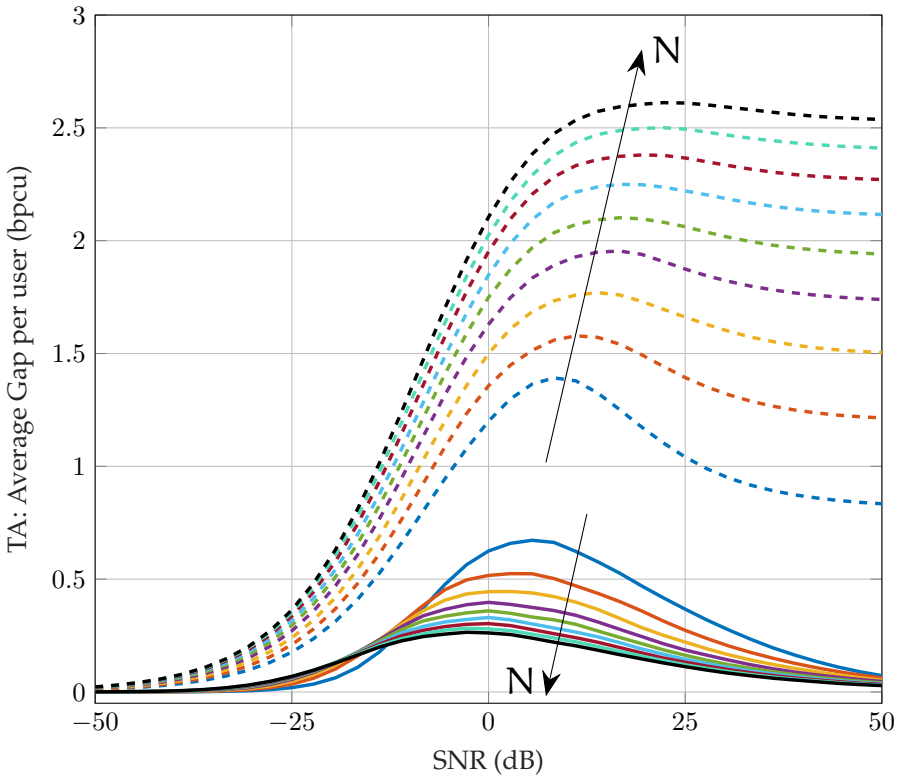

Figure 5.3: *Numerical evaluation of the average capacity gap per complex dimension in bit per channel use (bpcu) versus SNR, for* $N = 2, \ldots, 10$. *The solid curves are* $E[g_{TA}]/N$, *where* g_{TA} *is defined in* (5.5). *The dashed curves are* $E[g_{D,TA}]/N$, *where* $g_{D,TA}$ *is defined in* (5.6).

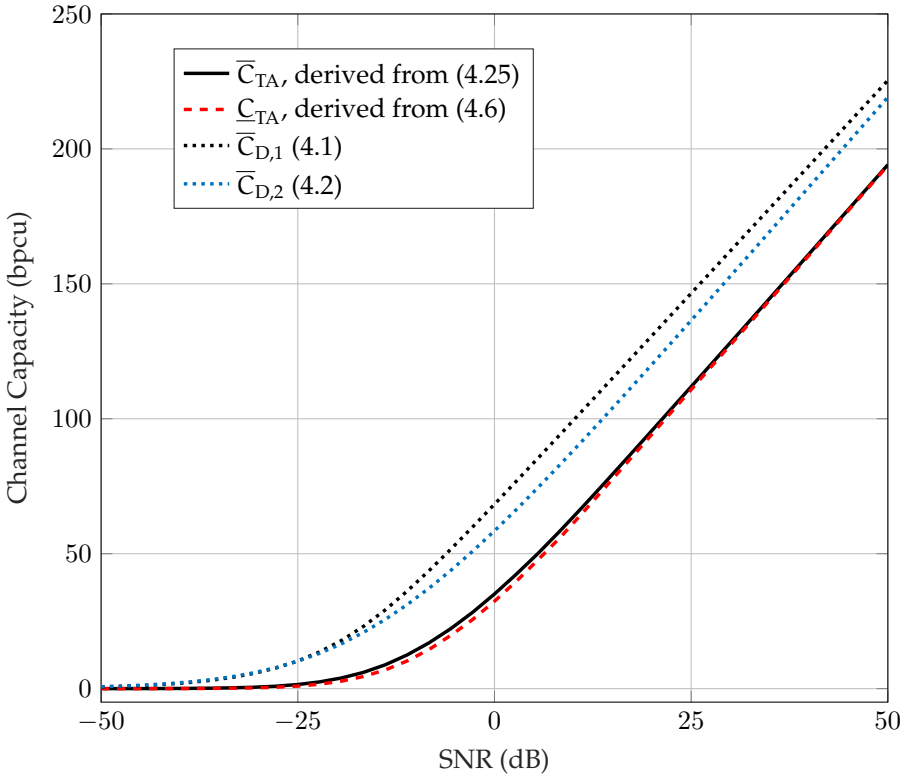

Figure 5.4: *Capacity bounds in bit per channel use (bpcu) versus SNR, for* $\mathsf{N} = 10$ *and for a random realization of* H'.

5.2 Per-Antenna Constraint

Let us now focus on the PA constraint characterized in Definition 2.3.2. Thanks to Remark 1, we will assume $\mathsf{R}_i = \mathsf{R}$, $\forall i$ without loss of generality. In the case of PA constraints, both the SP and the QPC can be applied. While the definition of the QPC is almost immediate, the derivation of the SP upper bound for the PA constraint requires some additional steps.

5.2.1 Sphere Packing Approach

Let us start with the SP approach. Notice that the intrinsic volumes $\mathrm{V}_j(\mathcal{X})$ can be evaluated in closed form. Nonetheless, the channel matrix H distorts $\mathcal{X}$ and, unfortunately, the intrinsic volumes of the resulting input constraint region $\mathsf{H}\mathcal{X}$ are not easy to evaluate. Thanks to the G-SP approach it is still possible to derive an upper bound. To do so, we need to find suitable enlarged regions that can be used to upper-bound the $\mathrm{V}_j(\mathsf{H}\mathcal{X})$'s, as in (4.20).

Given the PA constraint and Remark 1, it holds $\mathcal{X}_k = \mathcal{B}^2_{\mathsf{R}}$, for any k. Then, let us consider the squares $\mathcal{R}_k = \{\mathbf{x} : |x_i| \leq \mathsf{R},\ i = 1, 2\}$, for $k = 1, \ldots, \mathsf{N}$. Notice that $\mathcal{R}_k \supset \mathcal{X}_k$, therefore a constraint region $\mathcal{R}$ such that $\mathcal{R} \supset \mathcal{X}$ is given by

$$\mathcal{R} = \mathcal{R}_1 \times \cdots \times \mathcal{R}_{\mathsf{N}} = \{\mathbf{x} : |x_i| \leq \mathsf{R},\ i = 1, \ldots, 2\mathsf{N}\}. \tag{5.7}$$

The intrinsic volumes of $\mathsf{H}\mathcal{R}$ are still unknown, but an upper bound can be derived as follows. Let us denote by $\mathcal{P}$ a $(2\mathsf{N})$-dimensional polytope and by $\mathbb{F}_j(\mathcal{P})$ the set of all j-dimensional faces of $\mathcal{P}$.

From [98], the intrinsic volumes of a polytope are given by

$$\mathrm{V}_j(\mathcal{P}) = \sum_{\mathcal{F}\in\mathbb{F}_j(\mathcal{P})} \gamma(\mathcal{F},\mathcal{P})\mathrm{Vol}_j(\mathcal{F}), \quad j = 1,\ldots,2\mathrm{N}, \tag{5.8}$$

where $\gamma(\mathcal{F},\mathcal{P})$ is the normalized external angle of $\mathcal{P}$ at its face $\mathcal{F}$.

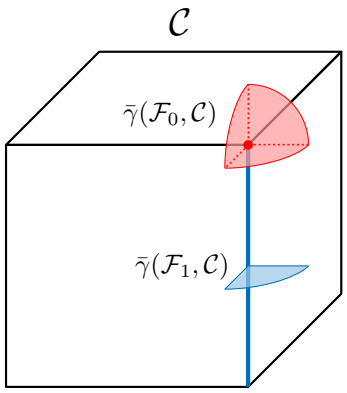

Figure 5.9: *Graphical representation of the external angles of a vertex $\mathcal{F}_0$ and an edge $\mathcal{F}_1$ for a cube $\mathcal{C}$.*

Let $\mathcal{F}$ be a j-dimensional face of $\mathcal{P}$. Then, the external angle $\bar{\gamma}(\mathcal{F},\mathcal{P})$ is defined as the fraction of the unit hypersphere $\mathcal{S}^{n-j} = \mathcal{S}_1^{n-j}$ covered by the cone of outward normals to the supporting hyperplanes of $\mathcal{P}$ at the face $\mathcal{F}$ [99,100]. Therefore, the normalized external angle is defined as $\gamma(\mathcal{F},\mathcal{P}) = \bar{\gamma}(\mathcal{F},\mathcal{P})/\mathrm{Vol}(\mathcal{S}^{n-j})$. In Fig. 5.9, it is shown a graphical representation of the external angles of a cube $\mathcal{C}$ for a vertex $\mathcal{F}_0$, the red point, and for an edge $\mathcal{F}_1$, the blue segment. Notice that vertices are 0-dimensional faces, edges are 1-dimensional faces, and so on. The normalized external angle is not trivial to evaluate for an arbitrary $\mathcal{P}$. Therefore, since $\gamma(\mathcal{F},\mathcal{P}) \leq 1$, let us upper-bound the intrinsic volumes

of $\mathcal{P}$ as follows

$$\mathrm{V}_j(\mathcal{P}) \leq \sum_{\mathcal{F}\in\mathbb{F}_j(\mathcal{P})} \mathrm{Vol}_j(\mathcal{F}), \quad j = 1, \ldots, 2\mathsf{N}. \tag{5.9}$$

Furthermore, let us consider the following results from exterior algebra. In [101], the authors prove that, by a set of j vectors $\mathbf{r}_1, \ldots, \mathbf{r}_j \in \mathbb{R}^{2\mathsf{N}}$ and by a base point $\mathbf{p} \in \mathbb{R}^{2\mathsf{N}}$, one can equivalently determine a j-dimensional parallelepiped, with $j \leq 2\mathsf{N}$. Let us consider $\mathbf{p}$ to be a vertex of a given parallelepiped. Moreover, let us define the vectors $\mathbf{r}_1, \ldots, \mathbf{r}_j$ in such a way that their magnitude and direction is equal to that of the j edges of the parallelepiped originating from the vertex in $\mathbf{p}$. Then, each point in the parallelepiped can be defined as

$$\mathbf{p} + t_1\mathbf{r}_1 + \cdots + t_j\mathbf{r}_j, \quad 0 \leq t_1, \ldots, t_j \leq 1. \tag{5.10}$$

The linear combinations given by the vectors $\mathbf{r}_1$, $\mathbf{r}_2$, and $\mathbf{r}_3$ with base point $\mathbf{p}$ span the parallelepiped. Fig. 5.10 shows a graphical example for a 3-dimensional parallelepiped. Volume is invariant with respect to translations, therefore, we can neglect the base point $\mathbf{p}$ and represent the geometric region $\mathcal{R}$ via the corresponding matrix R thanks to the following concepts of exterior algebra from [101].

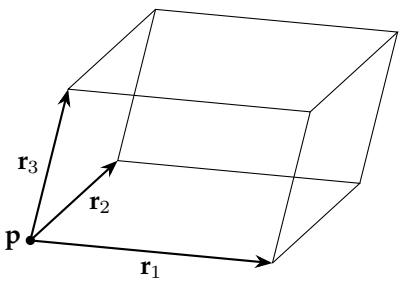

Figure 5.10: *Parallelepiped spanned by $\mathbf{r}_1$, $\mathbf{r}_2$, and $\mathbf{r}_3$ from the point $\mathbf{p}$.*

Let us define the matrix R as

$$\mathsf{R} \triangleq (\mathbf{r}_1, \mathbf{r}_2, \ldots, \mathbf{r}_{2\mathsf{N}}) = 2\mathsf{R} \cdot \mathsf{I}_{2\mathsf{N}}. \tag{5.11}$$

For now, let us focus on $\mathcal{R}$ and ignore the matrix H. Since $\mathcal{R}$ is a parallelepiped, it is also a polytope. By (5.8), we have that the jth intrinsic volumes $\mathrm{V}_j(\mathcal{R})$ depends on its j-dimensional faces. Notice that j column vectors from R span one of the faces in $\mathbb{F}_j(\mathcal{R})$. Therefore, by taking all possible combinations of j columns from the matrix R, counting also all the repetitions due to parallel identical faces, we are able to evaluate each $\mathrm{Vol}_j(\mathcal{F})$ for all $\mathcal{F} \in \mathbb{F}_j(\mathcal{R})$. Let $\mathcal{R}_{j,i}$ be the j-dimensional face spanned by the ith combination of j columns from R, out of $\binom{2\mathsf{N}}{j}$. For example, let $\mathcal{R}_{j,1}$ be the face spanned by the vectors $\mathbf{r}_1, \ldots, \mathbf{r}_j$. Then, like it was done for $\mathcal{R}$ and R, we can represent $\mathcal{R}_{j,1}$ with a $(2\mathsf{N}) \times j$ matrix defined as $\mathsf{R}_{j,1} = (\mathbf{r}_1, \mathbf{r}_2, \ldots, \mathbf{r}_j)$. Thanks to the results in [101], the j-dimensional volume of $\mathcal{R}_{j,1}$ can be evaluated as

$$\mathrm{Vol}_j(\mathcal{R}_{j,1}) = \sqrt{\left|\det\left(\mathsf{R}_{j,1}^T \cdot \mathsf{R}_{j,1}\right)\right|}. \tag{5.12}$$

The same can be done for any of the $\mathcal{R}_{j,i}$'s. Moreover, notice that $\mathsf{H}\mathcal{R}$ is still a polytope and, therefore, the volume of its faces can be evaluated similarly to those of $\mathcal{R}$. To ease the notation let us denote by $\mathcal{S} = \mathsf{H}\mathcal{R} \supset \mathsf{H}\mathcal{X}$ the distorted polytope and by $\mathsf{S} = (\mathsf{s}_1, \mathsf{s}_2, \ldots, \mathsf{s}_{2\mathsf{N}}) = \mathsf{H} \cdot \mathsf{R}$ the associated $(2\mathsf{N}) \times (2\mathsf{N})$ matrix. Notice that, given (5.8), to evaluate the intrinsic volumes of $\mathcal{S}$ we would still need to evaluate the external angles $\gamma(\mathcal{F}, \mathcal{S})$, with $\mathcal{F} \in \mathbb{F}_j(\mathcal{S})$. Let us denote by $\mathcal{S}_A$ a constraint region with the same faces of $\mathcal{S}$ and with $\gamma(\mathcal{F}, \mathcal{S}_A) = 1$. By (5.9), the jth

intrinsic volume of $\mathcal{S}_A$ upper-bounds $\mathrm{V}_j(\mathcal{S})$, i.e.,

$$\mathrm{V}_j(\mathsf{H}\mathcal{X}) < \mathrm{V}_j(\mathcal{S}) \tag{5.13}$$

$$\leq \mathrm{V}_j(\mathcal{S}_A) = 2^{2\mathsf{N}-j} \sum_{i=1}^{\binom{2\mathsf{N}}{j}} \sqrt{\left|\det\left(\mathsf{S}_{j,i}^T \cdot \mathsf{S}_{j,i}\right)\right|}. \tag{5.14}$$

Notice that $2^{2\mathsf{N}-j}$ is the multiplicity of each j-dimensional parallel face in a parallelepiped. The intrinsic volumes $\mathrm{V}_j(\mathcal{S}_A)$ in (5.14) are, in turn, upper bounds on $\mathrm{V}_j(\mathsf{H}\mathcal{X})$. Therefore, the $\mathrm{V}_j(\mathcal{S}_A)$'s can be used, as in (4.20), to evaluate the G-SP upper bound for the PA constraint.

Another set of upper bounds on the $\mathrm{V}_j(\mathsf{H}\mathcal{X})$'s can be derived by considering the smallest ball containing $\mathcal{X}$. Given the maximum radius of the input constraint region $r_{\max}(\mathcal{X}) = \mathsf{R}\sqrt{\mathsf{N}}$, it holds $\mathcal{B}^{2\mathsf{N}}_{\mathsf{R}\sqrt{\mathsf{N}}} \supset \mathcal{X}$. Then, let us define the set $\mathcal{S}_B \triangleq \mathsf{H}\mathcal{B}^{2\mathsf{N}}_{\mathsf{R}\sqrt{\mathsf{N}}} \supset \mathsf{H}\mathcal{X}$. Notice that $\mathcal{S}_B$ is an ellipsoid and, therefore, its intrinsic volumes can be evaluated as

$$\mathrm{V}_j(\mathcal{S}_B) = \mathrm{V}_j(\mathcal{E})\left(\mathsf{R}\sqrt{\mathsf{N}}\right)^j, \tag{5.15}$$

where $\mathrm{V}_j(\mathcal{E})$ is given by (5.3), with $\Sigma = \Lambda^2$ from $\mathsf{H} = \mathsf{U}\Lambda\mathsf{V}^T$. Both the intrinsic volumes of $\mathcal{S}_B$ and those of $\mathcal{S}_A$ are valid upper bounds on $\mathrm{V}_j(\mathsf{H}\mathcal{X})$. Then, for each j, let us consider the following upper bounds

$$\overline{\mathrm{V}}_j = \begin{cases} 1, & j = 0, \\ \min(\mathrm{V}_j(\mathcal{S}_A), \mathrm{V}_j(\mathcal{S}_B)), & j = 1, \ldots, 2\mathsf{N}-1, \\ \det(\mathsf{H})\mathrm{Vol}_{2\mathsf{N}}(\mathcal{X}), & j = 2\mathsf{N}. \end{cases} \tag{5.16}$$

The G-SP upper bound in Lemma 3 for the PA constraint can be, therefore, evaluated by plugging (5.16) into (4.20). Let us denote the result-

ing capacity upper bound by $\overline{\mathsf{C}}_{\mathrm{PA},1}$.

Moreover, a more accurate bound in the low SNR regime can be derived via the P-SP approach. Specifically, by considering once more the ball $\mathcal{B}^{2\mathsf{N}}_{\mathsf{R}\sqrt{\mathsf{N}}} \supset \mathcal{X}$, another upper bound is obtained via Lemma 4. The resulting bound is denoted by $\overline{\mathsf{C}}_{\mathrm{PA},2}$.

Let us now evaluate the performance of the SP approach for the PA constraint. The resulting capacity gap is defined as

$$g_{\mathrm{PA}} \triangleq \overline{\mathsf{C}}_{\mathrm{PA}} - \underline{\mathsf{C}}_{\mathrm{PA}}, \tag{5.17}$$

where $\underline{\mathsf{C}}_{\mathrm{PA}}$ is the P-EPI lower bound defined in (4.6) and $\overline{\mathsf{C}}_{\mathrm{PA}}$ is defined as

$$\overline{\mathsf{C}}_{\mathrm{PA}} = \min\big(\overline{\mathsf{C}}_{\mathrm{PA},1}, \overline{\mathsf{C}}_{\mathrm{PA},2}\big). \tag{5.18}$$

Like we did for the TA constraint, we show the numerical results provided by the evaluation of the gap for random channel matrix realizations. The entries of the channel matrix H' of Definition 2.1.2 are again drawn independently as $\mathsf{H}'_{i,j} \sim \mathcal{CN}(0,2),\ \forall i,j$. Fig. 5.5a shows a scatter plot of the capacity gaps obtained for each random matrix realization. In the same figure, with solid lines, we also show the averaged behavior. Both are derived for a wide SNR range and for $\mathsf{N} = 2,\ldots,10$. Fig. 5.5b shows the corresponding standard deviation of g_{PA}. Like already observed for the TA constraint, the gap is vanishing at low SNR thanks to the P-SP approach. Moreover, the gap tends to decrease also at high SNR but the convergence to zero is slower than that of the TA constraint. Nonetheless, thanks to the G-SP approach and Proposition 2 we know that, as the SNR increases, the gap eventually goes to

zero. The performance of the proposed bounds for the PA constraint are worse than those obtained for the TA constraint. This is due to difficulty in the evaluation of the intrinsic volumes of $\mathsf{H}\mathcal{X}$ for the PA constraint and the consequent need to upper-bound them. Nevertheless, Fig. 5.6 shows that the average ratio between g_{PA} and $\overline{\mathsf{C}}_{\mathrm{PA}}$ tends to zero as the SNR increases. Furthermore, in Fig. 5.7 and Fig. 5.8 the improvement obtained by the proposed bounds, compared to duality upper bounds of [39], is significant. The upper bounds $\overline{\mathsf{C}}_{\mathrm{D},1}$ and $\overline{\mathsf{C}}_{\mathrm{D},2}$ are those presented in [39, Theorem 10] and, in this work, defined in (4.1) and (4.2) respectively. Notice that the exact definition of (4.2) would require us to evaluate the box, among those containing the region $\mathsf{H}\mathcal{X}$, which has the smallest volume. Unfortunately, this is not a simple task and, therefore, we derive $\overline{\mathsf{C}}_{\mathrm{D},2}$ for the PA constraint by considering the small box containing the enlarged constraint region $\mathsf{H}\mathcal{B}^{2\mathsf{N}}_{\mathsf{R}\sqrt{\mathsf{N}}} \supset \mathsf{H}\mathcal{X}$. Finally, we choose the minimum between the considered upper bounds, i.e., $\overline{\mathsf{C}}_{\mathrm{D,PA}} \triangleq \min\big(\overline{\mathsf{C}}_{\mathrm{D},1}, \overline{\mathsf{C}}_{\mathrm{D},2}\big)$ and we define the capacity gap for the duality upper bounds as

$$g_{\mathrm{D,PA}} \triangleq \overline{\mathsf{C}}_{\mathrm{D,PA}} - \underline{\mathsf{C}}_{\mathrm{PA}}. \tag{5.19}$$

Fig. 5.7 shows that the average gap per complex dimension given by the G-SP and the P-SP approach is always smaller than the gap resulting from the duality bounds in [39]. Furthermore, Fig. 5.8 shows the capacity bounds for a random realization of H', given $\mathsf{N} = 10$. Again, the upper bound $\overline{\mathsf{C}}_{\mathrm{PA}}$ is significantly tighter than the upper bounds $\overline{\mathsf{C}}_{\mathrm{D},1}$ and $\overline{\mathsf{C}}_{\mathrm{D},2}$ of [39].

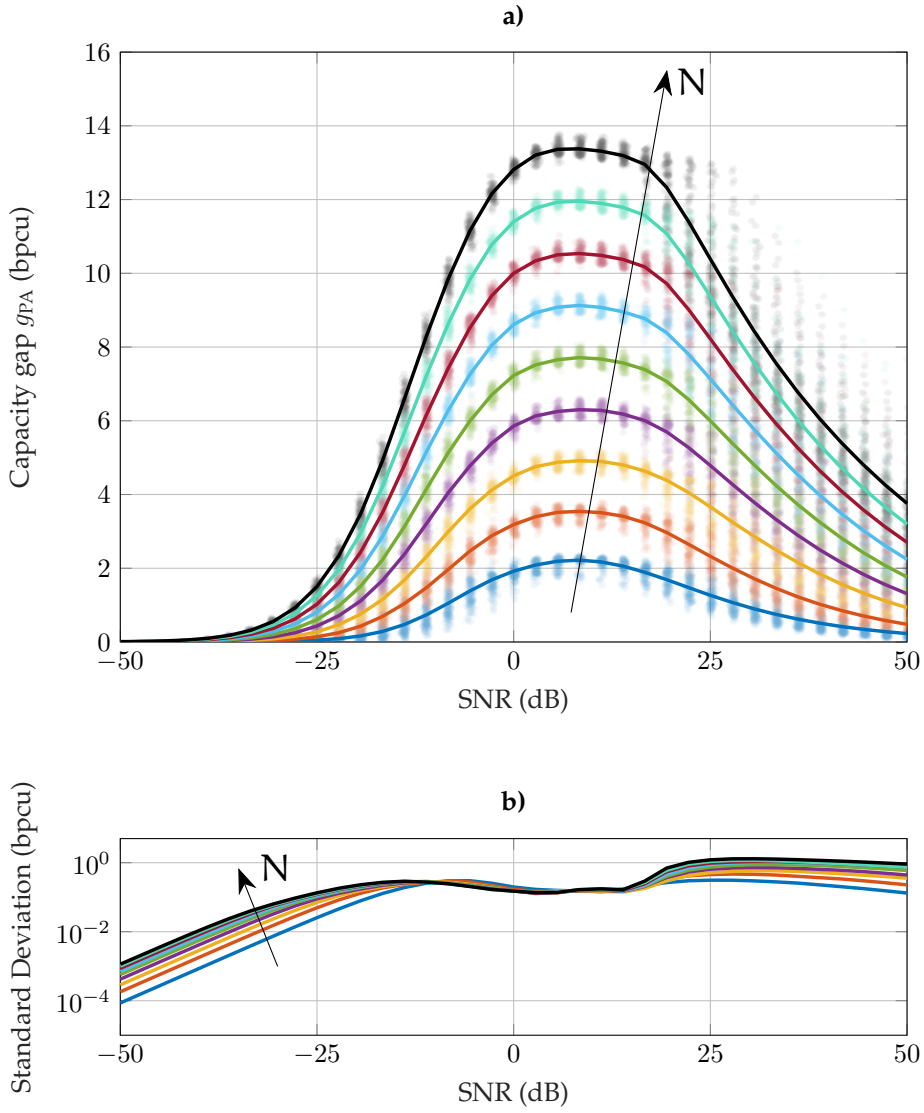

Figure 5.5: ***a)*** *Numerical evaluation of the capacity gap g_{PA}, defined in* (5.17)*, in bit per channel use (bpcu) versus SNR, for $\mathsf{N} = 2, \ldots, 10$. For all values of N, each filled circle shows the gap resulting from a random channel realization. The solid curves show the averaged behavior.* ***b)*** *Numerical evaluation of the standard deviation of g_{PA} in bpcu versus SNR, for $\mathsf{N} = 2, \ldots, 10$.*

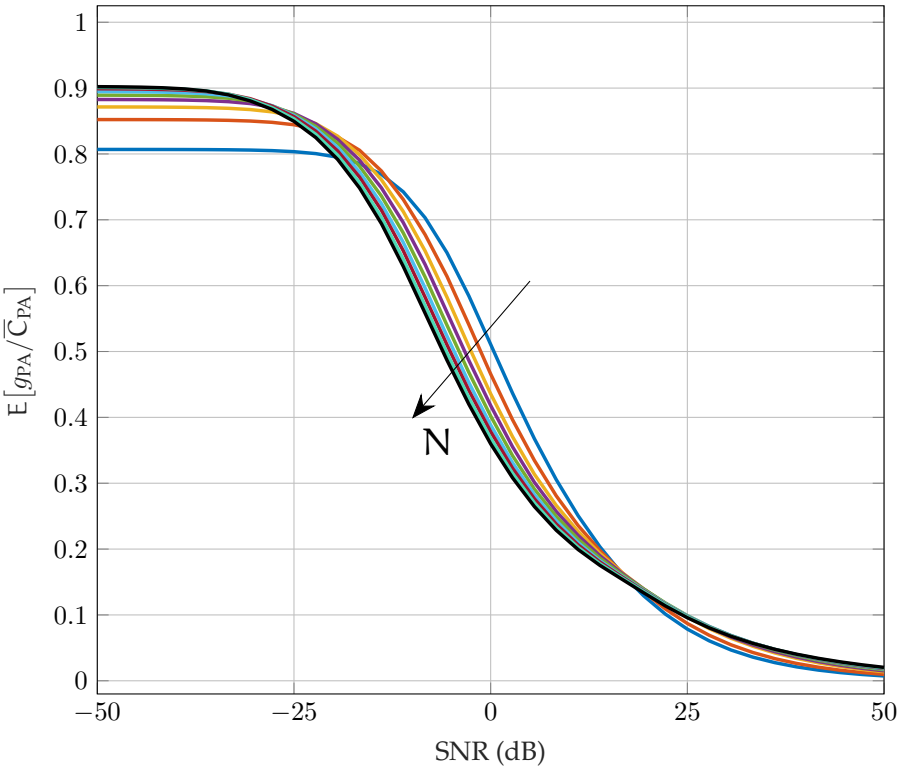

Figure 5.6: *Numerical evaluation of the average ratio between the capacity gap g_{PA}, defined in* (5.17)*, and the upper bound $\overline{C}_{PA}$, derived from* (5.18)*. The average ratio is plotted versus the SNR and for $N = 2, \ldots, 10$.*

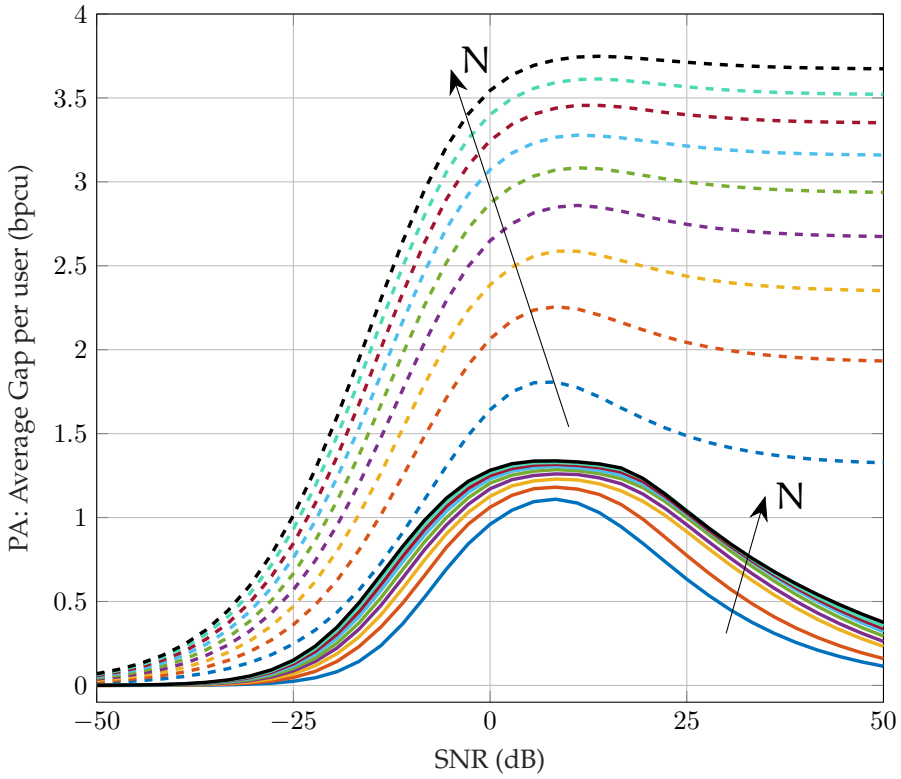

Figure 5.7: *Numerical evaluation of the average capacity gap per complex dimension in bit per channel use (bpcu) versus SNR, for* $\mathsf{N} = 2, \ldots, 10$. *The solid lines are* $\mathsf{E}[g_{PA}]/\mathsf{N}$, *with* g_{PA} *defined in* (5.17). *The dashed lines are* $\mathsf{E}[g_{D,PA}]/\mathsf{N}$, *with* $g_{D,PA}$ *defined in* (5.19).

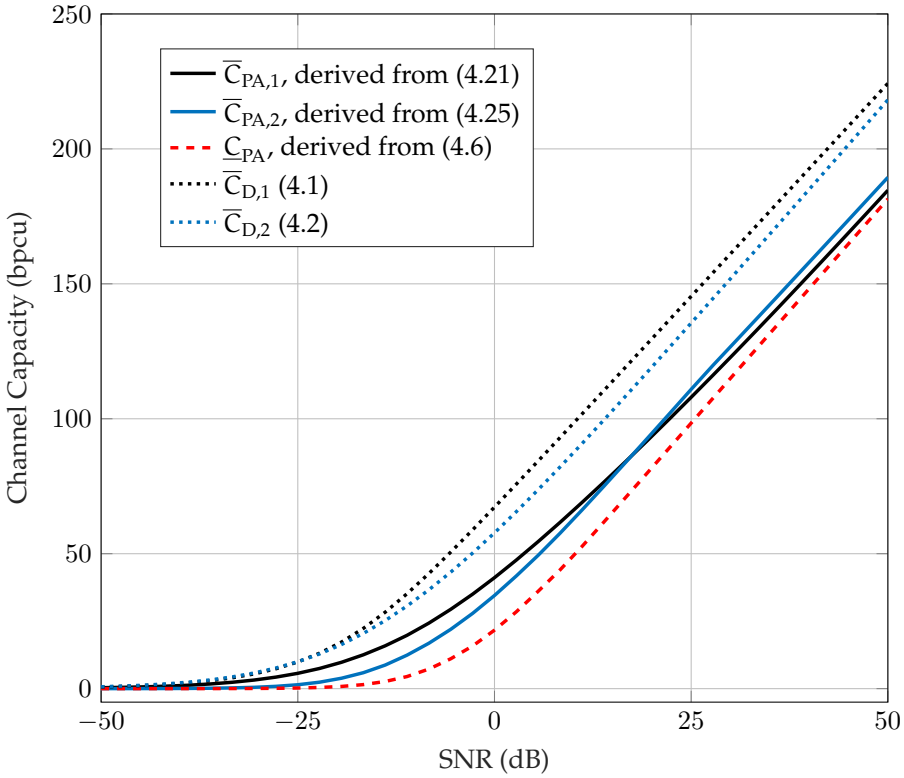

Figure 5.8: *Capacity bounds in bit per channel use (bpcu) versus SNR, for* $\mathsf{N} = 10$ *and for a random realization of* H'.

5.2.2 Quasi Parallel Channels Approach

The QPC approach is another viable solution to obtain upper bounds that can be applied to the PA constraint.

Let C_i be the capacity of the ith subchannel defined in the proof of Lemma 5, i.e.,

$$\mathsf{C}_i = \max_{f_{\mathbf{X}_i}:\, \mathbf{X}_i \in \mathcal{X}_i} \mathsf{h}(\mathsf{M}_i \mathbf{X}_i) - \mathsf{h}(\mathbf{Z}_i). \tag{5.20}$$

Since the channel matrix H is obtained by the vectorization of the complex-valued H' in Definition 2.1.1, we can assume the singular values of H to be equal 2-by-2, specifically, $\lambda_{2i}(\mathsf{H}) = \lambda_{2i-1}(\mathsf{H}),\ i = 1, \ldots, \mathsf{N}$. Notice that, therefore, the same holds for the covariance matrix D, for the D_i's, and also for the M_i's. Let us ease the notation by defining

$$\lambda(\mathsf{M}_i) \triangleq \lambda_1(\mathsf{M}_i) = \lambda_2(\mathsf{M}_i), \quad i = 1, \ldots, \mathsf{N}. \tag{5.21}$$

As mentioned in Remark 7, when the M_i's are scalar matrices, suitable upper bounds on the C_i's can be derived either through the bounds from [34] in Section 4.1. Notice that, for the considered case, the McKellips-Type upper bound from (3.61) becomes

$$\mathsf{C}_i \leq \overline{\mathsf{C}}_{\mathrm{McK},i} \triangleq \log\left(1 + \sqrt{\frac{\pi}{2}}\frac{\lambda(\mathsf{M}_i)\mathsf{R}}{\sigma_z} + \frac{\left(\lambda(\mathsf{M}_i)\mathsf{R}\right)^2}{2e\sigma_z^2}\right), \tag{5.22}$$

for $i = 1, \ldots, \mathsf{N}$.

Then, the QPC upper bound for the high SNR regime is given

by (5.22) is

$$\overline{\mathsf{C}}_1 \leq \overline{\mathsf{C}}_{\text{PA},3} \triangleq \left(\sum_{i=1}^{\mathsf{N}} \overline{\mathsf{C}}_{\text{McK},i} \right) + \frac{1}{2} \log \frac{\prod_{j=1}^{\mathsf{T}} \det(\mathsf{D}_j)}{\det(\mathsf{D})}. \tag{5.23}$$

Moreover, let $\overline{\mathsf{C}}_{\text{Ref},i} \geq \mathsf{C}_i$ denote the Refined upper bound introduced in Section 4.1. Then, by Theorem 4.3.1, we define

$$\overline{\mathsf{C}}_1 \leq \overline{\mathsf{C}}_{\text{PA},4} \triangleq \left(\sum_{i=1}^{\mathsf{N}} \overline{\mathsf{C}}_{\text{Ref},i} \right) + \frac{1}{2} \log \frac{\prod_{j=1}^{\mathsf{T}} \det(\mathsf{D}_j)}{\det(\mathsf{D})}. \tag{5.24}$$

Since $\overline{\mathsf{C}}_{\text{Ref},i}$ and $\overline{\mathsf{C}}_{\text{McK},i}$ converge to the subchannel capacities C_i, we have that thanks to Remark 11, Lemma 5 holds for both $\overline{\mathsf{C}}_{\text{PA},3}$ and $\overline{\mathsf{C}}_{\text{PA},4}$. Therefore, both upper bounds are asymptotically tight at high SNR. Notice that estimates of the C_i's could be evaluated via the numerical procedure devised in Algorithm 1. While providing a more accurate result than $\overline{\mathsf{C}}_{\text{Ref},i}$, in Section 3.4.2 it was shown that the refined upper bound $\overline{\mathsf{C}}_{\text{Ref},i}$ from [34] is already accurate and faster to evaluate. Furthermore, one of the main advantage provided by Algorithm 1, i.e., the evaluation of the PMF estimate, does not have particular significance in this case. Indeed, the optimal input PDFs for the *quasi* parallel subchannels, do not relate to that of the overall fading channel, aside from the special case described in Remark 10. Therefore, since i) $\overline{\mathsf{C}}_{\text{Ref},i}$ is computationally less heavy; ii) it provides a fairly tight capacity upper bound; and iii) the optimal PMFs of the subchannels are generally not related to the capacity-achieving distribution of the actual channel, we do not employ Algorithm 1 in this particular case.

Finally, as for the low SNR regime, notice that the QPC bound for the low SNR regime defined in Theorem 4.3.2, can be applied as it is

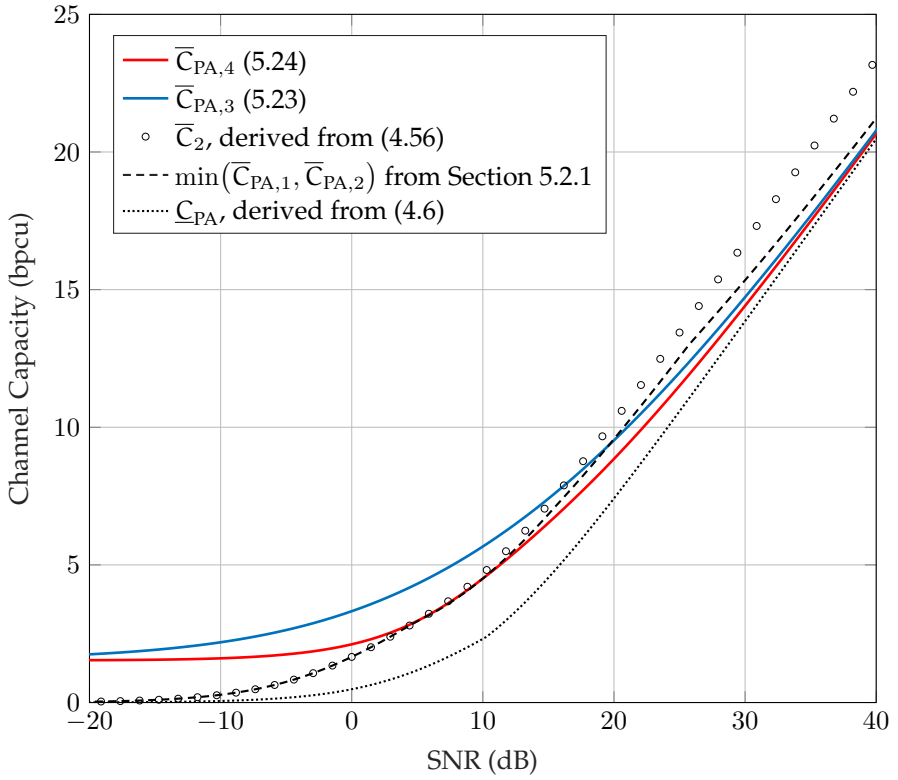

Figure 5.11: *Capacity bounds in bit per channel use (bpcu) versus SNR, for* $2\mathsf{N} = 4$, $\lambda(\boldsymbol{M}_1) = 0.52$, *and* $\lambda(\boldsymbol{M}_2) = 0.37$.

and does not need further derivations.

Let us provide some numerical results for the QPC approach. Consider a random realization of H and $\mathsf{N} = 2$. Fig. 5.11 shows the QPC capacity bounds for both the high, with $\overline{C}_{PA,3}$ and $\overline{C}_{PA,4}$, and low SNR regime, with $\overline{C}_2$. Furthermore, it shows the upper bound obtained via the SP approach and the P-EPI lower bound. Notice that, in the considered case, the QPC compound bound $\min(\overline{C}_{PA,4}, \overline{C}_2)$ outperforms the SP bound $\min(\overline{C}_{PA,1}, \overline{C}_{PA,2})$ at any SNR level.

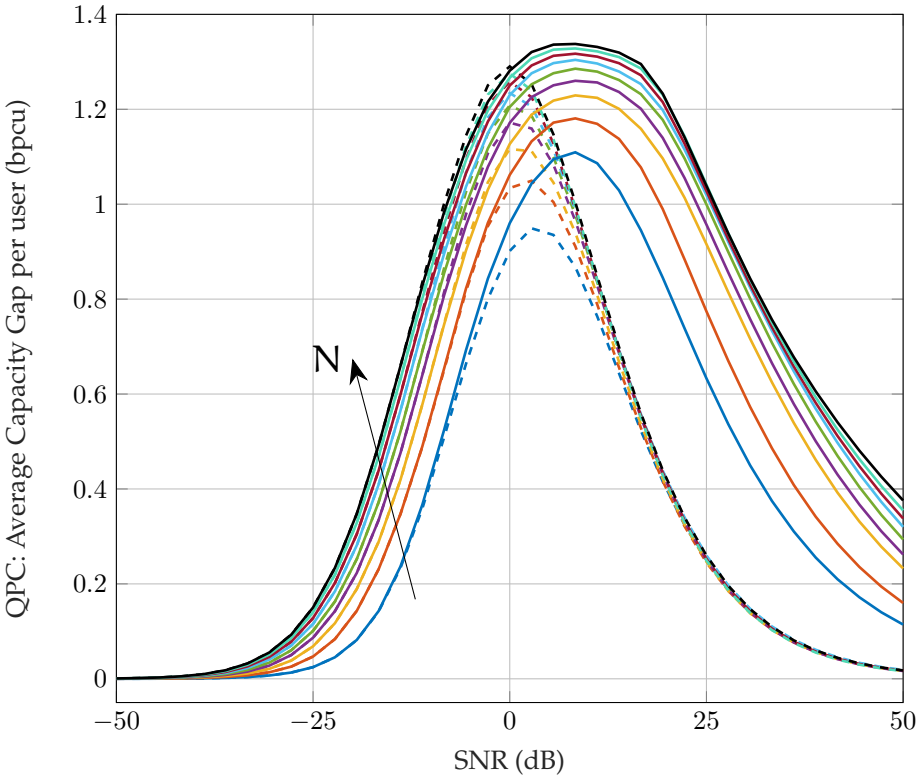

Figure 5.12: *Numerical evaluation of the average capacity gap per complex dimension in bit per channel use (bpcu) versus SNR, for* $\mathsf{N} = 2, \ldots, 10$. *The solid curves are* $\mathsf{E}[g_{PA}]/\mathsf{N}$, *with* g_{PA} *is defined in* (5.17), *and show the performance of the SP bound. The dashed curves are* $\mathsf{E}[g_{QPC}]/\mathsf{N}$, *with* g_{QPC} *is defined in* (5.25), *and show the performance of the QPC bound.*

Let us define the capacity gap provided by the QPC bounds as

$$g_{\text{QPC}} \triangleq \min\left(\overline{\mathsf{C}}_{\text{PA},4}, \overline{\mathsf{C}}_2\right) - \underline{\mathsf{C}}_{\text{PA}}. \tag{5.25}$$

In Fig. 5.12 it is shown a comparison between the average gap per complex dimension provided by the SP bound, i.e., $\mathsf{E}[g_{\text{PA}}]/\mathsf{N}$, and by the QPC bound, i.e., $\mathsf{E}[g_{\text{QPC}}]/\mathsf{N}$. Both are averaged over random realization of the channel matrix H'. As in the previous cases, the entries of H' are drawn independently as $\mathsf{H}'_{i,j} \sim \mathcal{CN}(0, 2),\ \forall i, j$. Notice that, in

average the QPC is tighter than the SP bound at almost any SNR level. Moreover, the average QPC gap convergence to zero at high SNR is significantly faster than that of the average SP gap.

Chapter 6

Conclusion

The pursuit of higher rates in wireless communication systems has made power consumption and the related environmental impact of such systems a growing concern. A better characterization of the problem from an information theoretic viewpoint can contribute to improve the overall energy efficiency of wireless communications systems. In this work, the capacity and the optimal input distribution has been investigated, for both nonfading and fading channels, under different configurations of input power constraints.

In the case of nonfading channels, a numerical procedure to estimate the capacity-achieving distribution has been derived, together with new insights on its properties. Furthermore, in the case of 2-dimensional real-valued channels, it is proposed a discrete approximate input distribution that can be practically implemented and achieves information rates extremely close to the capacity. The results on the optimal input distribution are extended to the case of vector Gaussian wiretap channels.

For the fading case, bounds on the channel capacity were derived.

The presented upper bounds are, currently, the best in the existing literature and asymptotically converge to the capacity as the Signal-to-Noise Ratio (SNR) increases. One family of upper bounds is based on a sphere packing argument and can be applied to any convex input constraint and for any full rank fading channel matrix. The second family specifically targets transmitter configurations employing multiple and parallel input constraints. For such constraints, the proposed bound further improves the performance obtained via the sphere packing upper bounds, by achieving an even faster convergence to the capacity at high SNR.

6.1 Future Avenues

Nonfading Vector Gaussian Channels:

The nonfading case has been thoroughly investigated. Nonetheless, an interesting line of research could be the derivation of tight bounds on the number of amplitude mass points in the capacity-achieving distribution. Another interesting topic could be the investigation of discrete and approximate input distributions for n-dimensional real-valued Multiple-Input Multiple-Output (MIMO) channels, with $n > 2$.

Fading Vector Gaussian Channels:

Notice that, in the nonfading case and at finite SNR, the gap between the presented capacity estimate and the Entropy Power Inequality (EPI) lower bound is far from zero, proving that the EPI approach does not provide a particularly tight lower bound. It is reasonable to expect the same shortcomings also for the EPI approach in the fading

case. Therefore, one interesting line of work could be the derivation of tighter lower bounds. Moreover, in the fading case not much is known about the capacity-achieving input distribution.

Another relevant research line could aim to derive insights on the structure of the optimal input distribution. For instance, for 2-dimensional real-valued channels, in which the most general input constraint region is an ellipse, it is not even clear if the support of the optimal input distribution is composed of points, curves or a mixture of both. Therefore, there is the need to develop numerical algorithms to estimate the capacity-achieving input distribution.

The presented upper bounds assume a static channel matrix. It would be interesting to extend the proposed upper bounds to the relevant case of block fading MIMO channels.

Finally, in this work the number of transmitting antennas was assumed equal to that of receiving antennas. While it is possible to directly apply the proposed bounds to some special cases with uneven number of transmitting and receiving antennas, it would be interesting to investigate a possible generalization of the proposed bounds to any MIMO channels, with arbitrary number of antennas both at the transmit and receive side.

Bibliography

[1] C. E. Shannon, "A mathematical theory of communication," *The Bell System Technical Journal*, vol. 27, no. 3, pp. 379–423, Jul. 1948.

[2] J. Winters, "On the capacity of radio communication systems with diversity in a Rayleigh fading environment," *IEEE Journal on Selected Areas in Communications*, vol. 5, no. 5, pp. 871–878, 1987.

[3] G. G. Raleigh and J. M. Cioffi, "Spatio-temporal coding for wireless communication," *IEEE Transactions on Communications*, vol. 46, no. 3, pp. 357–366, 1998.

[4] G. J. Foschini and M. J. Gans, "On limits of wireless communications in a fading environment when using multiple antennas," *Wireless Personal Communications*, vol. 6, no. 3, pp. 311–335, Mar. 1998.

[5] E. Telatar, "Capacity of multi-antenna Gaussian channels," *European Transactions on Telecommunications*, vol. 10, no. 6, pp. 585–595, Nov./Dec. 1999.

[6] G. Caire and S. Shamai, "On the achievable throughput of a multiantenna Gaussian broadcast channel," *IEEE Transactions on Information Theory*, vol. 49, no. 7, pp. 1691–1706, 2003.

[7] P. Viswanath and D. N. C. Tse, "Sum capacity of the vector Gaussian broadcast channel and uplink–downlink duality," *IEEE Transactions on Information Theory*, vol. 49, no. 8, pp. 1912–1921, 2003.

[8] S. Vishwanath, N. Jindal, and A. Goldsmith, "Duality, achievable rates, and sum-rate capacity of Gaussian MIMO broadcast channels," *IEEE Transactions on Information Theory*, vol. 49, no. 10, pp. 2658–2668, 2003.

[9] A. Goldsmith, S. A. Jafar, N. Jindal, and S. Vishwanath, "Capacity limits of MIMO channels," *IEEE Journal on Selected Areas in Communications*, vol. 21, no. 5, pp. 684–702, 2003.

[10] S. Verdù, "Multiple-access channels with memory with and without frame synchronism," *IEEE Transactions on Information Theory*, vol. 35, no. 3, pp. 605–619, 1989.

[11] D. Gesbert, M. Kountouris, R. W. Heath, C.-B. Chae, and T. Salzer, "Shifting the MIMO paradigm," *IEEE Signal Processing Magazine*, vol. 24, no. 5, pp. 36–46, 2007.

[12] T. L. Marzetta, "Noncooperative cellular wireless with unlimited numbers of base station antennas," *IEEE Transactions on Wireless Communications*, vol. 9, no. 11, pp. 3590–3600, 2010.

[13] F. Rusek, D. Persson, B. K. Lau, E. G. Larsson, T. L. Marzetta, O. Edfors, and F. Tufvesson, "Scaling up MIMO: Opportunities and challenges with very large arrays," *IEEE Signal Processing Magazine*, vol. 30, no. 1, pp. 40–60, 2012.

[14] H. Q. Ngo, E. G. Larsson, and T. L. Marzetta, "Energy and spectral efficiency of very large multiuser MIMO systems," *IEEE Transactions on Communications*, vol. 61, no. 4, pp. 1436–1449, 2013.

[15] J. Hoydis, S. Ten Brink, and M. Debbah, "Massive MIMO in the UL/DL of cellular networks: How many antennas do we need?" *IEEE Journal on Selected Areas in Communications*, vol. 31, no. 2, pp. 160–171, 2013.

[16] E. G. Larsson, O. Edfors, F. Tufvesson, and T. L. Marzetta, "Massive MIMO for next generation wireless systems," *IEEE Communications Magazine*, vol. 52, no. 2, pp. 186–195, 2014.

[17] Y. Kim, H. Ji, J. Lee, Y.-H. Nam, B. L. Ng, I. Tzanidis, Y. Li, and J. Zhang, "Full dimension MIMO (FD-MIMO): The next evolution of MIMO in LTE systems," *IEEE Wireless Communications*, vol. 21, no. 2, pp. 26–33, 2014.

[18] M. Kamel, W. Hamouda, and A. Youssef, "Ultra-dense networks: A survey," *IEEE Communications Surveys & Tutorials*, vol. 18, no. 4, pp. 2522–2545, 2016.

[19] Y. Chen, S. Zhang, S. Xu, and G. Y. Li, "Fundamental trade-offs on green wireless networks," *IEEE Communications Magazine*, vol. 49, no. 6, pp. 30–37, 2011.

[20] G. Chopra, R. K. Jha, and S. Jain, "A survey on ultra-dense network and emerging technologies: Security challenges and possible solutions," *Journal of Network and Computer Applications*, vol. 95, pp. 54–78, 2017.

[21] C. Freitag, M. Berners-Lee, K. Widdicks, B. Knowles, G. S. Blair, and A. Friday, "The real climate and transformative impact of ICT: A critique of estimates, trends, and regulations," *Patterns*, vol. 2, no. 9, p. 100340, 2021.

[22] J. Malmodin and D. Lundén, "The energy and carbon footprint of the global ICT and E&M sectors 2010–2015," *Sustainability*, vol. 10, no. 9, p. 3027, 2018.

[23] Z. Hasan, H. Boostanimehr, and V. K. Bhargava, "Green cellular networks: A survey, some research issues and challenges," *IEEE Communications Surveys & Tutorials*, vol. 13, no. 4, pp. 524–540, 2011.

[24] C. Han, T. Harrold, S. Armour, I. Krikidis, S. Videv, P. M. Grant, H. Haas, J. S. Thompson, I. Ku, C.-X. Wang *et al.*, "Green radio: radio techniques to enable energy-efficient wireless networks," *IEEE Communications Magazine*, vol. 49, no. 6, pp. 46–54, 2011.

[25] L. M. Correia, D. Zeller, O. Blume, D. Ferling, Y. Jading, I. Gódor, G. Auer, and L. Van Der Perre, "Challenges and enabling technologies for energy aware mobile radio networks," *IEEE Communications Magazine*, vol. 48, no. 11, pp. 66–72, 2010.

[26] J. G. Smith, "The information capacity of amplitude- and variance-constrained scalar Gaussian channels," *Information and Control*, vol. 18, no. 3, pp. 203–219, Apr. 1971.

[27] S. Shamai and I. Bar-David, "The capacity of average and peak-power-limited quadrature Gaussian channels," *IEEE Transactions on Information Theory*, vol. 41, no. 4, pp. 1060–1071, Jul. 1995.

[28] B. Rassouli and B. Clerckx, "On the capacity of vector Gaussian channels with bounded inputs," *IEEE Transactions on Information Theory*, vol. 62, no. 12, pp. 6884–6903, Dec. 2016.

[29] A. Dytso, S. Yagli, H. V. Poor, and S. Shamai, "The capacity achieving distribution for the amplitude constrained additive Gaussian channel: An upper bound on the number of mass points," *IEEE Transactions on Information Theory*, vol. 66, no. 4, pp. 2006–2022, April 2020.

[30] A. Tchamkerten, "On the discreteness of capacity-achieving distributions," *IEEE Transactions on Information Theory*, vol. 50, no. 11, pp. 2773–2778, Nov. 2004.

[31] T. Chan, S. Hranilovic, and F. Kschischang, "Capacity-achieving probability measure for conditionally Gaussian channels with bounded inputs," *IEEE Transactions on Information Theory*, vol. 51, no. 6, pp. 2073–2088, Jun. 2005.

[32] B. Mamandipoor, K. Moshksar, and A. K. Khandani, "Capacity-achieving distributions in Gaussian multiple access channel with peak power constraints," *IEEE Transactions on Information Theory*, vol. 60, no. 10, pp. 6080–6092, Oct. 2014.

[33] A. McKellips, "Simple tight bounds on capacity for the peak-limited discrete-time channel," in *International Symposium on Information Theory, 2004. ISIT 2004. Proceedings.*, Jun./Jul. 2004, pp. 348–348.

[34] A. Thangaraj, G. Kramer, and G. Böcherer, "Capacity bounds for discrete-time, amplitude-constrained, additive white Gaussian noise channels," *IEEE Transactions on Information Theory*, vol. 63, no. 7, pp. 4172–4182, Jul. 2017.

[35] B. Rassouli and B. Clerckx, "An upper bound for the capacity of amplitude-constrained scalar AWGN channel," *IEEE Communications Letters*, vol. 20, no. 10, pp. 1924–1926, 2016.

[36] J. Huang and S. Meyn, "Characterization and computation of optimal distributions for channel coding," *IEEE Transactions on Information Theory*, vol. 51, no. 7, pp. 2336–2351, 2005.

[37] I. Abou-Faycal, M. Trott, and S. Shamai, "The capacity of discrete-time memoryless Rayleigh-fading channels," *IEEE Transactions on Information Theory*, vol. 47, no. 4, pp. 1290–1301, 2001.

[38] A. ElMoslimany and T. M. Duman, "On the capacity of multiple-antenna systems and parallel Gaussian channels with amplitude-limited inputs," *IEEE Transactions on Communications*, vol. 64, no. 7, pp. 2888–2899, Jul. 2016.

[39] A. Dytso, M. Goldenbaum, H. V. Poor *et al.*, "Amplitude constrained MIMO channels: Properties of optimal input distributions and bounds on the capacity," *Entropy*, vol. 21, no. 2, p. 200, Feb. 2019.

[40] A. Chaaban, J.-M. Morvan, and M.-S. Alouini, "Free-space optical communications: Capacity bounds, approximations, and a new sphere-packing perspective," *IEEE Transactions on Communications*, vol. 64, no. 3, pp. 1176–1191, Feb. 2016.

[41] L. Li, S. M. Moser, L. Wang, and M. Wigger, "On the capacity of MIMO optical wireless channels," *IEEE Transactions on Information Theory*, vol. 66, no. 9, pp. 5660–5682, Mar. 2020.

[42] S. M. Moser, L. Wang, and M. Wigger, "Capacity results on multiple-input single-output wireless optical channels," *IEEE Transactions on Information Theory*, vol. 64, no. 11, pp. 6954–6966, 2018.

[43] A. Lapidoth, S. M. Moser, and M. A. Wigger, "On the capacity of free-space optical intensity channels," *IEEE Transactions on Information Theory*, vol. 55, no. 10, pp. 4449–4461, Sep. 2009.

[44] N. Sharma and S. Shamai, "Transition points in the capacity-achieving distribution for the peak-power limited AWGN and free-space optical intensity channels," *Problems of Information Transmission*, vol. 46, no. 4, pp. 283–299, Dec. 2010.

[45] S. M. Moser, M. Mylonakis, L. Wang, and M. Wigger, "Asymptotic capacity results for MIMO wireless optical communication," in *2017 IEEE International Symposium on Information Theory (ISIT)*, Jun. 2017, pp. 536–540.

[46] S. Hranilovic and F. R. Kschischang, "Capacity bounds for power-and band-limited optical intensity channels corrupted by Gaussian noise," *IEEE Transactions on Information Theory*, vol. 50, no. 5, pp. 784–795, 2004.

[47] A. Favano, M. Ferrari, M. Magarini, and L. Barletta, "The capacity of the amplitude-constrained vector Gaussian channel," in *2021 IEEE International Symposium on Information Theory (ISIT)*, Jul. 2021, pp. 426–431.

[48] A. Favano, L. Barletta, and A. Dytso, "On the capacity achieving input of amplitude constrained vector Gaussian wiretap channel," in *2022 IEEE International Symposium on Information Theory (ISIT)*, 2022, pp. 850–855.

[49] A. Favano, M. Ferrari, M. Magarini, and L. Barletta, "Capacity bounds for amplitude-constrained AWGN MIMO channels with fading," in *2020 IEEE International Symposium on Information Theory (ISIT)*, Jun. 2020, pp. 2032–2037.

[50] A. Favano, M. Ferrari, M. Magarini, and L. Barletta, "A sphere packing bound for AWGN MIMO fading channels under peak amplitude constraints," in *2020 IEEE Information Theory Workshop (ITW)*, Apr. 2021, pp. 1–5.

[51] ——, "A sphere packing bound for vector Gaussian fading channels under peak amplitude constraints," *IEEE Transactions on Information Theory*, pp. 1–1, 2022.

[52] ——, "The capacity of fading vector Gaussian channels under amplitude constraints on antenna subsets," *arXiv preprint arXiv:2207.01266*, 2022.

[53] R. Dobrushin, "General formulation of Shannon's main theorem in information theory," *American Mathematical Society Translations*, vol. 33, pp. 323–438, 1963.

[54] W. Yu and T. Lan, "Transmitter optimization for the multi-antenna downlink with per-antenna power constraints," *IEEE Transactions on Signal Processing*, vol. 55, no. 6, pp. 2646–2660, 2007.

[55] S. Loyka, "The capacity of Gaussian MIMO channels under total and per-antenna power constraints," *IEEE Transactions on Communications*, vol. 65, no. 3, pp. 1035–1043, 2017.

[56] M. Vu, "MISO capacity with per-antenna power constraint," *IEEE Transactions on Communications*, vol. 59, no. 5, pp. 1268–1274, 2011.

[57] A. Lapidoth and S. M. Moser, "Capacity bounds via duality with applications to multiple-antenna systems on flat-fading channels," *IEEE Transactions on Information Theory*, vol. 49, no. 10, pp. 2426–2467, October 2003.

[58] L. Barletta and S. Rini, "On the capacity of the oversampled Wiener phase noise channel," *arXiv preprint arXiv:2001.07485*, January 2020.

[59] Y. Yu, "On log-concavity of the generalized Marcum Q function," *arXiv preprint arXiv:1105.5762*, May 2011.

[60] M. Abramowitz and I. A. Stegun, *Handbook of Mathematical Functions with Formulas, Graphs, and Mathematical Tables*. US Government printing office, December 1965, vol. 55.

[61] D. E. Amos, "Computation of modified Bessel functions and their ratios," *Mathematics of Computation*, vol. 28, no. 125, pp. 239–251, January 1974.

[62] R. Blahut, "Computation of channel capacity and rate-distortion functions," *IEEE Transactions on Information Theory*, vol. 18, no. 4, pp. 460–473, 1972.

[63] S. Arimoto, "An algorithm for computing the capacity of arbitrary discrete memoryless channels," *IEEE Transactions on Information Theory*, vol. 18, no. 1, pp. 14–20, 1972.

[64] Y. Wu and S. Verdù, "Functional properties of minimum mean-square error and mutual information," *IEEE Transactions on Information Theory*, vol. 58, no. 3, pp. 1289–1301, March 2012.

[65] J. Dauwels, "Numerical computation of the capacity of continuous memoryless channels," in *Proceedings of the 26th Symposium on Information Theory in the BENELUX*, 2005, pp. 221–228.

[66] A. Dytso, M. Al, H. V. Poor, and S. Shamai, "On the capacity of the peak power constrained vector Gaussian channel: An estimation theoretic perspective," *IEEE Transactions on Information Theory*, vol. 65, no. 6, pp. 3907–3921, January 2019.

[67] H. S. M. Coxeter, *Regular polytopes*. Courier Corporation, 1973.

[68] J. J. Thomson, "XXIV. On the structure of the atom: an investigation of the stability and periods of oscillation of a number of corpuscles arranged at equal intervals around the circumference of a circle; with application of the results to the theory of atomic structure," *The London, Edinburgh, and Dublin Philosophical Magazine and Journal of Science*, vol. 7, no. 39, pp. 237–265, 1904.

[69] J. Batle, A. Bagdasaryan, M. Abdel-Aty, and S. Abdalla, "Generalized Thomson problem in arbitrary dimensions and non-euclidean geometries," *Physica A: Statistical Mechanics and its Applications*, vol. 451, pp. 237–250, 2016.

[70] A. D. Wyner, "The wire-tap channel," *Bell System Technical Journal*, vol. 54, no. 8, pp. 1355–1387, 1975.

[71] S. Leung-Yan-Cheong and M. Hellman, "The Gaussian wire-tap channel," *IEEE Transactions on Information Theory*, vol. 24, no. 4, pp. 451–456, 1978.

[72] S. Shafiee, N. Liu, and S. Ulukus, "Towards the secrecy capacity of the Gaussian MIMO wire-tap channel: The 2-2-1 channel," *IEEE Transactions on Information Theory*, vol. 55, no. 9, pp. 4033–4039, 2009.

[73] A. Khisti and G. W. Wornell, "Secure transmission with multiple antennas–Part II: The MIMOME wiretap channel," *IEEE Transactions on Information Theory*, vol. 56, no. 11, pp. 5515–5532, 2010.

[74] F. Oggier and B. Hassibi, "The secrecy capacity of the MIMO wiretap channel," *IEEE Transactions on Information Theory*, vol. 57, no. 8, pp. 4961–4972, 2011.

[75] T. Liu and S. Shamai, "A note on the secrecy capacity of the multiple-antenna wiretap channel," *IEEE Transactions on Information Theory*, vol. 55, no. 6, pp. 2547–2553, 2009.

[76] S. Loyka and C. D. Charalambous, "An algorithm for global maximization of secrecy rates in Gaussian MIMO wiretap channels," *IEEE Transactions on Communications*, vol. 63, no. 6, pp. 2288–2299, 2015.

[77] ——, "Optimal signaling for secure communications over Gaussian MIMO wiretap channels," *IEEE Transactions on Information Theory*, vol. 62, no. 12, pp. 7207–7215, 2016.

[78] M. Bloch and J. Barros, *Physical-Layer Security:From Information Theory to Security Engineering*. Cambridge University Press, 2011.

[79] F. Oggier and B. Hassibi, "A perspective on the MIMO wiretap channel," *Proceedings of the IEEE*, vol. 103, no. 10, pp. 1874–1882, Oct 2015.

[80] Y. Liang, H. V. Poor, and S. Shamai, "Information theoretic security," *Foundations and Trends in Communications and Information Theory*, vol. 5, no. 4–5, pp. 355–580, 2009.

[81] H. V. Poor and R. F. Schaefer, "Wireless physical layer security," *Proceedings of the National Academy of Sciences*, vol. 114, no. 1, pp. 19–26, 2017.

[82] A. Mukherjee, S. A. A. Fakoorian, J. Huang, and A. L. Swindlehurst, "Principles of physical layer security in multiuser wireless networks: A survey," *IEEE Communications Surveys & Tutorials*, vol. 16, no. 3, pp. 1550–1573, 2014.

[83] P. K. Gopala, L. Lai, and H. El Gamal, "On the secrecy capacity of fading channels," *IEEE Transactions on Information Theory*, vol. 54, no. 10, pp. 4687–4698, 2008.

[84] M. Bloch, J. Barros, M. R. Rodrigues, and S. W. McLaughlin, "Wireless information-theoretic security," *IEEE Transactions on Information Theory*, vol. 54, no. 6, pp. 2515–2534, 2008.

[85] A. Khisti, A. Tchamkerten, and G. W. Wornell, "Secure broadcasting over fading channels," *IEEE Transactions on Information Theory*, vol. 54, no. 6, pp. 2453–2469, 2008.

[86] Y. Liang, H. V. Poor, and S. Shamai, "Secure communication over fading channels," *IEEE Transactions on Information Theory*, vol. 54, no. 6, pp. 2470–2492, 2008.

[87] O. Ozel, E. Ekrem, and S. Ulukus, "Gaussian wiretap channel with amplitude and variance constraints," *IEEE Transactions on Information Theory*, vol. 61, no. 10, pp. 5553–5563, 2015.

[88] M. Soltani and Z. Rezki, "The degraded discrete-time Poisson wiretap channel," *arXiv preprint arXiv:2101.03650*, 2021.

[89] S.-H. Nam and S.-H. Lee, "Secrecy capacity of a Gaussian wiretap channel with one-bit ADCs is always positive," in *2019 IEEE Information Theory Workshop (ITW)*. IEEE, 2019, pp. 1–5.

[90] A. Dytso, M. Egan, S. M. Perlaza, H. V. Poor, and S. Shamai, "Optimal inputs for some classes of degraded wiretap channels," in *2018 IEEE Information Theory Workshop (ITW)*, 2018, pp. 1–5.

[91] M. Lotz, M. B. McCoy, I. Nourdin, G. Peccati, and J. A. Tropp, "Concentration of the intrinsic volumes of a convex body," in *Geometric Aspects of Functional Analysis*. Springer, Jul. 2020, pp. 139–167.

[92] J. B. Conway, *A course in functional analysis*. Springer, 2019, vol. 96.

[93] M. Henk and M. A. H. Cifre, "Intrinsic volumes and successive radii," *Journal of Mathematical Analysis and Applications*, vol. 343, no. 2, pp. 733–742, 2008.

[94] V. Jog and V. Anantharam, "A geometric analysis of the AWGN channel with a (σ, ρ)-power constraint," *IEEE Transactions on Information Theory*, vol. 62, no. 8, pp. 4413–4438, Aug. 2016.

[95] R. T. Rockafellar, *Convex Analysis*. Princeton University Press, Jan. 1997, vol. 36.

[96] D. Zaporozhets and Z. Kabluchko, "Random determinants, mixed volumes of ellipsoids, and zeros of Gaussian random fields," *Journal of Mathematical Sciences*, vol. 199, no. 2, pp. 168–173, May 2014.

[97] R. A. Horn and C. R. Johnson, *Matrix Analysis*. Cambridge University Press, 2012.

[98] P. McMullen, "Non-linear angle-sum relations for polyhedral cones and polytopes," in *Mathematical Proceedings of the Cambridge Philosophical Society*, vol. 78, no. 2. Cambridge University Press, Oct. 1975, pp. 247–261.

[99] B. Grünbaum, "Grassmann angles of convex polytopes," *Acta Mathematica*, vol. 121, no. 1, pp. 293–302, Dec. 1968.

[100] W. Xu and B. Hassibi, "Compressed sensing over the Grassmann manifold: A unified analytical framework," in *2008 46th Annual Allerton Conference on Communication, Control, and Computing*, 2008, pp. 562–567.

[101] M. Khosravi and M. D. Taylor, "The wedge product and analytic geometry," *The American Mathematical Monthly*, vol. 115, no. 7, pp. 623–644, Aug./Sep. 2008.